SCHOOL OF COMPUTATION, INFORMATION AND TECHNOLOGY - INFORMATICS

TECHNICAL UNIVERSITY OF MUNICH

Master's Thesis in Informatics

# Analysis of Aircraft Noise Data in the Area of the Airport of Hamburg

**Patrick Bettermann**

SCHOOL OF COMPUTATION, INFORMATION AND TECHNOLOGY - INFORMATICS

TECHNICAL UNIVERSITY OF MUNICH

Master's Thesis in Informatics

# Analysis of Aircraft Noise Data in the Area of the Airport of Hamburg

# Analyse von Fluglärmdaten im Bereich des Flughafens von Hamburg

| | |
|---|---|
| Author: | Patrick Bettermann |
| Supervisor: | Prof. Dr. Hans-Joachim Bungartz |
| Advisor: | Dr. Arthur Schady |
| Submission Date: | 15.02.2024 |

I confirm that this master's thesis is my own work and I have documented all sources and material used.

Munich, 15.02.2024 Patrick Bettermann

# Acknowledgments

I would like to express my sincere gratitude to Dr. Arthur Schady for his invaluable guidance throughout the research process and for sharing his extensive experience in atmospheric physics and acoustics. I have benefited greatly from your wealth of knowledge, you taught me a lot beyond the master's thesis and prepared me perfectly for the time after my studies.

Thank you to Professor Dr. Hans-Joachim Bungartz, who always helped me in the shortest amount of time when I had problems and trusted me to make this project possible.

I thank my colleagues at the Traffic Noise and Sound Propagation group Dr. Katharina Elsen, Hessel Juliust, and Sirine Gharbi. Discussing acoustics and your works gave me a lot of ideas for this thesis and helped me navigate this field of research which was new to me as a computer scientist. A special thanks to Sirine for giving me thorough feedback on my work.

My appreciation goes to Tobias Joppa and Feryal Berber from the Airport of Hamburg for providing me with the necessary data, proofreading my work, and taking the time to give me a unique once-in-a-lifetime tour around the airport and the measuring stations. The visit gave me a lot of inspiration and important impressions to complete this work.

Finally, I would like to thank the Applied Meteorology group at the Institute of Atmospheric Physics at DLR who offered me the perfect conditions to do my research.

# Abstract

Outdoor sound propagation can be modeled numerically, but it is difficult to validate the results using measurements. The main objective of this master's thesis was to quantify meteorological effects on outdoor sound propagation using noise measurements and weather data obtained by the Hamburg airport for air traffic control purposes. 91,000 A320 measurements from the period August 22 - August 23 were recorded. This data is supplemented by weather profiles measured at the Hamburg Weathermast. In addition to the precise modeling of the noise emissions generated at the source, of the aircraft, the modeling of atmospheric effects is also crucial to accurately determine the noise measured on the ground. To analyze the data, we first perform a Principal Component Analysis (PCA) to investigate the correlation of the combined noise, flight, and weather parameters. The Analysis of Variance (ANOVA) method is used to investigate whether there are significant differences in the A-weighted maximum sound pressure level $L_{AS,max}$ values between different meteorological parameters. In addition, we use the mean decrease in impurity (MDI) and permutation importance of a random forest model to evaluate how weather parameters can be used in the prediction of noise from aircraft overflights. A positive and negative temperature gradient differed on average by 2.13 - 2.61 dB, p-value < 0.05. A measured difference of 1.2 dB on average, p-value 0.00, was found between the upwind and downwind classes. When predicting noise with a Random Forest model, the removal of the weather parameters would lead to a loss of 14.85% accuracy on the training data. Overall, the noise can be predicted with an accuracy of 1 dB at a specific measuring station for the A320 type depending on the state of the source, e.g. the aircraft's configuration and flight procedures. From the measurement data, it is possible to derive audible differences for humans depending on the weather conditions. However, we can't yet predict noise for all aircraft types and locations.

# Kurzfassung

Die Schallausbreitung im Freien kann numerisch modelliert werden, aber es ist schwierig, die Ergebnisse anhand von Messungen zu überprüfen. Das Hauptziel dieser Masterarbeit war die Quantifizierung der meteorologischen Effekte auf die Schallausbreitung im Freien anhand von Lärmmessungen und Wetterdaten, die der Hamburger Flughafen für Zwecke der Flugsicherung erhebt. Neben der genauen Modellierung der Lärmemissionen, die an der Quelle, dem Flugzeug, entstehen, ist auch die Modellierung der atmosphärischen Effekte von entscheidender Bedeutung, um den am Boden gemessenen Lärm genau zu bestimmen. 91,000 A320-Messungen aus dem Zeitraum August 22 bis August 23 wurden aufgezeichnet. Diese wurden durch Wetterprofile ergänzt, die am Hamburger Wettermast gemessen wurden. Um die Daten zu analysieren führen wir zunächst eine Hauptkomponentenanalyse (PCA) durch, um die Korrelation der kombinierten Lärm-, Flug- und Wetterparameter zu untersuchen. Mit der Varianzanalyse (ANOVA) wird untersucht, ob es signifikante Unterschiede in den A-bewerteten maximalen Schalldruckpegeln $L_{AS,max}$ zwischen Klassen verschiedener meteorologischer Parametern gibt. Darüber hinaus verwenden wir die "mean decrease in impurity"(MDI) - Metrik und die "permutation importance Metrik eines eines Random-Forest-Modells, um zu bewerten, wie Wetterparameter für die Vorhersage von Fluglärm verwendet werden können. Ein positiver und ein negativer Temperaturgradient unterschieden sich durchschnittlich um 2,13 - 2,61 dB, p-Wert < 0,05. Ein gemessener Unterschied von durchschnittlich 1,2 dB, p-value 0,00, wurde zwischen der Auf- und Abwindklasse festgestellt. Bei der Vorhersage von Lärm mit einem Random Forest Modells würde das Entfernen der Wetterparameter aus dem Datensatz zu einem Verlust von 14,85% Genauigkeit auf den Trainingsdaten führen. Insgesamt lässt sich der Lärm mit einer Genauigkeit von 1 dB an einer bestimmten Messstation für den Typ A320 vorhersagen, abhängig vom Zustand der Quelle, in Bezug auf z.B. Flugzeugkonfiguration und Flugverfahren. Aus den Messdaten lassen sich hörbare Unterschiede für den Menschen in Abhängigkeit von den Wetterbedingungen ableiten. Allerdings können wir noch nicht für alle Flugzeugtypen und Standorte Lärm vorhersagen.

# Contents

# 1. Introduction

This master's thesis is a data science approach to aircraft noise immission modeling with measured noise under consideration of weather data gathered around the airport of Hamburg. To better protect residents living near the airport from noise, it is essential to take into account the influence of meteorology on noise. Using the existing weather data recorded at the airport and the respective noise measurement stations (wind speed and direction, relative humidity, and air temperature), supplemented by vertical profiles of these parameters measured at the 280-meter-high Hamburg weather mast, we calculate the positive and negative effects of the weather on the noise heard by residents. The new approach of this work is to investigate how Hamburg Airport can use data that it already records for air traffic control purposes to improve the protection of residents from noise. Furthermore, as a new approach, we evaluate how the Hamburg weather mast can be used as an additional source of weather data to account for effects such as noise refraction. Aircraft noise immission is the sound level measured on the ground as opposed to the noise emitted by the aircraft. The investigation of aircraft noise emissions examines all noise-generating components, e.g. the engines, wings, landing gear, take-off weight (TOW), thrust setting, and high-lift components [1]. Studies of these components are outside of the scope of this work because of the lack of availability of this type of data. We focus on a specific aircraft type, the Airbus A320-200 passenger aircraft as it's one of the most flown aircraft worldwide. Using mathematical methods, we filter out the dependency on sound source-specific parameters as much as possible. Using the data from Hamburg Airport, we determine the influence of the atmosphere as a sound-transporting medium on the sound immissions measured on the ground. The aircraft position data from the radar is combined with weather data from the airport and the weather mast of the University of Hamburg to obtain the meteorological conditions that influenced the measured aircraft noise.

Atmospheric acoustics is a complex topic due to the complex and inhomogeneous nature of the atmosphere. Often numerical schemes are employed to simulate the governing PDEs over a given time. AKU3D a finite-difference time-domain sound propagation model [2] and AKUMET a sound particle model [3] are two such schemes developed by the DLR. These models can simulate sound propagation for complex meteorological fields as well as local topographical conditions like hills or ground impedance.

On the one hand, we look at the known influence of meteorological parameters on the measured noise, on the other hand, we also look at specific measuring stations in detail.

We are investigating the extent to which AI methods can be used to filter the influence of the measured weather parameters wind, temperature, and humidity on noise immissions and what information is needed to predict the noise from overflights at measuring stations.

The structure of this work is as follows: In chapter 2, current research in the field of

aeroacoustics is introduced. Some projects with a focus on aircraft noise immission modeling will be highlighted. Chapter 3 will first introduce the theory of atmospheric physics. The structure of the atmosphere plays a crucial role as it is the medium of sound propagation for aircraft noise [4]. We will go on to the topic of acoustics, what the different noise parameters mean, and what one should pay attention to when working with noise data. The theory of acoustics is the foundation for the subject of aeroacoustics where we look at noise generation through aerodynamic forces or turbulent flows. Various effects like sound refraction occur in the atmosphere that influence the propagation of sound which we examine in this work. The collection of data at the airport of Hamburg and the measuring stations, in particular, will be described in chapter 4. The weather instruments inside the Noise Monitoring Terminal (NMT) have limited capabilities because they measure the weather at a single point close to the ground, therefore extended weather profiles from the weather mast are used. This data allows us to compute vertical gradients and use them as parameters for statistical methods to model and quantify the influence of the atmosphere. Chapter 5 defines the methods used for this work. Multiple statistical methods and machine learning methods are used to build a model from the various data sources described in chapter 4. First, a Principal Component Analysis (PCA)[5] is performed in chapter 5.3 on several location-specific data sets to compute correlations in the data, visualize groups in the data set and determine significant parameters. The data is grouped according to several of these parameters for the Analysis of Variance (ANOVA) statistical method in chapter 6. As part of a complete statistical analysis, the mean difference in dB between the groups is calculated and the influence of atmospheric effects is quantified. We're interested in the question of whether and how noise immission can be predicted using machine learning methods. We train a random forest regression model [6] and determine the feature importance for all parameters in chapter 7 as a further metric to determine how much influence a specific weather parameter has on outdoor sound propagation. We go on to combine the information and findings of the previous chapters to predict the noise at a specific Noise Measuring Terminal for A320-200 overflights before concluding the work in chapter 8. Due to the data basis, only the A320 is considered in this work. In addition to this type, the Boeing 777, the Airbus A330, or, for example, the Boeing 737-800, which is very similar to the A320 in terms of size, flight behavior, and area of operation, also land at Hamburg Airport, along with other types. The B777 and the A330 are wide-body long-haul aircraft that are heavier than the A320. As a result, these types climb more slowly on take-off, depending on the load, and therefore fly closer to the microphones and need more thrust. Depending on the type, this results in a $\Delta L$ in the sound pressure level compared to the A320. We briefly look at these differences in chapter 6. In addition, the aircraft types also differ in the frequency spectrum of the noise emissions. We cannot take these differences into account as the spectrum was not recorded during the noise measurements. If these differences of $\Delta L$ are taken into account, the results of the A320 concerning the influence of meteorological effects can be transferred to other types with an offset.

# 2. State of the art

Aircraft noise has a significant impact on the health of the people affected. Effects on the number of prescriptions for antihypertensive drugs, sleep behavior and prescriptions of related drugs, and the deterioration of children's learning behavior due to aircraft noise were investigated using epidemiological data from 2000-2007 [7]. Effects on health, especially in the vicinity of airports, were investigated by Franssen et al. at Schiphol Airport in the Netherlands [8]. Here, an increase in the number of prescriptions for sleep, cardiovascular, and high blood pressure medication was observed. It should be noted that these effects were not linked to noise exposure during the night, but to noise exposure in the late afternoon. The International Civil Aviation Organization (ICAO), the UN's governing body for international civil aviation has for this reason set the goal for its member countries to reduce the adverse effects and protect the population, especially vulnerable groups like children, chronically ill, and the elderly from aircraft noise. One of the goals of the ICAO is to limit or reduce the number of people affected by significant aircraft noise [9]. To reduce the number of people affected by noise through aircraft traffic around airports the noise generation and propagation models must be accurate. There are various approaches to modeling the complex meteorological relationships in the atmosphere and how they influence sound propagation. Various technologies such as numerical simulations or empirical methods can be used for this purpose. The relevant physical effects are described in more detail in chapter 3. In general, we have to distinguish between emission and immission modeling. Yunus et al. [10] developed an atmospheric propagation model using ray acoustics while considering vertical wind velocity and air temperature profiles. The noise emission of the aircraft is modeled by sampling noise sources in a hemisphere around the aircraft and then propagating the noise on the ground. They conclude that refractive sound shadow zones appear under the right conditions, i.e. when the direction of sound propagation is opposed to the wind direction. It is concluded that the weather has a significant and hearable difference in the sound pressure level. **Isermann et al. [1]** provide a general introduction to the modeling of aircraft emissions. They describe different possibilities of source modeling of best-practice models such as Noise-power-distance (NPD) based models or models that explicitly model the source in its entirety. Scientific models are presented, with the difference that they model the source as the sum of its components. This makes it possible to perform more accurate calculations, as not all components are equally relevant along the trajectory. Different models are suitable depending on the context. Isermann et al. [1] identify various objectives:

a) Support of land use planning and noise legislation;

b) Modeling of noise mitigation measures;

c) Development of noise abatement flight procedures;

d) Modeling of noise reduction at the source;

e) Low-noise aircraft design.

Engine noise and airframe are identified as the two contributors to aircraft noise. In more advanced scientific models these are modeled in detail, however, the necessary data is generally only available to large institutions like NASA or DLR or main manufacturers like Boeing or Airbus [1]. **Johansson et al [11]** employ a data-driven approach to analyze A321 neo fly-over noise measurements not far away from the runway. Various linear methods like Analysis of Variance (ANOVA) [12] or hierarchical regression [13] are used to investigate the influence of specific meteorological parameters on the measured sound pressure level variance. The authors determine a significant dependence of noise immissions on the distance to the microphone (60 % of the variation of the noise data) aircraft speed and the configuration (together 20 %), while meteorological parameters have a relatively smaller impact (around 2-5 %). They note that temperature and relative humidity mainly contribute to the variation of the noise data while the wind is negligible. Johansson et al. [11] compare aircraft configurations with each other to calculate the influence of individual parameters such as distance or pitch on the emitted noise. **Zellmann et al. [14]** present a middle way between highly simplified and highly complex parameterized models for the calculation of aircraft noise. Modeling the source in its entirety is often not possible due to missing data or parameters and one has to ask oneself which parameters are relevant or how to replace missing data from measurement data. They work with a data set of flight tracks, sound pressure level measurements which contain similar parameters as the data set in this work, and meteorological profiles to calculate the emitted noise and the flight parameters. The Parametric Aircraft Noise Analysis Module (PANAM) is a program to predict noise immission on the ground for a homogeneous atmosphere and different types of aircraft **Bertsch** [15]. An extension for PANAM is presented to assess the uncertainty of noise simulations **Bertsch et al. [16]**. Noise emissions are predicted based on information about the aircraft engines and the airframe, the configuration and position of the aircraft, and the position of the receiver on the ground relative to the aircraft. To project the emissions to immissions, effects that occur during sound propagation in the atmosphere are also taken into account. In a recent paper, **Römer et al. [17]** combine uncertainty of the parametric input and uncertainty from the simplification of the noise calculation in an uncertainty quantification study. They use a component-based method for noise calculation in a time-stepping procedure and extend the PANAM [18] model. Especially in multi-parameter simulations, they emphasize the need to pay attention to the uncertainty of input parameters. Whenever results from simulation are compared with measured values, uncertainty quantification is crucial. Several models already exist for modeling aircraft noise immissions [1][15]. However, these models don't take atmospheric effects such as sound refraction or atmospheric absorption into account sufficiently, but these effects do play a role in outdoor sound propagation. We consider vertical weather profiles of these parameters and investigate the extent to which these measurements, which are not carried out directly at the airport, can be used there.

# 3. Fundamentals of Outdoor Sound Propagation

## 3.1. Vertical profiles and daily evolution of meteorological parameters

The atmosphere's primary properties are its pressure, density, temperature, composition, and motion of the molecules [4]. These properties vary greatly depending on where you are in the atmosphere, which is around 40 km high. At ground level, the temperature tends to decrease with altitude, both in summer and in winter. The first layer in the atmosphere is called the troposphere and extends between 8-16km upwards [4]. Density and pressure decrease with altitude due to gravity. Horizontal gradients generally disappear because gravity sorts the layers in the atmosphere accordingly. The atmosphere establishes the hydrostatic equilibrium [4]. The part of the troposphere closest to the ground is called the atmospheric boundary layer (ABL). Depending on the location, time of day, and season, the temperature can also rise with altitude. This situation is called an inversion. Especially for take-offs and landings of airplanes, it is crucial to pay attention to the weather conditions in the atmospheric boundary layer, as temperature, wind, humidity, and pressure have different effects on the lift of the flights [19]. From a certain altitude, the decrease in temperature stops. This layer of the atmosphere is called the tropopause. The stratosphere begins above the tropopause. This extends up to an altitude of 50 km and is characterized by a temperature inversion. In figure (3.1), one can see from an atmospheric pressure of around 50 hPa, i.e. an altitude of around 20 km, that the temperature increases with increasing altitude. There are also the mesosphere and the thermosphere at much greater heights. Aircraft during approach or departure move inside the ABL which is the layer we focus on.

At sea level, the average atmospheric pressure is 1 atm or approx. 1013.25 hPa. The air pressure as a logarithmic scale then decreases linearly with altitude. Figure (3.1) shows the temperature curve depending on altitude and air pressure. The data for figure (3.1) and figure (3.2) is published on the website of the University of Wyoming [1]. The data used here is from station 10868.

The troposphere consists of the boundary layer, which is of particular interest to us because it is the part of the atmosphere where starts and landings of aircraft take place, up to a height of approx. 1 km and the free atmosphere. The boundary layer is defined as the part of the tropopause that is directly influenced by the presence of the Earth's surface, Stull [20]. In the boundary layer, turbulence occurs as transport processes, triggered by the heat of solar

[1] https://weather.uwyo.edu/upperair/sounding.html

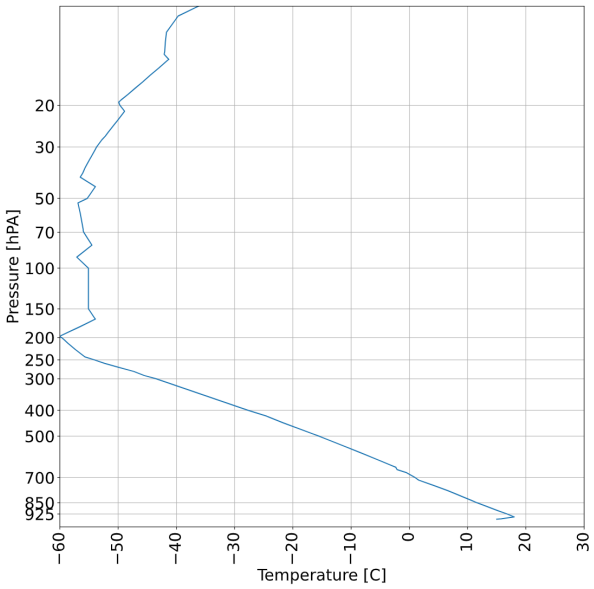


Figure 3.1.: Temperature measurements from the ascent of a weather balloon with radiosonde in Oberschleissheim near Munich on June 01, 2023 published by the University of Wyoming. The height is given by the measured pressure value in hPa. The measurements start at ground level and go up to a height of around 33km.

radiation on the Earth's surface. The boundary is structured into three components: the mixed layer, the residual layer, and the stable boundary layer. The composition of these three layers changes over a day. About 30 minutes after sunrise, the turbulent mixed layer begins to form. The warm air heated by sunlight on the ground rises. The resulting turbulence tends to distribute the temperature and relative humidity evenly throughout the layer. Towards the afternoon, the mixed layer reaches its maximum expansion [20]. About half an hour before sunset, the thermals stop forming due to a lack of cold air advection. The name residual layer comes from the fact that the average initial value of the state and concentration variables is the same as that of the mixed layer. Variables such as the potential temperature usually decrease slowly at night. The lower part of the residual layer slowly transforms into the stable boundary layer during the night through contact with the ground. This zone is characterized by calm winds at night.

## 3.2. Acoustics

Sound waves in the atmosphere consist of pressure oscillations where particles move in a longitudinal direction [4]. The frequency [Hz] (f) and the sound pressure amplitude [Pa] ($\hat{p}$) characterize a sound wave. For humans, frequencies between 20 Hz and 20 kHz are normally hearable [21]. The sound pressure level is a logarithmic scale that refers to the sound pressure

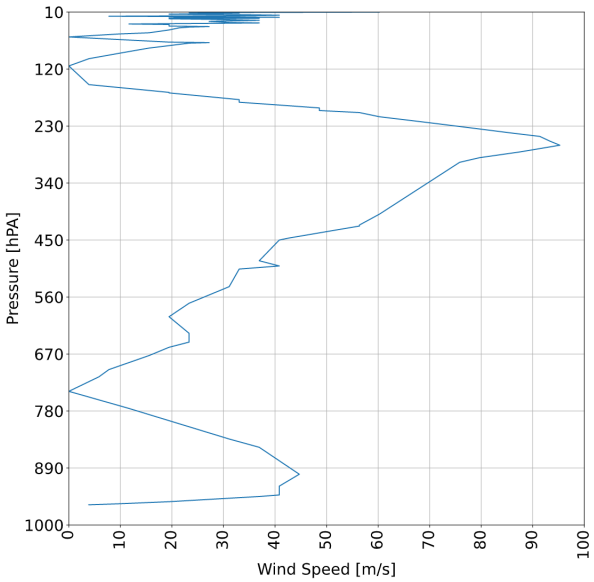


Figure 3.2.: Wind speed measurements from the ascent of a weather balloon with radiosonde in Oberschleissheim near Munich on June 01, 2023 published by the University of Wyoming. The height is given by the measured pressure value in hPa. The measurements start at ground level and go up to a height of around 33km.

amplitude

$$SPL = 10lg\left(\frac{\hat{p}^2}{p_0^2}\right) dB \tag{3.1}$$

where $p_0^2 = 2 \cdot 10^{-5} Pa$ is the reference pressure amplitude at the threshold of hearing. From this equation, it follows that the doubling of sound sources, e.g. from one to two leads to an increase in sound pressure level of approximately 3 dB [4]. People do not perceive all frequencies equally well, or are not disturbed by all frequencies to the same extent. For this reason, the sound pressure level is weighted according to certain frequencies. The often used 'A-weighting' takes frequencies between 1kHz and 6kHz more into account.
For dry air where we do not consider the effect of humidity on sound propagation the sound speed $c$ is defined as:

$$c = \sqrt{\kappa R_d T}, \tag{3.2}$$

where $\kappa = \frac{c_p}{c_v}$ with $c_p = 1005 J/(kgK)$ and $c_v = 718 J/(kgK)$ is the ratio of the specific heat capacities of dry air at constant pressure and constant volume, and $R_d = 287 J/(kgK)$ the gas constant of dry air [22].
The speed of sound for 0°C and 1013 hPa is

$$c_0 = 331.5 m/s \tag{3.3}$$

For 20°C, the speed of sound is

$$c_0 = 342 m/s. \tag{3.4}$$

The speed of sound is dependent on the temperature [$°C$] (T).

If we do not consider a homogeneous atmosphere but only a horizontally homogeneous atmosphere vertical refraction of the sound waves occurs and needs to be accounted for. A vertical effective sound speed gradient $\partial c_{eff}/\partial z$ leads to sound refraction. The effective sound speed can be computed by adding the sound speed in calm air $c$ and the horizontal wind component in the direction of the sound propagation:

$$c_{eff} = c_{air} + Vcos(\alpha), \tag{3.5}$$

where **V** is the horizontal wind speed, $\alpha$ is the angle between the direction of the wind vector and the direction of sound propagation and $z$ is the height of ground in meters [22].

## 3.3. Noise equations

In practice, the noise or sound pressure level [dB] (SPL) is measured as a time series over a time t. The function L(t) is defined by the maximum level $L_{max}$ and the duration $t$ of the noise. For aircraft noise, the maximum A-weighted sound pressure level of the aircraft with the "SLOW" rating (immission at a certain observer) [dBA] ($L_{AS,max}$) is used [1]. Iserman et al. [1] describe the A-weighted single event sound level [dB] ($L_E$) as

$$L_E = 10 \times log\left(\frac{1}{t_0} \times \int_{t_1}^{t_2} 10^{L(t)/10} dt\right) = L_{max} + 10 \times lg\left(\frac{t_{eff}}{t_0}\right) \tag{3.6}$$

for a normalizing time $t_0$ of 1 second and the effective duration $t_{eff}$ which is defined as follows

$$\int_{t_1}^{t_2} 10^{L(t)/10} dt = t_{eff} \times 10^{L_{max}/10}. \tag{3.7}$$

Long-term effects of noise are generally defined by the equivalent continuous sound level, [dBA] ($L_{eq}$), which is determined from a series of $N$ noise events $L_{E,i}$ over a characterization time $T_C$ and a normalization time $t_0$ [1],

$$L_{eq} = 10 \times log\left(\frac{t_0}{T_c} \times \sum_{i=1}^{N} 10^{L_{E,i}/10}\right). \tag{3.8}$$

Since decibels are a logarithmic scale, the energetic mean value formation as in equation (3.8) can be misleading for the actual noise situation. A single very loud noise event can greatly increase the average value over a long period, even if the exposure is only very brief. In addition, individual very loud events are particularly disturbing but are averaged out over a series of events. A specific single-event sound level can be the result of a short noise with a high maximum level or a long noise event with a lower maximum level [1]. The human perception of loud and quiet results from the magnitude. Therefore, in this work $L_{AS,max}$ is used as the metric of loudness.

To calculate the mean value over several noise events, it is important to adapt to the logarithmic decibel scale. According to Taraldsen et al. [23], let $L_i$ be a series of observed

sound pressure levels. We calculate values $P_i = P_0 10^{L_i/10}$ with $P_0$ as reference value. $\overline{P}$ is calculated as mean of values $P_i$ with $\overline{P} = (P_1 + ... + P_n)/n$, with $n$ being the number of noise events. Then $\overline{P}$ is converted back to the decibel scale with

$$L_{\overline{P}} = 10log\left(\frac{\overline{P}}{P_0}\right). \tag{3.9}$$

$L_{\overline{P}}$ refers to the mean of the sound pressure level $L$ over a series of noise events $L_i$, [dBA] ($L_{\overline{P}}$).

## 3.4. Effects on sound pressure level

Depending on the type of source or the state of the atmosphere, the propagation of the sound wave is influenced in many ways [4]. Sound can be refracted, reflected, or absorbed. These effects usually depend on the air temperature, the relative humidity, the frequency spectrum of the sound wave, or the relative impedance of the ground.

**Geometrical spreading** The shape of the source and the number of dimensions we consider determine the shape of the wavefront with which the sound propagates. If we assume a point source the sound intensity then decreases in proportion to $1/d^2$, where d is the distance to the source because of spherical spread proportions. Doubling the distance would reduce the SPL by 6dB. If it were a line source, the SPL would decrease by approximately 3 dB when the distance is doubled because of cylindrical spread proportions. The SPL then decreases with the ratio 1/d frequency independent [4].

**Air absorption** In addition to the decrease in sound energy due to geometric propagation, part of the energy is released as thermal energy due to the friction of the particle weave about the sound wave. This attenuation depends on the temperature, the relative humidity, and the frequency of the sound wave. Very high frequencies in particular are strongly attenuated, while low frequencies are affected less. Figure (3.9) shows the attenuation due to the atmosphere in dB per 100m for different frequencies as a function of relative humidity and temperature. This attenuation accounts for part of the difference between emitted SPL at the source and measured SPL at the receiver. The attenuation through absorption $A_a$ can be calculated with

$$A_a = -20log_{10}\left[\frac{P(r)}{P(0)}\right] = -20log_{10}[exp(-\alpha r)] = \text{ar dB} \tag{3.10}$$

where P(r) is the sound pressure after traveling the distance $r$ and $a$ is the attenuation coefficient in dB per meter. The absorption of sound in still air in Nepers per meter can be calculated with the equation from Bass et al. [24],

$$\begin{aligned}\alpha = f^2\Big[1.84\times10^{-11}\left(\frac{p_s}{p_{s0}}\right)^{-1}\left(\frac{T}{T_0}\right)^{\frac{1}{2}} + \left(\frac{T}{T_0}\right)^{\frac{5}{2}} \times \{1.278\times10^{-2}[exp(-2239.1/T)]/ \\ [f_{r,O} + (f^2/f_{r,O})] + 1.068\times10^{-1}\times[exp(-3352/T)]/[f_{r,N} + (f^2/f_{r,N})]\}\Big],\end{aligned} \tag{3.11}$$

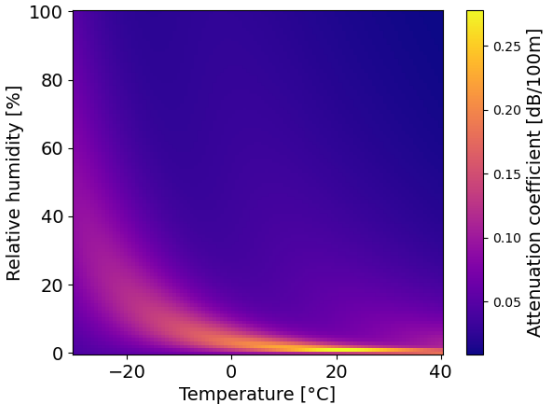


Figure 3.3.: Attenuation for f = 50 Hz

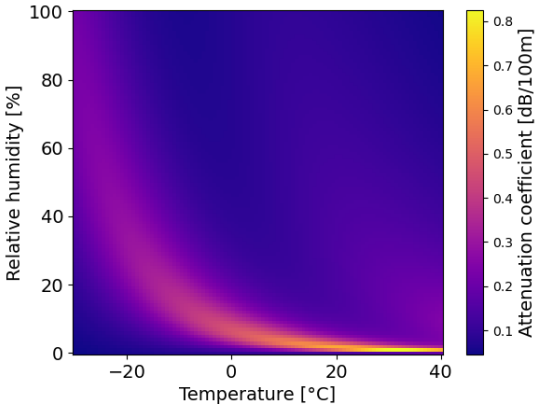


Figure 3.4.: Attenuation for f = 250 Hz

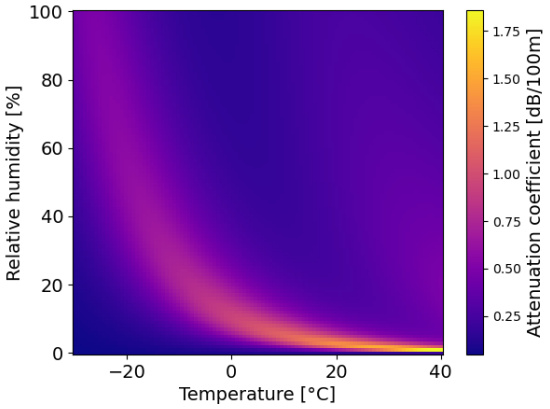


Figure 3.5.: Attenuation for f = 500 Hz

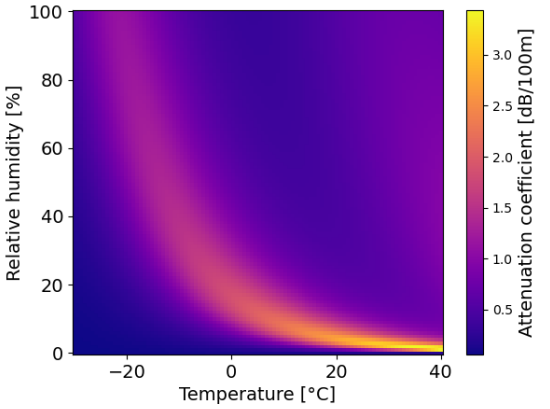


Figure 3.6.: Attenuation for f = 1000 Hz

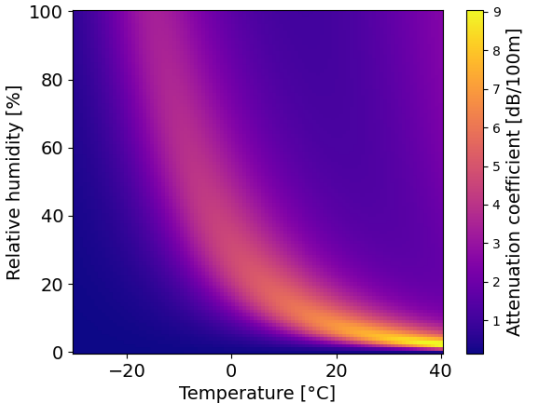


Figure 3.7.: Attenuation for f = 2500 Hz

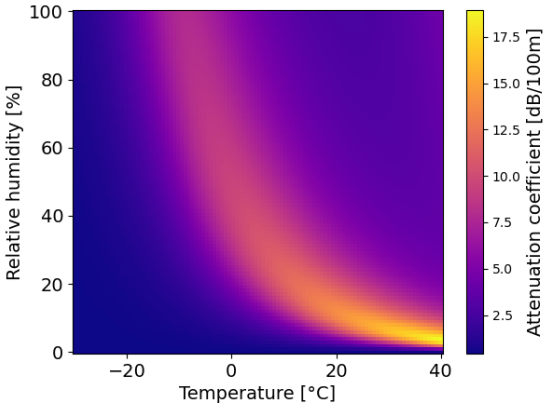


Figure 3.8.: Attenuation for f = 5000 Hz

Figure 3.9.: Attenuation coefficient of atmospheric absorption as a function of temperature and relative humidity for a series of different frequencies

where $f$ is the acoustic frequency in Hz, $p_s$ is the atmospheric pressure, $p_{s0}$ is the reference atmospheric pressure (1 atm), $T$ is the atmospheric temperature in Kelvin, $T_0$ is the reference atmospheric temperature in Kelvin (293.15 K), $f_{r,O}$ is the relaxation frequency of molecular oxygen and $f_{r,N}$ is the relaxation frequency of molecular nitrogen. Neper is a unit of logarithmic scale like the decibel scale where 1NP = 20log$_e$e dB. It is based on Euler's number [25] where the level ratio $L$ is defined as,

$$\begin{aligned} L &= 10log_{10}\frac{x_1^2}{x_2^2}dB \\ &= 20log_{10}\frac{x_1}{x_2}dB \\ &= ln\frac{x_1}{x_2}Np \end{aligned} \tag{3.12}$$

**Sound refraction** Sound refraction occurs when there are temperature gradients or gradients of the wind speed $U$ in the atmosphere and thus gradients of the sound speed $c$ [4]. Then the sound does not propagate straight ahead but the sound rays are curved in the direction of the lower temperature or wind speed $U$. Heimann, Schady, and Feng [4] note that the curvature of the sound rays is proportional to the velocity gradients in the atmosphere. Furthermore, sound refraction mostly occurs in the atmospheric boundary layer near the ground. For elevated sources like airplanes, the effect only occurs for farther away sources. Upward refraction typically occurs during the day when the ground is relatively warmer than the cold air, thus creating sound shadow zones at the ground where residents live. Downward refraction typically occurs during the night in the case of a temperature inversion in the atmosphere. Then the sound is refracted towards the colder ground.

**Sound diffraction** Sound diffraction typically occurs around convex surfaces where a part of the sound wave is diffracted into the protected space, i.e. around a noise barrier into the direction of the houses behind the barrier [4]. This is mainly relevant to the noise emitted by cars on highways or trains. For aircraft noise, this effect is of minor concern.

**Sound reflection** Sound is reflected on the ground or off the surface of a building or any obstacle. The reflection mainly depends on the angle of incidence and the impedance of the reflecting surface relative to the impedance of the air ($Z = \rho c$) with $\rho$ being the density of the air [4]. Media such as concrete have a high impedance and thus reflect a lot of sound energy, while media such as grass have a low impedance and reflect less sound. Sound reflection is mainly relevant for near-ground to near-ground sound propagation.

# 4. Measurements and Data

Sound propagation in the atmosphere is a complex topic that depends on many parameters and thus many different types of data need to be utilized to draw conclusions about dependencies. The theory of outdoor sound propagation is discussed in chapter (3). This chapter aims to define the data and measurements related to the source (aircraft) and the receiver of sound (microphone on the ground). The data set is extended by measurements from the weather mast of the University of Hamburg. Vertical profiles of temperature, wind direction, wind speed, and relative humidity measurements at different heights will complement the weather data.

## 4.1. Position data

At the time where the maximum sound pressure level $L_{AS,max}$ is measured ($T_{Las,max}$), the airport's data management system notes the position of the aircraft in latitude and longitude, the speed in knots, the altitude in ft, the elevation angle between NMT and aircraft, the current heading of the aircraft in degrees and multiple IDs to identify and match the data. This information is provided by the Automatic Dependent Surveillance-Broadcast system (ADS-B), which determines its position via satellite navigation and passes it on to air traffic control [26].

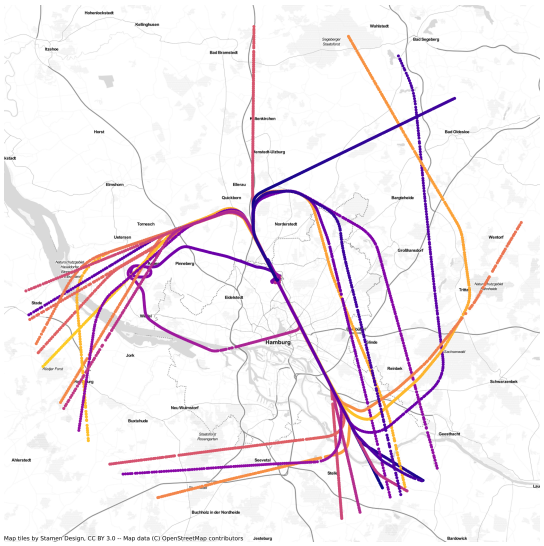


Figure 4.1.: Flight tracks around Hamburg airport from 2023-06-15 from 09:30 - 10:30. The dark blue lines are the earlier flights while the yellow flight tracks are later flights.

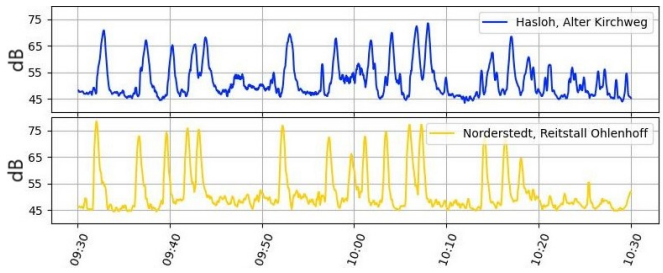


Figure 4.2.: Consecutive noise measurements at NMTs 01 and 11. Starting planes on runway 33 first pass NMT 11 Norderstedt, Reitstall Ohlenhoff, and a few minutes later NMT 01 Hasloh, Alter Kirchweg. We note the overall lower sound pressure level of the blue plot since aircraft are higher in the air at the point of measurement at this NMT.

In figure (4.1) we see that airliner operations always follow standard Standard Instrument Arrival (STAR) routes. Noise measurements at the same NMT are comparable because the aircraft follow fixed tracks in the vicinity of the airport.

To be able to use the GPS coordinates for evaluation, they are processed in a geodata frame from the Geopandas library in Python. The Coordinate Reference System (CRS) of the data frame is set to the World Geodetic System 84 (EPSG:4326) initially since the source of the data is saved in this CRS. Then we project the data to the EPSG 3857 coordinate system to use the coordinates with OpenStreetMap tiles and create maps with the data.

## 4.2. Noise Monitoring Terminals

There are fifteen so-called Noise Monitoring Terminals (NMTs) in the vicinity of the airport of Hamburg. These continuously measure the sound pressure levels in decibels. The microphones are usually located 6-10 meters above the ground as recommended by DIN 45643 [27]. Sometimes they are located on top of a long mast, sometimes on top of single-family homes and some are on the roof of larger public buildings like schools. The NMTs are located under or near the flight path of airplanes approaching or departing from Hamburg Airport. Typically the distance in three dimensions between passing aircraft and the NMTs ranges from a few hundred meters to a few kilometers depending on where the NMT is located. The closer the aircraft is to the airport the closer they are to the ground and thus closer to the NMT.

| NMT | wind-speed [m/s] | -direction [°] | T [°C] | air pressure [mBar] | relative humidity [%] | m over ground |
|---|---|---|---|---|---|---|
| 02 | x | x | | | | ∼ 9 |
| 03 | x | x | | | | ∼ 9 |
| 06 | x | x | x | | | ∼ 2 |
| 13 | | x | x | x | x | ∼ 3 |
| 14 | x | x | x | x | x | ∼ 3 |

Table 4.2.: Overview of the weather stations

| NMT number | Weather from | Name | (Lat ° N, Long ° E) |
|---|---|---|---|
| 01 | 03 | Hasloh, Alter Kirchweg | (53.698194, 9.926267) |
| 02 | 02 | Harkshörn, Grundschule | (53.733783, 9.998408) |
| 03 | 03 | Quickborn, Goethe-Schule | (53.723772, 9.914022) |
| 04 | METAR | Norderstedt, Altes Rathaus | (53.680611, 9.976847 ) |
| 05 | METAR | Langenhorn, Kohrswort | (53.641469, 10.006639) |
| 06 | 06 | Lufthansa Werft | (53.623753, 9.985658) |
| 07 | 06 | Langenhorn, Kortenkamp | (53.649556, 10.026608) |
| 08 | 06 | Niendorf, Empfängerstation | (53.634486, 9.981875) |
| 09 | 03 | Quickborn, Droysenkehre | (53.742253, 9.957981) |
| 10 | METAR | Stellingen, Wasserwerk | (53.604647, 9.936033) |
| 11 | 06 | Norderstedt, Reitstall Ohlenhoff | (53.674994 , 9.9636) |
| 12 | METAR | Groß Borstel, Seniorenwohnheim | (53.615267, 9.972339) |
| 13 | 13 | Poppenbüttel, Kiwittredder | (53.6656, 10.059489) |
| 14 | 14 | Lurup | (53.595349, 9.894492) |
| C02 | METAR | Mobile Meßstelle 2 | (53.744033, 10.214648) |

Table 4.1.: There are fifteen Noise Monitoring Terminals (NMTs) in the area around the airport of Hamburg. The table shows the number and name of the NMT that are used to identify the different stations. Some stations measure weather (wind speed, direction, and temperature), while others use values from nearby NMTs. Some NMTs get their value from the airport's METAR reports. The exact position is noted in latitude and longitude [28].

Complete list of all fifteen NMTs around the airport of Hamburg and nearby villages. The position of each NMT is given by coordinates in the EPSG:4326 coordinate reference system (CRS). These coordinates will be used to calculate the distance on the ground between the aircraft and the microphones. The noise measurements at NMT 06 Lufthansa Werft from the specified period are not used for this work but we will use the weather measurements from this NMT for NMT 11. The corresponding weather station is noted for each NMT. Some NMTs with no weather station nearby get their weather information from the METAR which

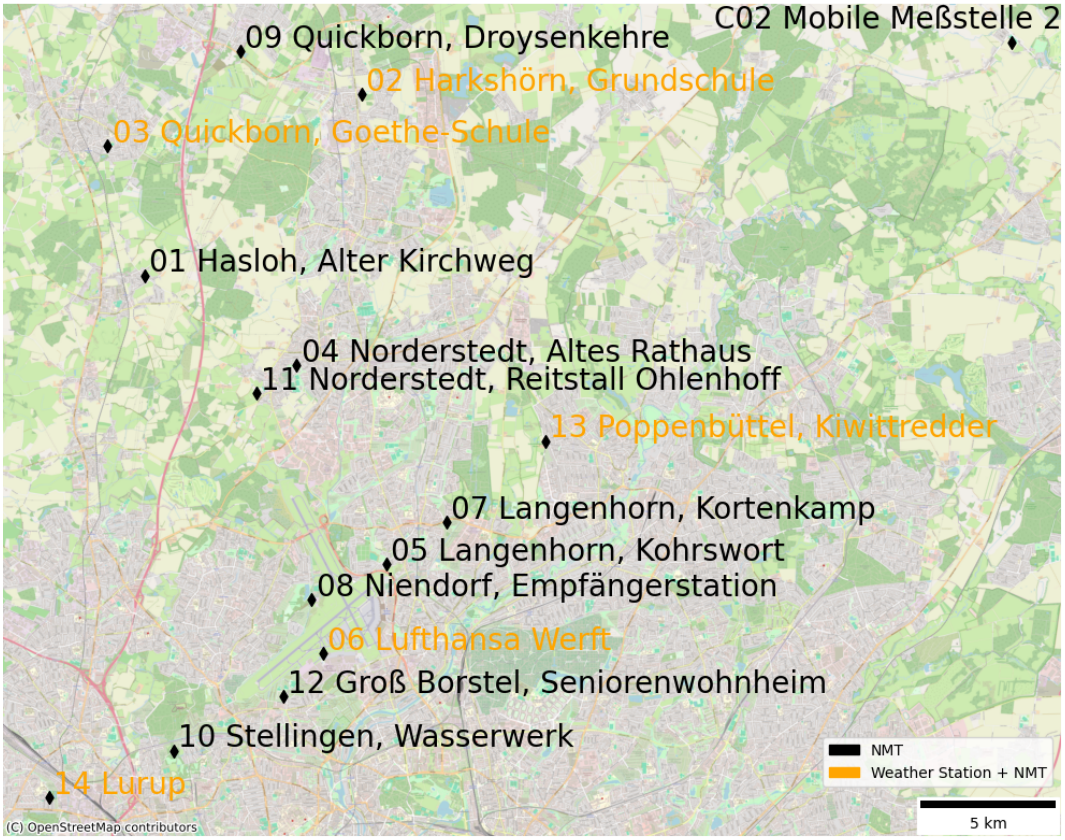


Figure 4.3.: The plot shows all fifteen NMTs in the area of the airport of Hamburg. When we compare the position of the NMTs with the plot of the flight tracks (fig 4.1) we see that the NMTs are located along the main start and landing routes.

is provided by the "Deutscher Wetterdienst (DWD)" every 20 minutes [28]. All of the NMTs measure the sound pressure level. Only four of the fifteen NMTs have the technical capability to measure weather data. NMT 02 and NMT 03 can also measure wind direction and wind speed while NMT 06 also measures the temperature. Furthermore, NMTs 13 and 14 measure air pressure and relative humidity. The wind speed measurement is not available due to erroneous data.
When a sound event is registered at one of the NMTs without a weather station the system automatically fills in the weather variables from the corresponding weather station according to table (4.1).

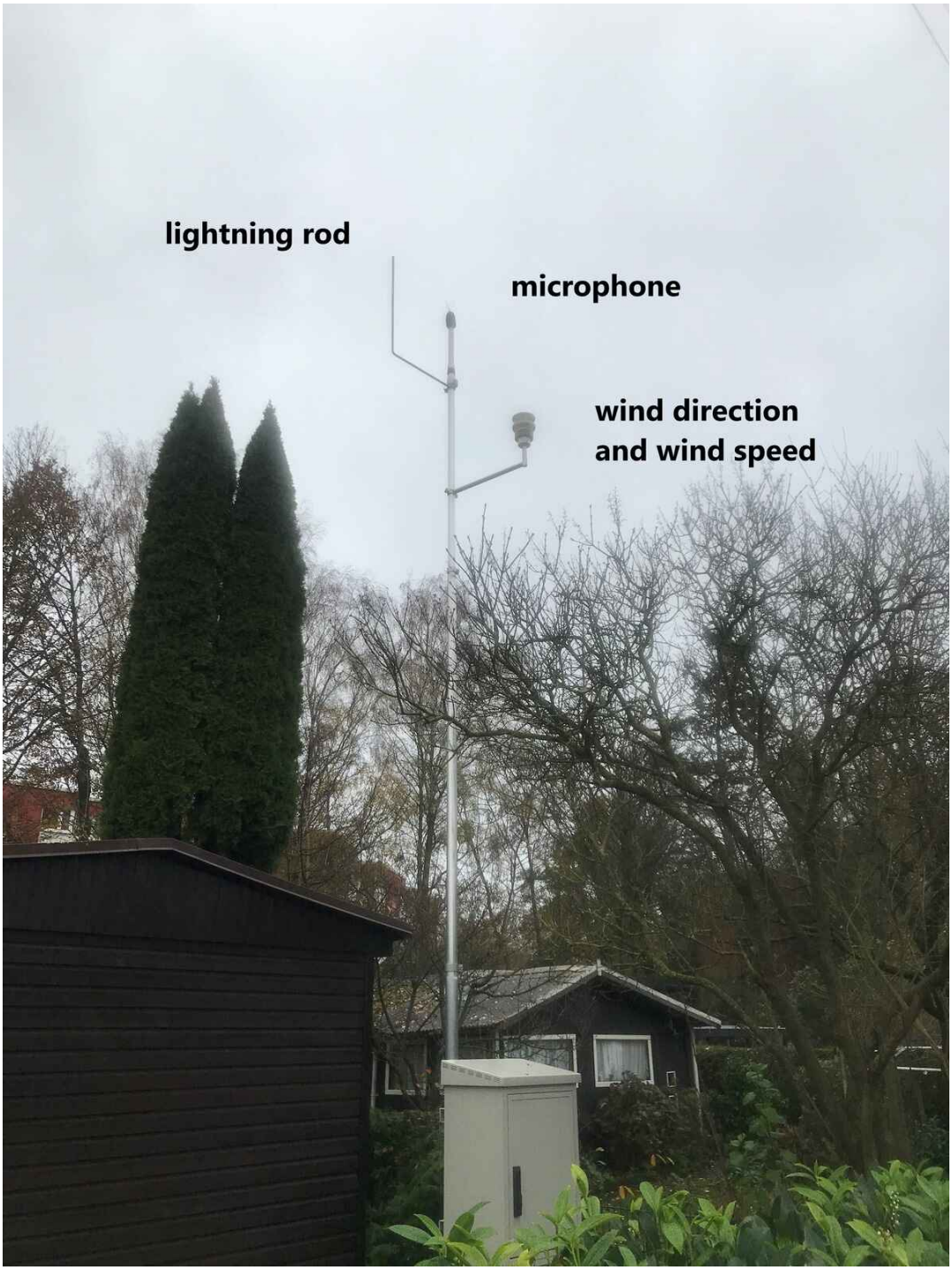


Figure 4.4.: Outside view of the technical structure of a Noise Monitoring Terminal (NMT). The photo shows NMT 14 Lurup. An NMT consists of a long mast that carries a lightning rod to protect the NMT, a microphone to measure the sound level, and instruments to measure the wind direction and wind speed. Not all of the NTMs consist of wind measuring equipment. These NMTs receive the wind data from nearby NMTs or METAR reports from the airport.


Figure 4.5.: Inside view of the Noise Monitoring Terminal (NMT). Hamburg airport employs the TANOS management system from the company Topsonic. The photo shows the technical equipment in figure (4.4). The equipment is used to save and transfer the data to the central data management system of the airport. It consists of a router, sound level meter, fuses, and a battery in case the electricity goes out.

The microphones inside the NMT measure the sound pressure level as a time series for every second. From this we can compute the equivalent continuous sound pressure level *Leq* which is an important metric to determine how much residents are affected by noise over a long period of time. Acoustics is a field of physics where human perception is a crucial factor. Multiple small planes starting over a long period could have the same total sound energy as a single loud noise event like the start of a large Boeing 747. For some residents, the latter event is much more noticeable while for others a series of small planes might disturb their living conditions more. The airport's TANOS system continuously measures the sound pressure level and attempts to detect individual noise events such as aircraft overflights.
The noise event detection process works as follows: A threshold value is defined for each measuring point based on local conditions such as trees or proximity to the aircraft. If the level exceeds the threshold value, a noise event is registered. The system then automatically saves all relevant data. The time series of the sound pressure level is recorded, as is the maximum sound pressure level. Using the data from the ADS-B, the position of the aircraft at the time of the measurement is determined and given an ID so that all the data can be combined. In

addition, the weather data of the NMT is stored, as well as additional information about the flight, such as the aircraft type, the route, the airline, which approach or departure route was used, whether it was a take-off or a landing, and some other information. With the ID of the measurement and the time stamp, the time series of the sound pressure level and the calculated values such as $LAS_{max}$ and $Leq$ can be combined with weather data and analyzed. This allows us to measure the influence of weather data on measured noise data. We can also combine data from the airport with third-party data.

It is not only the atmosphere as a medium, or the source and receiver of the noise, that affects sound propagation outdoors. Local topographical conditions also influence sound propagation. At many measuring points, the angle of incidence of aircraft noise, which would be the angle we have to tilt our head up if we look at an aircraft from the ground, is high. However, especially near airports, the noise can come from an almost horizontal direction, see figure (4.7). Properties of the ground or the surrounding area, such as woodland or buildings, have a greater influence when the angle incidence is low. Scientific works like Defrance et al. [29] examine in detail the dependence of topographical conditions on sound propagation outdoors. Topographical factors are not differentiated here. In addition, the type of source (point source, line source, or other) has an influence. Chapter (2) shows other works regarding the noise emissions of aircraft. With our data, we focus on noise immissions and how they relate to the weather.

## 4.3. Noise data

The data used in this study includes noise measurements from August 2022 to August 2023. In total, there were 115,796 unique flights in this period. Each of them includes 1-10 noise measurements at measuring stations. On average an airplane flies over 3.6 stations with a standard deviation of 1.3 stations. Overall there are 414,205 single noise events. The noise level is recorded as a continuous time series by the NMTs. The time series for one such NMT can be seen in figure (4.6).

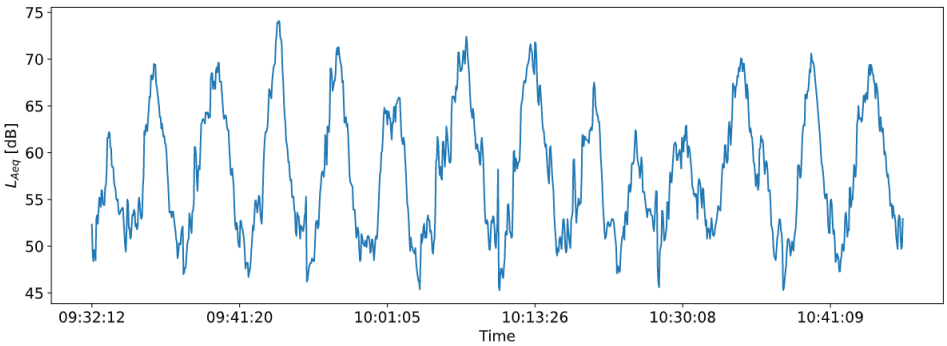


Figure 4.6.: Noise event level for NMT 01 Hasloh, Alter Kirchweg for 15th June 2023 from 09:32 to 11:49. The peaks represent a series of noise events from overflights while the background noise level is around 53 dB.

First, we need to define what a noise event is. For this work we want to detect an airplane that flies over the NMT and in the process creates a peak in the sound pressure level measurements. As seen in figure (4.6) there might be an intermediate peak when the aircraft approaches the NMT and another peak as the aircraft flies further away from the NMT. At each time step, we have an A-weighted noise level $L_A$ which peaks at some point, usually very close to the NMT. $L$ is usually measured with a time weighting "SLOW", $L_{AS}$ [1]. The "SLOW" rating reacts more slowly to impulsive noise. The measurement threshold for detecting an overflight must be at least 5 dB above the background noise level. This is determined individually for each measuring point. The closer an airplane gets to the NMT, the louder the noise becomes. The level must exceed the measurement threshold by the maximum level threshold. A noise event is generated when the measurement threshold is exceeded by the maximum level threshold and a minimum time is exceeded. A noise event has ended when the level does not exceed the threshold again within the listening time after falling below the measurement threshold. Both the minimum time and the listening time are set individually on each NMT. Normally these are 5 seconds [30]. The peak of the "A-weighted" "SLOW"-weighted sound pressure level is called $L_{AS,max}$. For further chapters in this work, the $L_{AS,max}$ value is used for evaluations, unless otherwise specified.

## 4.4. Weather data

Multiple weather data sources are used in this work. On the one hand we use the weather measurements from the NMTs as shown in figure (4.2). On the other hand, weather measurements from the Hamburg Weather Mast are used [31].

| height m | wind speed [m/s] | wind direction [°] | temperature [°C] | relative humidity [%] |
|---|---|---|---|---|
| 2 | | | x | x |
| 10 | x | x | x | x |
| 50 | x | x | x | x |
| 70 | | | x | x |
| 110 | x | x | x | x |
| 175 | | | x | x |
| 250 | x | x | x | x |
| 280 | x | x | x | x |

Table 4.3.: Measurements from the Hamburg Weather Mast that are used in this work

The measurements from the Hamburg weather mast include wind speed and direction, as well as temperature and relative humidity at various heights between 2m and 280m above the ground. These supplement the weather data set with important weather profiles. This makes it possible, for example, to include vertical gradients in the analysis, e.g. the vertical

temperature gradient, which is crucial for sound refraction, see chapter (3).

The temperature gradients and wind gradients are calculated from the data measured at the Hamburg Weathermast. The gradients are calculated for the heights $[10m, 70m, 110m, 175m]$ as follows:

$$\Delta T_{10m} = \frac{T_{70m} - T_{2m}}{70m - 2m} \qquad \Delta T_{70m} = \frac{T_{110m} - T_{10m}}{110m - 10m}$$
$$\Delta T_{110m} = \frac{T_{175m} - T_{70m}}{175m - 70m} \qquad \Delta T_{175m} = \frac{T_{280m} - T_{110m}}{280m - 110m}$$

where $T_y$ is the temperature in height $y$. The wind speed gradients for the heights $[50m, 110m, 175m]$ are calculated in the same fashion:

$$\Delta WS_{50m} = \frac{WS_{110m} - WS_{10m}}{110m - 10m} \qquad \Delta WS_{110m} = \frac{WS_{175m} - WS_{70m}}{175m - 70m}$$
$$\Delta WS_{175m} = \frac{WS_{280m} - WS_{110m}}{280m - 110m}$$

where $WS_y$ is the wind speed in height $y$.

As with the noise measurements, the data originates from the period 01.08.2022 to 31.08.2023. These are 10-minute averages. The time difference between the 10-minute intervals results from the final value minus the initial value divided by the reduced number of measured values in the file because Windows adds an empty row at the end.

$$\Delta t = \frac{t_2 - t_1}{n - 1} \tag{4.1}$$

The start time of the 10-minute averaging interval is indicated in the file name. The interval for noon therefore contains the values for 12:00 to 12:09. The measurements for the noon 10-minute average therefore originate from measurements between 11:59 and 12:09 [31]. The data from the Hamburg Weather Mast are used in addition to the weather measurements from Hamburg Airport throughout the paper, in particular as comparative values and when height profiles of weather parameters are used. One question that arises is to compare the extent to which the very precise and extensive measurements of the weather mast, which is located approx. 13.7 km from Hamburg Airport, can be used for weather-related issues at the airport, e.g. concerning aircraft noise.

Figure 4.7.: NMT 05
Langenhorn, Kohrswort

Figure 4.8.: NMT 07
Langenhorn, Kortenkamp

Figure 4.9.: NMT 11
Norderstedt, Reitstall Ohlenhoff

Figure 4.10.: NMT 12
Poppenbüttel, Kiwittredder

# 5. Statistical Methods

We try to understand the effects of atmospheric and non-atmospheric parameters on the propagation of noise at this specific location. The target variable will therefore be the maximum loudness of a noise event called $L_{AS,max}$. Other important noise parameters like the Equivalent Continuous Sound Level $L_{eq}$ or the A-weighted sound exposure level (immission at certain observer), [dBA] ($L_{AE}$) could be used as target variables. The maximum loudness was chosen since this variable describes better the magnitude of the noise event that residents around the airport hear compared to integrated quantities like $L_{eq}$ or $L_{AE}$. These variables are also heavily correlated as shown in chapter 5.3.

Intuitively, from the literature we have some idea about which parameters affect the target variable and to what extent. However, the goal is to quantify the importance of parameters as accurately as possible within the range of error of the measured data. Even if all data was measured perfectly there would still be factors that we couldn't include in the data set due to availability of the data or safety regulations like the configuration of the airplanes during start or landing like thrust settings or whether or not the landing gear is deployed.

## 5.1. Principal Component Analysis (PCA)

We start with the principal component analysis (PCA) as one of the core methods of multivariate data analysis. PCA makes it possible to filter out similar groups of entries from complex data sets or to find new grouping parameters that better describe the data. For example, it is possible to find characterizing features for wine varieties or chemical compounds or to filter out distinctive properties of images. The method is universally applicable to all possible types of data. The main objective of PCA is to reduce the dimensionality of a multidimensional data set. This could, for example, be a data matrix containing noise measurements with the meteorological conditions prevailing at the time of measurement, as well as other parameters related to air traffic. In other words, dimension reduction is about presenting the data in a new, more meaningful base. Due to this very generally formulated objective, PCA can be found in almost all scientific disciplines in which data is analyzed. In addition to dimension reduction, other application examples include data compression, feature extraction and data visualization [32]. In principle, PCA works in such a way that the data set in its original basis is represented by a new basis, with the new basis vectors representing linear combinations of the original parameters. The first principal component is chosen so that the variance along this axis is maximized. In other words, maximizing the variance means trying to orient the axis in the data matrix in such a way that it explains the data as well as possible. The alternative formulation of this problem is to minimize the

error, i.e. the distance between the entry and the axis. The second principal component is orthogonal to the first principal component and again maximizes the variance. Principal components are added until the largest percentage of the original variance is explained by the new principal components [33].

**Algorithm** The PCA is computed by means of the singular value decomposition (SVD). The algorithm as defind by Kurita et al. [32] and Svante et al. [33] is used. We define a data matrix $\mathbf{X} = [x_1, ..., x_N]$ where $x_N$ are parameters of data set with $N$ variables each. The sample mean vector $\overline{x}$ and the sample covariance matrix $\sum$ can be written as

$$\overline{x} = \frac{1}{N}\sum_{i=1}^{N} x_i, \tag{5.1}$$

$$\sum = \frac{1}{N}\sum_{i=1}^{N}(x_i - \overline{x})(x_i - \overline{x})^T = \frac{1}{N}\tilde{X}\tilde{X}^T, \tag{5.2}$$

where matrix $\tilde{X}$ is centered data matrix $X$ and defined as $\tilde{X} = [x_1 - \overline{x}, ..., x_N - \tilde{X}]$. The data matrix $\tilde{X}$ can be decomposed by the SVD as

$$\tilde{X} = S\Delta V^T \tag{5.3}$$

where S contains the left singular values, V contains the right singular values, and $\Delta$ is the diagonal matrix of singular values. We rewrite the covariance matrix as

$$\sum = \frac{1}{N}\tilde{X}\tilde{X}^T = \frac{1}{N}S\Delta V^T V\Delta S^T = \frac{1}{N}S\Delta^2 S^T. \tag{5.4}$$

To obtain the eigenvector equation we multiply $S$ from the right

$$\sum S = S\frac{1}{N}\Delta^2. \tag{5.5}$$

Kurita et al [32] note that from this it follows that the loading vectors $A$ are equal to $S$ and that the diagonal matrix of eigenvalues $\Lambda$ is equal to $\frac{1}{N}\Delta^2$ if the number of principal components L is equal to the rank of the data matrix $\overline{X}$ with reference to the eigenvector equation

$$\sum A = A\Lambda. \tag{5.6}$$

The optimal linear projection of PCA is given by $Y = A^T\tilde{X}$ [32]. With equations (5.3) and from the relation in equation (5.5) we can write

$$Y = A^T\tilde{X} = S^T S\Delta V^T = \Delta V^T \tag{5.7}$$

where the parameter scores $y_{1i}$ are defined as $y_{1i} = a_1^T(x_i - \overline{x}), (i = 1, ..., N)$. They represent the coordinates on the new component. $A = [a_1, ...a_2]$ with $a_n = (a_{11}, ..., a_{M1})^T$ is the set of loading vectors of the linear combinations of the original variables. The variance of the first new component is exactly equal to the biggest eigenvalue $\lambda_1$ of the covariance matrix. The

```
loadings = sorted_eigenvectors * np.sqrt(sorted_eigenvalues)
```

Source Code 5.1.: Computation of the loadings in Python

corresponding eigenvector defines the orientation of the new component or axis in reference to the old axis, whereas loadings are eigenvectors that hold information about the magnitude of the rotated information. They can be computed by multiplying the eigenvector with the square root of the corresponding eigenvalue.

If we take equation (5.7) then the data matrix $\tilde{X}$ can be represented as the product of the score vectors Y and the loading vectors A:

$$\tilde{X} = S\Delta V^T = AY = AA^T\tilde{X} \tag{5.8}$$

More components are added in an iterative process where the eigenvector with the second largest eigenvalue $\lambda_2$ will be the second added component, and so on.

In Python, the algorithm would look similar to this. We assume that the data matrix $\tilde{X}$ is already normalized, and standardized and that all features are quantifiable. Nominal data could be handled with a one-hot encoding, increasing the dimensionality of the data matrix in the process. The Python library Pandas was used to store $\tilde{X}$ in a data frame and Numpy was used to calculate the covariance matrix and the eigenvalues- and vectors. The variable $n$ denotes the number of dimensions the data matrix will be reduced to.

```
X_centered = X - X.mean()
X_centered.dropna(inplace=True) # remove incomplete samples
covariance_matrix = np.cov(X_centered , rowvar = False)
eigen_values, eigen_vectors = np.linalg.eigh(covariance_matrix)
sorted_index = np.argsort(eigen_values)[::-1]
sorted_eigenvalues = eigen_values[sorted_index]
sorted_eigenvectors = eigen_vectors[:, sorted_index]
eigenvector_subset = sorted_eigenvectors[:, 0:n]
X_reduced = np.dot(eigenvector_subset.transpose(), X_centered.transpose()).transpose()
```

Source Code 5.2.: PCA algorithm using the Python libraries Pandas and Numpy

After we conduct the PCA we can create a biplot showing the data represented by the new components. First, the data needs to be reduced to either two or three dimensions so we can visualize it. The shown code works for two dimensions. The scores represent the coordinates of the data in the new coordinate system while the loadings can be used to show how the parameters load onto the components. From this plot, we can show the parameters correlate and how they correspond to the components. The new basis could also reveal previously hidden groups in the data. For this code, we assume to have some PCA-object that holds the reduced data matrix $X_{reduced}$ and the loading matrix. The Python library matplotlib is imported and used under the name *plt*. The arrows that annotate the loadings are scaled for better visibility.

```python
def plot_biplot(self, target, title, scaling):
        mean = [self.X_reduced[i, :].mean() for i in range(0,2,1)]
        loadings_matrix = self.loadings
        fig = plt.figure(figsize=(15,15))

        plt.scatter(self.X_reduced[:, 0], self.X_reduced[:, 1], c=self.X_centered[target],
            cmap=plt.cm.get_cmap("Spectral",10), alpha=0.7)

        for i, elem in enumerate(loadings_matrix):
            plt.arrow(0, 0, loadings_matrix[i,0] * scaling, loadings_matrix[i,1] * scaling,
            color = 'k', alpha = 1,linestyle = '-', linewidth = 1.5, overhang=0.2)
            plt.text(loadings_matrix[i,0]* (scaling+0.5), loadings_matrix[i,1] * (scaling+0.5),
                self.df_centered.columns[i], color = 'k', ha = 'center', va = 'center',fontsize=15)

        plt.rcParams.update({'font.size': 25})
        plt.xlabel("PC1", size=22)
        plt.ylabel("PC2", size=22)
        plt.title(f"Scores and Loadings Biplot {target} {title}")
```

Source Code 5.3.: PCA biplot code to show the scores and loading of the reduced data matrix in Python e.g. figure (5.1)

## 5.2. Analysis of Variance (ANOVA)

We're using standard linear regression to construct an initial model for noise propagation in the atmosphere. With regards to the differential equations in chapter (3) we know that a linear model will be insufficient, however, the regression parameters will provide insights into the importance of single parameters. From these results, we can then build a model for the noise propagation in the atmosphere in the context of measured data. The Analysis of Variance or short ANOVA is a collection of established statistical methods to analyze the differences in variance among and within groups [12]. In principle, we divide the data into several groups according to a parameter, e.g. how strongly the wind opposes the sound, and then compare the average noise measurement value between the groups to see if there are any differences. Some assumptions need to be fulfilled so that the results of statistical tests are reliable:

- The data is distributed normally
- Sample variances are equal
- The groups and the measurements are independent

The first two assumptions can be tested while the third assumption independence is inherent to the experimental setup or the study design. Levene's test [34] will be used to check for homogeneity of variances and quantile-quantily plots [35] will be used to visually confirm if the data (the standardized residuals) are normally distributed. Noise measurements

| Source of variation | (Df) | (SS) | (MS) | F-value | significance |
|---|---|---|---|---|---|
| Group (between) | $Df_b = a - 1$ | $SS_b$ | $MS_b = SS_b/Df_b$ | $MS_b/MS_e$ | p-value |
| Residuals (within) | $Df_E = a(n-1)$ | $SS_E$ | $MS_E = SS_E/Df_E$ | | |
| Total | $Df_T = an - 1$ | $SS_T$ | | | |

Table 5.1.: Calculation of the ANOVA table

from overflights of airplanes and weather measurements are assumed to be independently measured. The measurements were taken from distinct samples.
In the one-way (one factor) ANOVA [36] we have one independent variable (factor) and at least two groups. We compare the variance of mean between groups to the variance of means within the groups. In general, the null hypotheses $H_0$ is that all group means $\mu_0, ...\mu_n$ are equal: $\mu_0 = ... = \mu_n$. We reject the null hypothesis if one group's mean is different from the other group's means. Our motivation is to categorize the noise measurements into different groups according to local atmospheric parameters such as wind direction or temperature gradients at the time of measurement and to compare whether these have an influence on the average noise measured. Johansson et al. [11] have used ANOVA in a similar context for noise measurements of landing A321 aircraft.

The basic ANOVA is a linear model that assumes that a value $y = \mu + \alpha + e$ can be decomposed into the population mean $\mu$, the effects of an independent variable $\alpha$ and some error $e$ [36]. The idea is to test the mean differences against naturally occurring variability as represented by the error term $e$. The total sum of squares is the sum of squares between groups ($SS_b$) plus the sum of squares within groups ($SS_E$)

$$SS_T = SS_b + SS_E \tag{5.9}$$

For these to become variances they are averaged by the degree of freedom which is partitioned similarly.

$$Df_T = Df_b + Df_E \tag{5.10}$$

The ANOVA table shows the source of variation, the degree of freedom (Df), the Sum of Squares (SS), the Mean Square (MS), the F-value, and the significance.

where $N$ is the total number of samples, $a$ is the number of groups, and $n$ the number of samples within each group. The sum of squares is defined as

$$SS_b = \sum_i a_j(\overline{y_j} - \overline{y})^2 \tag{5.11}$$

$$SS_E = \sum_i \sum_j (y_{ij} - \overline{y_i})^2 \tag{5.12}$$

Since the ANOVA test only tells us that there are differences between the groups, but not which groups differ, a post-hoc test is necessary. To find out which pairs are specifically different, we apply Tukey's honestly significantly differentiated (HSD) post-hoc test. For equal group sizes, the HSD is defined as follows [37]

$$HSD = q_{a,\alpha,df}\sqrt{\frac{ME_E}{n}} \tag{5.13}$$

where $q$ is a studentized range statistic with $\alpha$ is the significance level (0.01) and $df$ is the degrees of freedom.

As a metric of effect size, $\eta^2$ and $\omega^2$ are used.

$$\eta^2 = \frac{SS_b}{SS_T} \tag{5.14}$$

Eta-squared describes the ratio of variance explained in the dependent variable by a parameter while controlling for other parameters.

$$\omega^2 = \frac{SS_b - Df_b \cdot MS_E}{SS_T + MS_E} \tag{5.15}$$

Omega-squared is a less biased estimator of the variance explained by the population.

The Levene test for equal variances tests for the null hypotheses $H_0$ that the variances between the groups are equal: $\sigma_1^2 = \sigma_2^2 = ... = \sigma_k^2$. The alternative hypothesis is that at least the variance of one pair is different. For a variable $Y$ with a sample size of $N$ divided into $k$ subgroups, where $N_i$ is the sample size of subgroup $i$. The test statistic is defined as

$$W = \frac{(N-k)}{(k-1)} \frac{\sum_{i=1}^{k} N_i(\overline{Z}_{i.} - \overline{Z}_{..})^2}{\sum_{i=1}^{k}\sum_{j=1}^{N_i}(Z_{ij} - \overline{Z}_{i.})^2} \tag{5.16}$$

where $Z_{ij} = |Y_{ij} - \overline{Y}_{i.}|$ and $\overline{Y}_{i.}$ is the mean of the i-th subgroup. $\overline{Z}_{i.}$ are the group means of the $Z_{ij}$ and $\overline{Z}_{..}$ is the overall mean of the $Z_{ij}$ [34].

## 5.3. Application of the PCA for Noise

The combined data set of noise measurements, flight information, position data, and weather parameters contains a total of 80 parameters. A total of 14497 data records from the A320-200 are available for NMT 11 Norderstedt, Reitstall Ohlenhoff which will be examined in this chapter. PCA plots for the other NMTs can be found in the appendix. Many different parameters like the distance and the aircraft type have an influence on $L_{AS,max}$. As the data set is too extensive to recognize patterns, the dimensionality of the data is first reduced using PCA in order to make dependencies visible. In the next step, it is then possible to further filter the data for the statistics. PCA also makes the covariances between the parameters visible. On the one hand, this is interesting to understand on which measurement data the noise depends, but also how much the weather measurements from the airport

correlate with the weather measurements from the Hamburg weather mast. If there is a strong correlation, measured weather profiles from the weather mast can be included in the analysis to better depict the physical processes in the atmosphere. PCA is applied in such a way that grouping parameters are identified step by step according to which the data sets can be divided for further analysis with the aim that in the end the relative influence on the variance of $L_{AS,max}$ of the weather parameters is maximized. Before PCA is applied, the data is normalized and standardized so that parameters with high values do not carry excessive weight. The sklearn.preprocessing.MinMaxScaler library [1] is used for normalization. The $L_{AS,max}$ measurements are normalized to the interval [0,1].

```
X_std = (X - X.min(axis=0)) / (X.max(axis=0) - X.min(axis=0))
X_scaled = X_std * (max - min) + min
```

Source Code 5.4.: Definition of the MinMaxScaler from sklearn

The standard scaler from sklearn [2] is used to set the mean value of the data series to 0 with unit variance.

```
z = (x - u) / s
```

Source Code 5.5.: Definition of the StandardScaler from sklearn

where $x$ is the sample, $u$ the mean of the parameter, and $s$ the standard deviation. For NMT 11 Reitstall, Ohlenhoff we have 49768 measurements of different types of airplanes. The associated runway 33 is the main take-off direction. Restricted to the A320-200, 14497 measurements remain. PCA is applied and the scores and loadings are displayed in a biplot. For this purpose, the data set is reduced to two dimensions. The scores are the coordinates of the original data, displayed in the new coordinate system of the principal components. The loadings show how the original parameters are represented by the principal components. In figure 5.1, the scores are categorized according to whether it is a take-off or a landing.

[1] https://scikit-learn.org/stable/modules/generated/sklearn.preprocessing.MinMaxScaler.html
[2] https://scikit-learn.org/stable/modules/generated/sklearn.preprocessing.StandardScaler.html

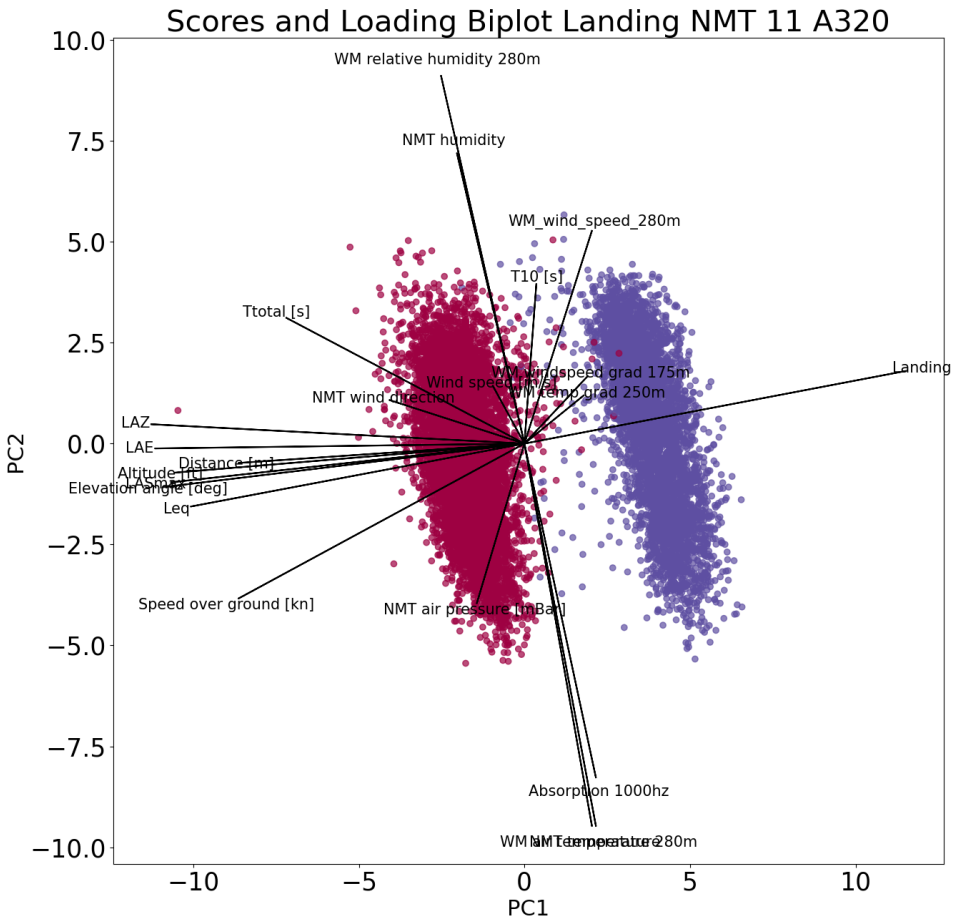


Figure 5.1.: Scores and loading biplot for a reduced A320 data set at NMT 11 Norderstedt, Reitstall Ohlenhoff. The measurements from departures are colored in purple. Measurements from landings are colored in red. The biplot for the other NMTs can be found in the appendix.

After running the PCA, you can see the grouping of the measured values into take-offs and landings. The parameter Landing [True/False] contributes significantly to the first component. Together with the parameters distance, speed, altitude, and elevation angle, most of the variance is explained along this axis. Three of the four parameters describe the distance between the NMT and the aircraft at the time of measurement in space. It should also be noted that the $L_{AS,max}$ parameter correlates very strongly with these four parameters. In this case, it is a correlation and not only a covariance between the parameters even though the covariance matrix was computed originally, as the data set is centered. The data is standardized and the parameters can be compared with each other. The second main component is determined

by temperature-related parameters such as the temperature at the NMT and at the weather mast, the air humidity, and the atmospheric absorption as a composite variable. Here it can be seen that the weather measurements of the NMT correlate very strongly with those of the weather mast. It should also be noted that the wind speed profile and the temperature profile are both linear profiles.

| | Parameter | PC 1 | PC 2 | % of variance explained |
|---|---|---|---|---|
| 01 | Departure [True/False] | 0.95 | 0.21 | 0.95 |
| 02 | Height [ft] | -0.94 | -0.14 | 0.90 |
| 03 | Elevation angle [°] | -0.92 | -0.15 | 0.87 |
| 04 | Distance to NMT [m] | -0.80 | -0.11 | 0.65 |
| 05 | WM air temperature 280m [$°C$] | 0.22 | -0.76 | 0.63 |
| 06 | WM relative humidity 280m [%] | -0.25 | 0.75 | 0.62 |
| 07 | NMT temperature [$°C$] | 0.19 | -0.76 | 0.61 |
| 08 | $L_{AS,max}$ [dB] | -0.77 | -0.12 | 0.61 |
| 09 | Speed over ground [kn] | -0.67 | -0.36 | 0.58 |
| 10 | Absorption 1000Hz [$\frac{dB}{m}$] | 0.21 | -0.68 | 0.51 |
| 11 | $T_{total}$ [s] | -0.63 | 0.20 | 0.44 |
| 12 | NMT relative humidity [%] | -0.18 | 0.60 | 0.39 |
| 13 | WM wind speed 280m [m/s] | 0.15 | 0.45 | 0.23 |
| 14 | NMT wind direction [°] | -0.45 | 0.11 | 0.21 |
| 15 | WM wind direction 280m [°] | -0.40 | 0.20 | 0.20 |
| 16 | NMT air pressure [mBar] | -0.11 | -0.36 | 0.14 |
| 17 | $T_{10}$ [s] | -0.10 | 0.29 | 0.09 |
| 18 | WM wind speed grad. 175m [$\frac{m/s}{m}$] | 0.24 | 0.16 | 0.08 |
| 19 | WM temperature grad. 250m [$\frac{°C}{m}$] | 0.23 | 0.12 | 0.07 |
| 20 | NMT wind speed [m/s] | -0.14 | 0.11 | 0.03 |

Figure 5.2.: Loadings of the parameters onto the first two principal components for the data matrix from NMT 11 with A320 measurements

The table shows the corresponding loadings for the NMT 11 Norderstedt, Reitstall Ohlenhoff data. The explained variance per variable is computed by squaring and adding up the loadings for each principal component,

$$\text{variance component i that is explained} = PC1_i^2 + PC2_i^2 \tag{5.17}$$

where $PCj_i$ is the loading of parameter $i$ on principal component $j$.

There are various methods in the literature for deciding how many components should be chosen to represent the data. Abdi et al. [6] mention the "scree" or "elbow" test where we plot the eigenvalues in decreasing order. We look for a point in the graph where the slope of the eigenvalues goes from steep to flat and select the eigenvalues before that point. These are the most meaningful ones. In figure (5.3) we see that this point is approximately between

| | PC1 | PC2 | PC3 | PC4 | PC5 | PC6 | PC7 | PC8 | PC9 | PC10 |
|---|---|---|---|---|---|---|---|---|---|---|
| variance | 0.28 | 0.17 | 0.11 | 0.08 | 0.08 | 0.07 | 0.04 | 0.03 | 0.03 | 0.02 |
| cum. variance | 0.28 | 0.45 | 0.56 | 0.64 | 0.72 | 0.79 | 0.83 | 0.86 | 0.89 | 0.91 |

Table 5.2.: percentage of variance explained with the principal components in figure (5.1)

the 7th and the 8th eigenvalue. The first seven eigenvalues and the corresponding principal components represent 83% of the total variance in the data set according to table (5.2).

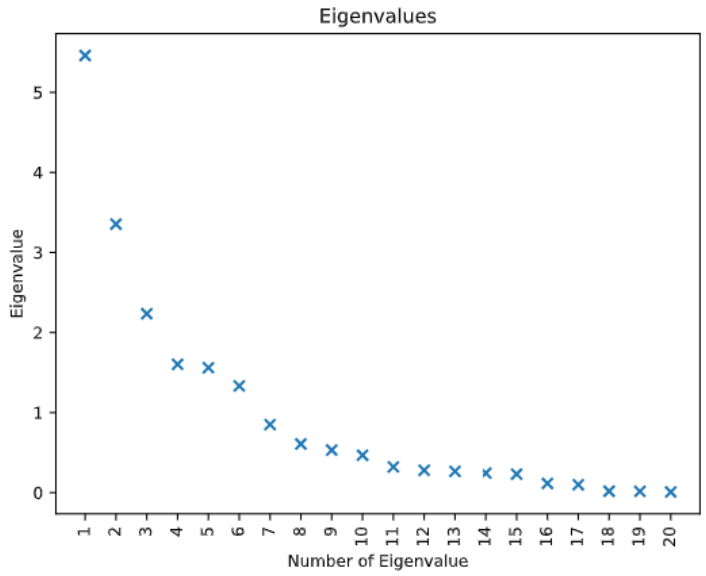


Figure 5.3.: Scree test to determine how many eigenvalues for figure (5.1) sufficient to represent the data set

We summarize that the first 7 eigenvalues are significant enough. The first 7 components are sufficient to present 83 % of the data in a meaningful way. Compared to the 20 parameters from the reduced data set and the 80 parameters from the original data set, the data can be presented in a much more compact way. With a view to machine learning applications, the training time of neural networks can be significantly reduced. As a second result, take-offs and landings are considered separately in further analyses, as these two groups differ in terms of take-offs and landings and the influence of weather parameters is hardly significant in comparison.

# 6. Statistics of measured Data

This chapter uses statistical methods to answer the two research questions "What is the relationship between weather and noise pollution in the vicinity of Hamburg Airport?" and "What is the relationship between weather and noise pollution at individual measuring stations?".
First, we calculate the average noise values according to NMT and group by aircraft type according to equation (3.9). The NMT-ID as a parameter is important because the topographical conditions in the vicinity of the measuring station have a decisive influence on sound propagation. We want to filter out these influencing factors as far as possible. All statistics are therefore usually performed for a specific NMT. In figure (6.2) you can see the different, sometimes very different, average noise levels. The map (6.2) shows the average noise in the period 01.08.2023 - 31.08.2023 for all NMTs and all aircraft types. The red color represents the noise, the louder, the darker the red color. The number of recorded overflights is represented by the size of the circle. In this map, both take-offs and landings are recorded to capture the entire noise impact on residents as completely as possible. Without looking at the data in detail, it is already clear that noise pollution is highest in the airport's immediate vicinity. NTMs 05, 07, 11, and 12 are all very close to the airport. Here the aircraft are already very close to the ground and the distance between the source of noise and the receiver is short. Most aircraft take off in a north-westerly direction to avoid flying over the city of Hamburg, some depart towards the west. The area around NMTs 08, 11, 01, and 03 is therefore very noisy, as take-offs are comparatively much louder than landings. During take-off, the engines are operated under take-off thrust, while aircraft use less thrust on the glide path to the runway when landing. Approx. 50 % of the landings come from the north-east. The series of measuring stations from NMTs 13, 07, and 05 is therefore mainly overflown by landing aircraft. A further 28% land from the north and 20% from the south-east.

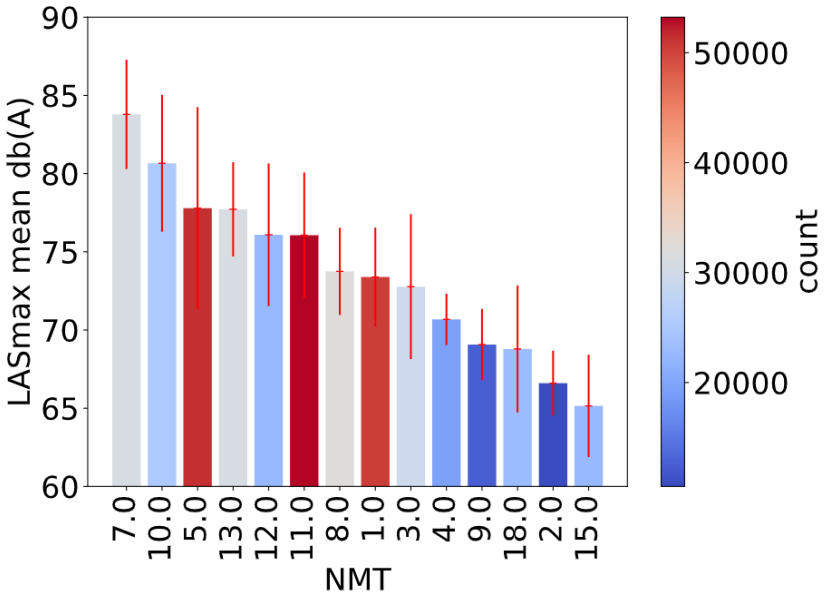


Figure 6.1.: Average $L_{AS,max}$ by NMT ID and standard deviation

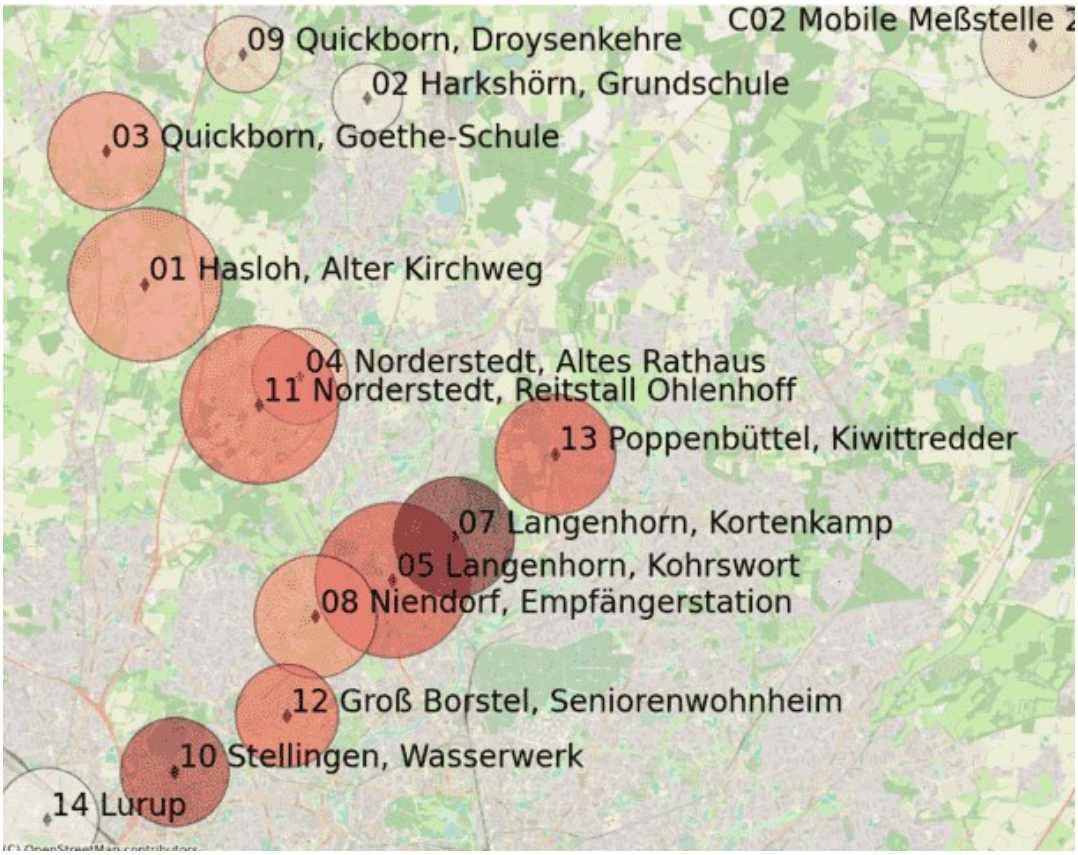


Figure 6.2.: Map of NMTs in the vicinity of Hamburg Airport. For each NMT, the average noise level (from the figure (6.1) shown as a combination of the average noise measurements and the number of overflights

The type of aircraft is another important factor influencing the noise measurements. Although this work exclusively uses data from the A320-200 type (comprised of the A3202 and A320A type in plot (6.3)), we would like to briefly show the average noise measured for the other widely used types as comparative values. Only aircraft types with at least 1000 measurements in the period 01.08.2022 - 31.08.2023 in the area of Hamburg Airport were included in the statistics. The Airbus aircraft hangar in nearby Finkenwerder should also be briefly mentioned at this point. Flights with destination Finkenwerder represent a not insignificant proportion of flights in the area of Hamburg Airport (formerly Hamburg-Fuhlsbüttel). In addition, these are often test flights for new airliners. These can include unusual aircraft operations such as the use of the so-called ram-air turbine. In an emergency, this is released from the aircraft fuselage by gravity and produces emergency power, but also generates a very distinctive noise. In addition, the heavily loaded Beluga transport planes land in Finkenwerder, bringing entire aircraft parts to Hamburg for production. As these flights have highly unusual characteristics and different routes than the flights with Fuhlsbüttel as their destination, this data is filtered out by the airport and is not included in this work.

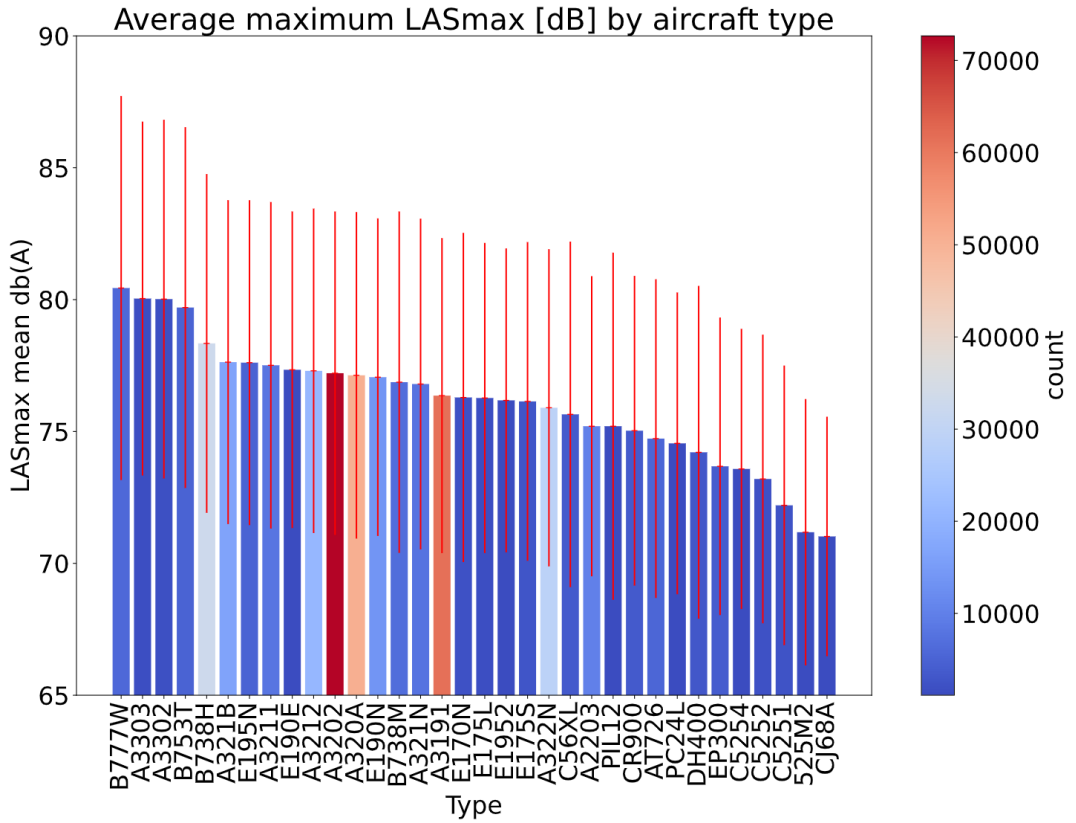


Figure 6.3.: Average maximum $L_{AS,max}$ [dB] by aircraft type for all NMTs combined

In the graphic (6.3) we see the energetic average maximum sound levels, $\overline{L}_{AS,max}$ by aircraft type. The loudest aircraft at Hamburg Airport is also the largest, as you would expect. The

Boeing 777 and the A330-200 and -300 are on average 3-4 dB louder at approximately 80 dB compared to an average noise of approximately 76 dB of the smaller singe-aisle aircraft (aircraft with only one aisle between the two rows of seats, opposed to larger aircraft with two aisles between three rows of seats) such as the A320. This is a significant increase in noise as a 3 dB increase would be a doubling of noise sources.

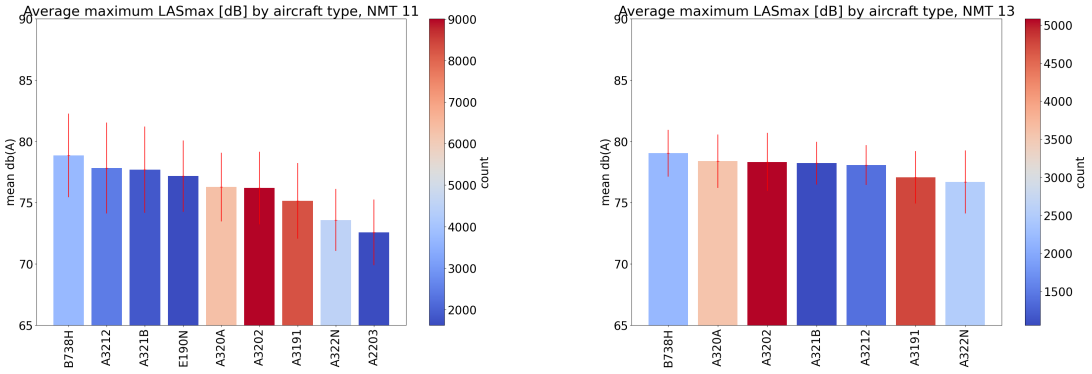


Figure 6.4.: Average maximum $\overline{L}_{AS,max}$ [dB] by aircraft type at NMT 11 Norderstedt, Reitstall Ohlenhoff and NMT 13 Poppenbüttel, Kiwittredder

Airplanes often fly the same routes between two cities. Since it could be that one type of airplane always flies over a certain route, which is louder due to the topographical conditions and the distance to the measuring point, we compare the average noise per airplane type with at least 1000 measurements again for two specific NMTs. For NMT 11 Norderstedt, Reitstall Ohlenhoff and for NMT 13 Poppenbüttel, Kiwittredder we calculate $\overline{L}_{AS,max}$ [dB] separately. The Boeing 737-800 (symbol B738H) is 1-2 dB louder than the A321 and the A320 in both cases. On all three types the CFM-56 engines are used, therefore this difference is due to the different aerodynamics and possibly different flight operations.

## 6.1. Engine type

As the primary noise-generating component of an aircraft, the engines are an important parameter for the dependent variable $L_{AS,max}$. When investigating parameters that influence noise, we first consider other station-independent parameters in addition to the location and aircraft type. The A320-200 series uses a range of engines. The older ceo models largely use the CFM-56 engines, which are also used by Boeing 737 types. However, the newer A320 neo aircraft use Pratt & Whitney's PurePower PW1100G-JM geared turbofan, and CFM International's LEAP-1A [1]. Figure (6.5) compares the different engine types that are used. Only values from starts are used as starts and landings are too distinct to be compared together as we've seen in chapter 5.3. The engines used on the A320 neo are colored orange, and the engines of the A320 ceo in red. Measurements of take-offs were chosen as data,

[1] https://aircraft.airbus.com/en/aircraft/a320-the-most-successful-aircraft-family-ever/a320neo

as the engine has to call up much more power during take-off than during a landing. The proportion of the total noise generated by the engine is greater during take-off, so differences are more noticeable. In order to make the differences between the engines independent of the topography of the measuring points, we look explicitly at NMT 11, the main take-off direction. This has the most data compared to the other measuring points.

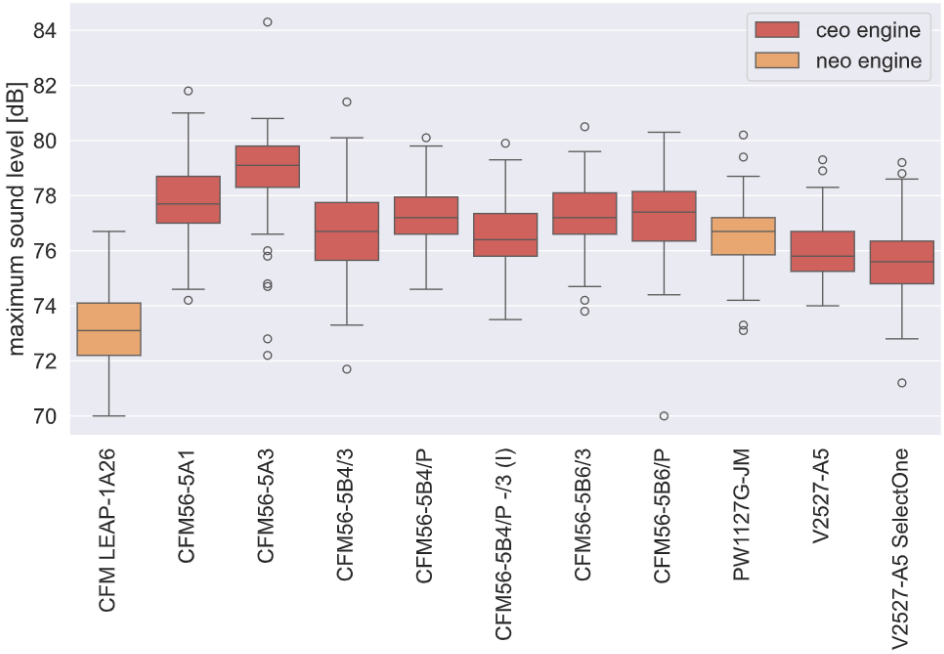


Figure 6.5.: Boxplot for NMT 11 departure data, grouped by A320 engine types

We can see that the new CFM LEAP-1A engines are significantly quieter, in some cases by 3-5 dB on average. The exact pairwise comparisons are broken down in more detail in table (6.2).

The One-Way ANOVA method [5] confirms that the parameter "engine type" has a significant effect on the measured maximum noise $L_{AS,max}$. Both the value of $\omega^2$ and that of $\eta^2$ indicate a large effect size. Table (6.1) first shows the average values per engine type at NMT 11, the sample size per group $N$, the standard deviation $sd$, the standard error $se$, and the 95% confidence interval. The sample size is equal for all populations. This is important so that assumptions of equal variances hold and for the sum of squares computations.

| | sum$^2$ | df | mean$^2$ | F-value | p-value | $\eta^2$ | $\omega^2$ |
|---|---|---|---|---|---|---|---|
| C(Engine type) | 1525.14 | 10.00 | 152.51 | 78.28 | 0.00 | 0.49 | 0.48 |
| Residual | 1585.96 | 814.00 | 1.95 | | | | |

Figure 6.6.: ANOVA results for the engine parameter of A320 measurements

Table 6.1.: Mean $L_{AS,max}$ [dB] values grouped by engine type of the A320. Ceo (current engine option) and neo (new engine option) engine options are shown

| Engine | N | mean | sd | se | 95 % confidence interval lower CI | upper CI |
|---|---|---|---|---|---|---|
| CFM LEAP-1A26 | 75 | 73.22 | 1.34 | 0.15 | 72.91 | 73.53 |
| CFM56-5A1 | 75 | 77.86 | 1.42 | 0.16 | 77.54 | 78.19 |
| CFM56-5A3 | 75 | 78.82 | 1.76 | 0.20 | 78.41 | 79.22 |
| CFM56-5B4/3 | 75 | 76.65 | 1.69 | 0.19 | 76.26 | 77.03 |
| CFM56-5B4/P | 75 | 77.22 | 1.10 | 0.13 | 76.97 | 77.48 |
| CFM56-5B4/P -/3 (I) | 75 | 76.58 | 1.23 | 0.14 | 76.30 | 76.86 |
| CFM56-5B6/3 | 75 | 77.21 | 1.33 | 0.15 | 76.90 | 77.52 |
| CFM56-5B6/P | 75 | 77.16 | 1.63 | 0.19 | 76.78 | 77.53 |
| PW1127G-JM | 75 | 76.51 | 1.19 | 0.14 | 76.24 | 76.79 |
| V2527-A5 | 75 | 76.00 | 1.14 | 0.13 | 75.74 | 76.26 |
| V2527-A5 SelectOne | 75 | 75.63 | 1.35 | 0.16 | 75.31 | 75.94 |

In order to determine the pairwise differences between the engine types, we carry out a post-hoc test [2]. Table (6.2) shows the mean difference in decibel between each pair of engine types, the standard error, the t-value since we look at the difference in mean here, the p-value (only pairs with a significant p-value $< 0$ are shown), and the 95% confidence interval.

[2] https://docs.scipy.org/doc/scipy/reference/generated/scipy.stats.tukey_hsd.html

Table 6.2.: Tukey posthoc test for engine types: pairwise comparisons

| groups | mean diff | std error | t-value | p-value | 95% ci upper | 95% ci lower |
|---|---|---|---|---|---|---|
| CFM LEAP-1A26 : CFM56-5A1 | 4.64 | 0.16 | 20.61 | 0.00 | 9.10 | 0.19 |
| CFM LEAP-1A26 : CFM56-5A3 | 5.60 | 0.18 | 21.93 | 0.00 | 10.06 | 1.14 |
| CFM LEAP-1A26 : CFM56-5B4/3 | 3.43 | 0.18 | 13.78 | 0.00 | 7.88 | -1.03 |
| CFM LEAP-1A26 : CFM56-5B4/P | 4.01 | 0.14 | 20.01 | 0.00 | 8.46 | -0.45 |
| CFM LEAP-1A26 : CFM56-5B6/3 | 3.99 | 0.15 | 18.32 | 0.00 | 8.44 | -0.46 |
| CFM LEAP-1A26 : CFM56-5B6/P | 3.94 | 0.17 | 16.15 | 0.00 | 8.39 | -0.51 |
| CFM LEAP-1A26 : PW1127G-JM | 3.29 | 0.15 | 15.93 | 0.00 | 7.75 | -1.16 |
| CFM LEAP-1A26 : V2527-A5 | 2.78 | 0.14 | 13.73 | 0.00 | 7.24 | -1.67 |
| CFM56-5A1 : CFM56-5B4/3 | -1.22 | 0.18 | 4.77 | 0.00 | 3.24 | -5.67 |
| CFM56-5A1 : PW1127G-JM | -1.35 | 0.15 | 6.31 | 0.00 | 3.10 | -5.80 |
| CFM56-5A1 : V2527-A5 | -1.86 | 0.15 | 8.86 | 0.00 | 2.60 | -6.32 |
| CFM56-5A3 : CFM56-5B4/3 | -2.17 | 0.20 | 7.71 | 0.00 | 2.28 | -6.62 |
| CFM56-5A3 : CFM56-5B4/P | -1.59 | 0.17 | 6.65 | 0.00 | 2.87 | -6.06 |
| CFM56-5A3 : CFM56-5B6/3 | -1.61 | 0.18 | 6.31 | 0.00 | 2.85 | -6.07 |
| CFM56-5A3 : CFM56-5B6/P | -1.66 | 0.20 | 5.99 | 0.00 | 2.79 | -6.11 |
| CFM56-5A3 : PW1127G-JM | -2.31 | 0.17 | 9.40 | 0.00 | 2.16 | -6.77 |
| CFM56-5A3 : V2527-A5 | -2.82 | 0.17 | 11.64 | 0.00 | 1.65 | -7.28 |
| CFM56-5B4/P : V2527-A5 | -1.22 | 0.13 | 6.69 | 0.00 | 3.23 | -5.67 |
| CFM56-5B6/3 : V2527-A5 | -1.21 | 0.14 | 5.98 | 0.00 | 3.25 | -5.66 |
| CFM56-5B6/P : V2527-A5 | -1.16 | 0.16 | 5.03 | 0.00 | 3.30 | -5.62 |

The differences between the new neo engines CFM LEAP-1A26 and the older CFM56-5A/B ceo engines are the biggest. The CFM LEAP-1A26 : CFM56-5A3 group is the most noticeable with a difference of 5.6 dB. For a point source that emits sound, an increase of 6 dB would mean halving the distance between the transmitter and receiver. Finally, we check the assumption of the normality of the ANOVA method with a histogram compared with a normal distribution in red and a QQ plot of the standardized residuals. We visually confirm the assumption as fulfilled.

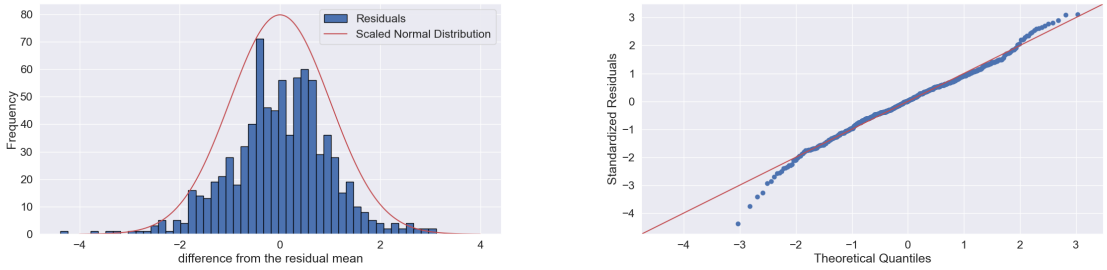


Figure 6.7.: Histogram (left) and QQ-plot (right) of standardized residuals for the engine type parameter

## 6.2. Distance between aircraft and NMT

The effect of the non-atmospheric parameters will be analyzed and then used as a baseline to compare the effect of the atmospheric parameters. The distance between the aircraft and the microphone in the NMT on the ground, together with the engine type, aircraft type and location of the measurement by narrowing down the data, have the greatest influence on the noise [1].

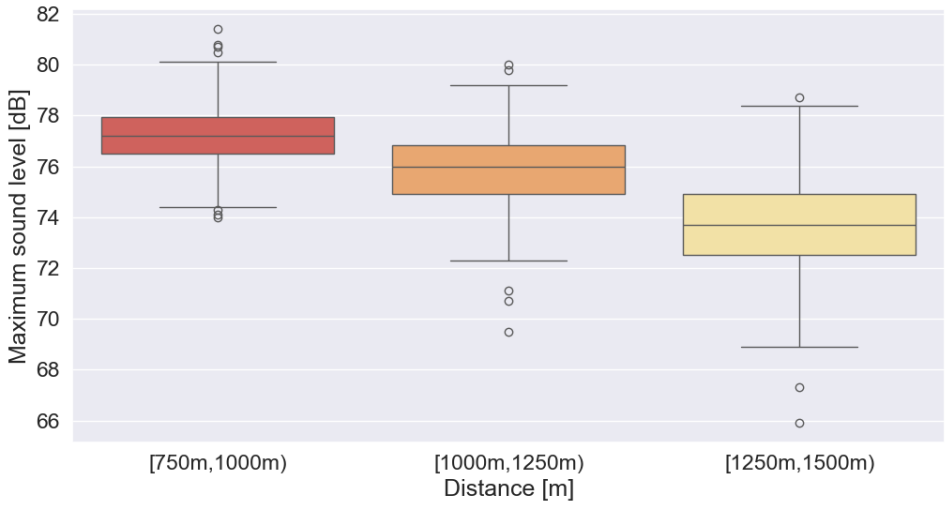


Figure 6.8.: Boxplot for NMT 11 departure data grouped into 250m groups. The distance is the distance $d$ at time $T_{Las,max}$, $d_{T_{LAS,max}}$.

The boxplot shows visible differences in the mean maximum loudness among the groups. Specifically, $L_{AS,max}$ measured values of A320-200 aircraft at NMT 11 Reitstall, Ohlenhoff are classified into the three distance groups $[750m, 1000m)$, $[1000, 1250m)$ and $[1250m, 1500m)$. The distance $d_{T_{LAS,max}}$ denotes the distance between the aircraft and the NMT at the time

| | sum$^2$ | df | mean$^2$ | F-value | p-value | $\eta^2$ | $\omega^2$ |
|---|---|---|---|---|---|---|---|
| C(Distance) | 2411.70 | 2.00 | 1205.85 | 557.54 | 0.00 | 0.48 | 0.48 |
| Residual | 2582.39 | 1194.00 | 2.16 | | | | |

Figure 6.9.: ANVOA results for the distance parameter of A320 measurements

Table 6.3.: Statistics of the $L_{AS,max}$ values grouped into distance groups

| Distance | [750m,1000m) | [1000m,1250m) | [1250m,1500m) |
|---|---|---|---|
| N | 399 | 399 | 399 |
| mean | 77.17 | 75.90 | 73.73 |
| sd | 1.17 | 1.43 | 1.75 |
| se | 0.06 | 0.07 | 0.09 |
| 95 % ci lower limit | 77.06 | 75.76 | 73.56 |
| 95 % ci upper limit | 77.29 | 76.04 | 73.91 |

$T_{Las,max}$. The distance between the aircraft and NMt is calculated as

$$d = \sqrt{h_i^2 - s_{i,j}^2} \tag{6.1}$$

where $d$ is the distance parameter, $h_i$ is the height over ground of airplane $i$, and $s_{ij}$ is the distance on ground between aircraft $i$ and NMT $j$. To confirm this finding the One-Way ANOVA method from scipy.stats is computed and reported.

The null hypothesis $H_0$ is that the means of the three groups are equal. The p-value is below the threshold of 0.05 therefore we reject $H_0$ and conclude that the "distance" parameter has a significant effect on the mean measured maximum sound level $L_{\overline{p}}$. Figure (6.3) shows the $L_{\overline{p}}$ value per group, the number of samples per group $N$, the standard deviation, the standard error, and the 95% confidence interval.

From table (6.4) we can see the pairwise differences between the distance groups and then compare them with the behavior of the geometric spreading of sound (3). The average sound pressure level $L_{\overline{p}}$ decreases by 3.44 dB between the groups [750m,1000m) and [1250,1500). The distance between the shortest and the longest distance in the two intervals is doubled. For a point source, doubling the distance would mean a reduction of SPL by 6 dB. However, we note that the distance doesn't strictly double between the intervals as this statement cannot be made when we compare intervals where the distance values at the borders of the intervals are closer to each other while other values are further apart.

Table 6.4.: Tukey posthoc test for the distance parameter, pairwise comparisons

| groups | [1000m,1250m) [1250m,1500m) | [750m,1000m) [1000m,1250m) | [750m,1000m) [1250m,1500m) |
|---|---|---|---|
| mean difference | -2.17 ($\Delta 250m$) | -1.27 ($\Delta 250m$) | -3.44 ($\Delta 500m$) |
| std error | 0.08 | 0.07 | 0.07 |
| t-value | 19.11 | 13.78 | 32.57 |
| p-value | 0.00 | 0.00 | 0.00 |
| lower limit | -5.49 | -2.05 | 0.12 |
| upper limit | 1.16 | 4.59 | 6.76 |

Finally, we check the assumptions of the ANOVA method again. The histogram and the Quantile-Quantile plot of the standardized residuals confirm the assumption that the data are normally distributed. There are a few outliers at the edges of the QQ plot, but the ANOVA method is quite robust against such violations. With a value of 0.99, the Shapiro-Wilk test [3] shows that we do not reject the hypothesis that the data are normally distributed and conclude that both visually and confirmed by the test that the distance samples came from a normal distribution. The assumptions to draw reliable and meaningful results from the ANOVA method are met.

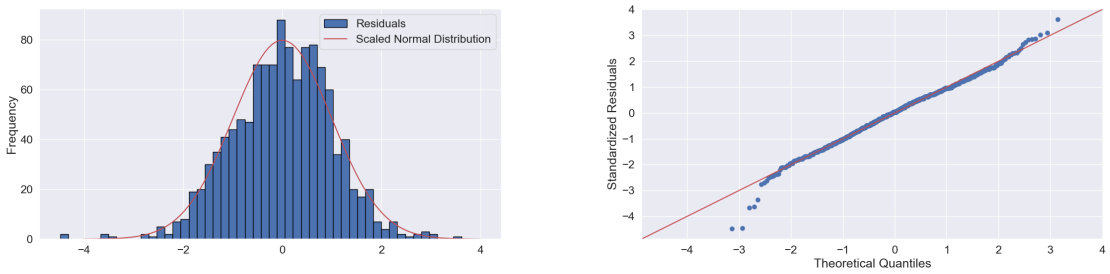


Figure 6.10.: Histogram and QQ plot of standardized residuals for the distance parameter

## 6.3. Starts/Landings

In Chapter (5.3), we have already seen that take-offs and landings differ greatly in terms of noise pollution for the surrounding area. At NMT 11, Reitstall Ohlenhoff we have 4672 landings and 9822 take-offs from the A320-200. For the ANOVA, we sample both groups so that both have the same number of samples. Using the ANOVA method and the post-hoc test, we obtain a difference of almost 5 dB and a p-value of 0.00.

[3] https://docs.scipy.org/doc/scipy/reference/generated/scipy.stats.shapiro.html

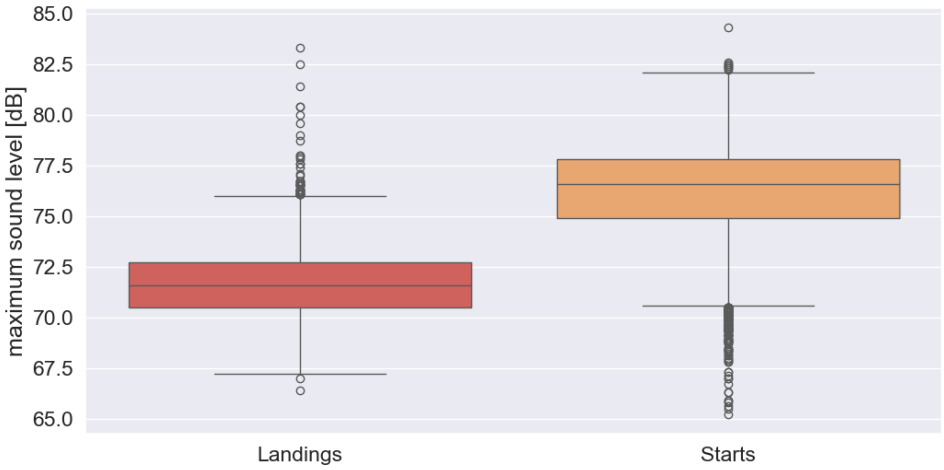


Figure 6.11.: Boxplot for NMT 11 grouped by starts and landings of the A320

## 6.4. Winglets

The A320 Neo aircraft have modern sharklets on their wings. These are approx. 2.5 m high and, according to the manufacturer, should ensure lower fuel consumption in flight [4]. The data set contains sufficient noise measurements for the ceo variants with conventional winglets and for the neo variant with sharklets. However, the $L_{\overline{P}}$ values of these two groups do not differ. Compared to parameters such as the distance to the receiver or the engine type, the winglets are negligible as parameters.

## 6.5. Dependencies of $L_{AS,max}$ at single stations

To further evaluate the importance of the multiple parameters on the sound pressure level we're going to look at several specific NMTs around the airport of Hamburg. First, we're looking at data from starts at NMT 11 Norderstedt, Reitstall Ohlenhoff which is located towards the north-west of the airport. It is situated right underneath the path of planes landing on runway 15 or departing on runway 33. As in chapter (5.3) we analyze the influence of parameters on the noise propagation in the atmosphere. We'll apply the Analysis of Variance method (ANOVA). In general, our target variable will be the maximum loudness $L_{AS,max}$ of a noise event. The data will be split into multiple groups for a specific parameter and the variance within the groups is compared with the variance among the groups. If the assumption of the ANOVA method is satisfied and the p-value is below the threshold of 0.05, then the null hypotheses $H_0$ that there is no difference between the groups will be rejected and a statistically significant effect of the parameter on the target variable can be concluded.

[4] https://www.airbus.com/en/products-services/commercial-aircraft/passenger-aircraft/a320-family

**Weather** Previous work has mainly investigated basic atmospheric variables such as temperature, wind direction, and speed [1]. As noted in chapter (2) aircraft noise prediction models such as PANAM consider a homogeneous atmosphere in the analysis. Effects such as sound refraction are not considered resulting in an overestimation of noise at long distances [18]. In a more recent version of PANAM from 2019 [17], the ambient humidity and temperature on the frequency-dependent atmospheric absorption coefficient, and effects such as refraction and scattering are considered. By supplementing the noise and flight data set with measurements of weather profiles from the Hamburg weather mast, it is possible to investigate these effects. While earlier works note that the weather is a small factor for outdoor sound propagation as we discussed in chapter (2) we note that weather parameters are significant when we look at single NMTs. The local setting can differ greatly due to circumstances like buildings, tree lines, hills, and other features of the landscape which affect the temperature and the wind. Therefore the local effect of atmospheric attenuation and sound refraction might differ when comparing NMTs. In this chapter, we'll study the difference in the magnitude of influence of the atmospheric effects for single NMTs.

The theory of atmospheric physics and outdoor sound propagation is explained in chapter (3). In this section, the measured data are analyzed using the influence of temperature gradients and various wind profiles. These values can vary greatly depending on the measuring point, time of year, and time of day. The figures (6.12), (6.13), (6.14), and (6.15) show the weather parameters wind speed, wind direction, and temperature at NMT 14 Lurup. The figures each show the development of the three parameters over the 14th of each month from 00:00 to 24:00. The wind direction (light blue crosses) largely stays approximately constant over the day. At NMT 14, wind directions between approx. 90° and 180° mean favorable downwind conditions. In December the wind seems to come more from this direction, while in June and September, the wind tends to come from the north, which leads to light upwind or cross-wind conditions. The wind speed (dark blue line) tends to increase from noon until the early evening hours. In spring and summer, the temperature (red line) seems to rise around 07:00 am, changing the negative sign of the temperature gradient of the night to a positive sign in the morning. This effect does not seem to be as pronounced in the cold months, as temperatures do not rise as much during the day.

**Wind: Comparison NMT 02 and NMT 03** For each overflight of an A320 landing at Hamburg airport, we measure one maximum sound level for the overflight $LAS_{max}[dB]$ at each NMT that is on the route of the aircraft. The time $TLAS_{max}[s]$ is where the sound level $LAS_{max}$ was measured is noted and used to look up the corresponding wind direction and speed at the NMT during that time.

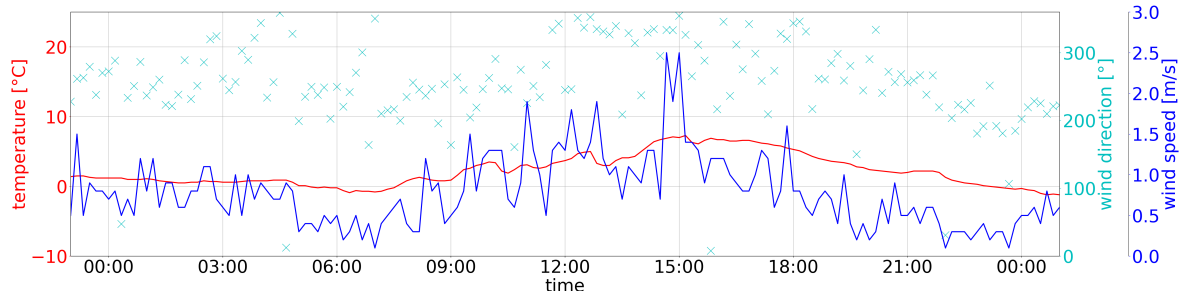


Figure 6.12.: Weather at NMT 14 Lurup, March 14th, 2023

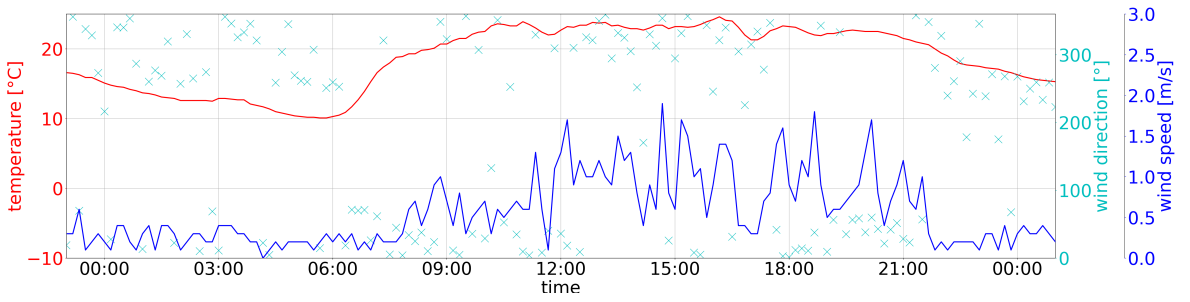


Figure 6.13.: Weather at NMT 14 Lurup, June 14th, 2023

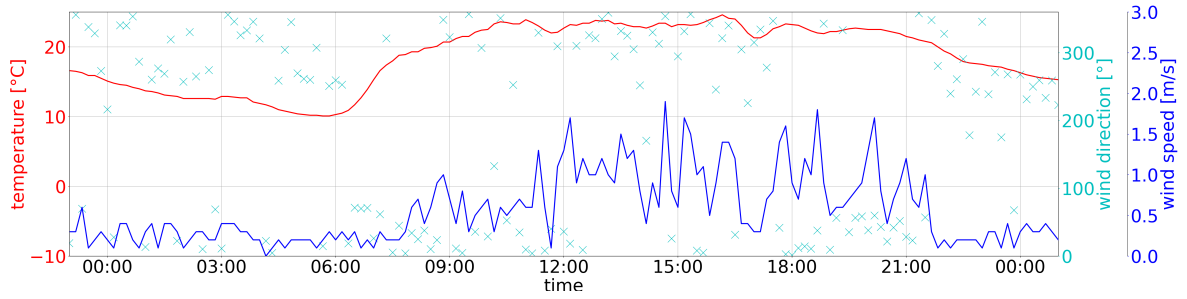


Figure 6.14.: Weather at NMT 14 Lurup, September 14th, 2022

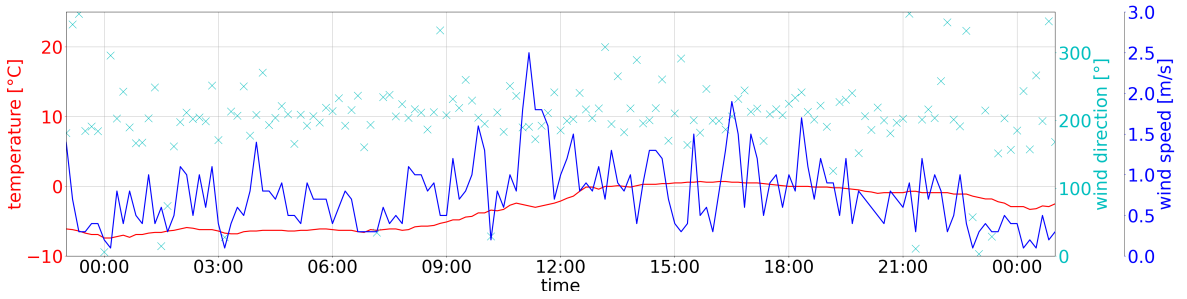


Figure 6.15.: Weather at NMT 14 Lurup, December 14th, 2022

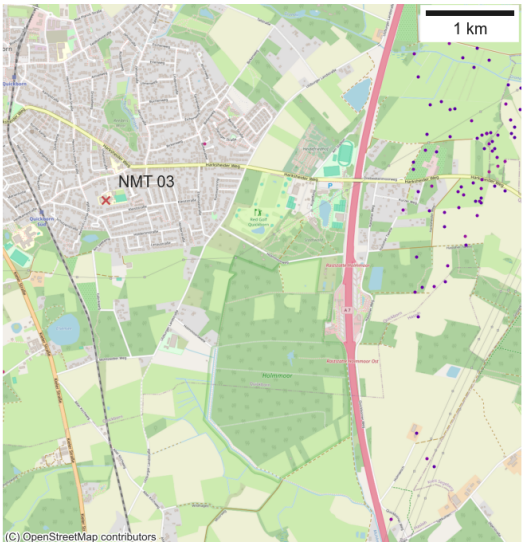


Figure 6.16.: NMT 03

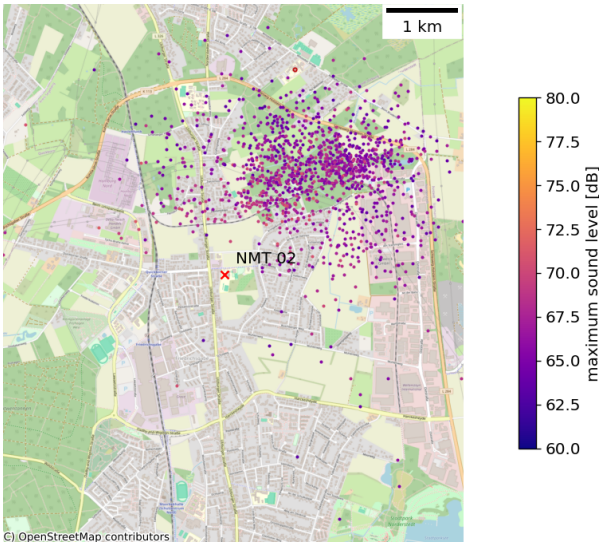


Figure 6.17.: NMT 02

Figure 6.18.: Positions of the aircraft at time $T_{Las,max}$ for NMT 03 (6.16) and NMT 02 (6.17) which are located in the north of the airport. For NMT 02 we see that the aircraft turns towards the east on this departure route while the aircraft passes NMT 03 on a north-south line.
The position data for this plot is matched exactly to the second to the corresponding noise measurement. The data set is therefore reduced to entries where we can join the two data sets exactly. Both plots share the same color bar where the color represents the value of $L_{AS,max}$.

The depicted departure route AMLUH1G is the main route for the time frame of August 2022 to August 2023. Using the extensive data from 46,604 departures for this specific path we try to derive the influence of the wind direction parameter on the measured noise at the two NMTs. Planes on this route usually stay to the north-east of NMT 02 Harkshörn, Grundschule while they're located east to NMT 03 Quickborn, Goethe-Schule. With this setup, we would expect the effect of the wind direction parameter to be directly opposed for the two measuring points if they would completely adhere to the theory. Therefore we formulate the null hypothesis that there is no significant effect of the wind direction on $L_{AS,max}$ at the NMTs. To test this hypothesis we separate the data into groups of 60° and again use the Analysis of Variance method to analyze the difference in means of these groups.

In Figure (6.21) we can see that the NMT 02 is slightly louder overall. If we look at figure (6.18), we see that the airplanes are much closer to NMT 02 at the time when the sound pressure level $L_{AS,max}$ occurs, $T_{Las,max}$, than is the case at NMT 03. In the case of NMT 03, it was impossible to assign as many time points of noise measurements exactly to the aircraft's position, which is why fewer position markers appear here. As the aircraft on the AMLUH1G route flies a right turn past NMT 03, the markings here are relatively scattered around the station.

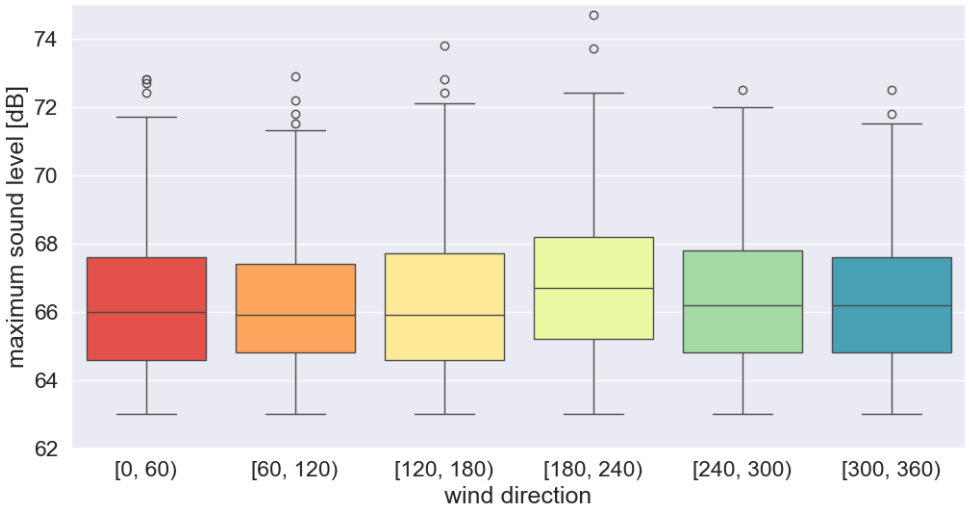


Figure 6.19.: NMT 02 wind direction boxplot

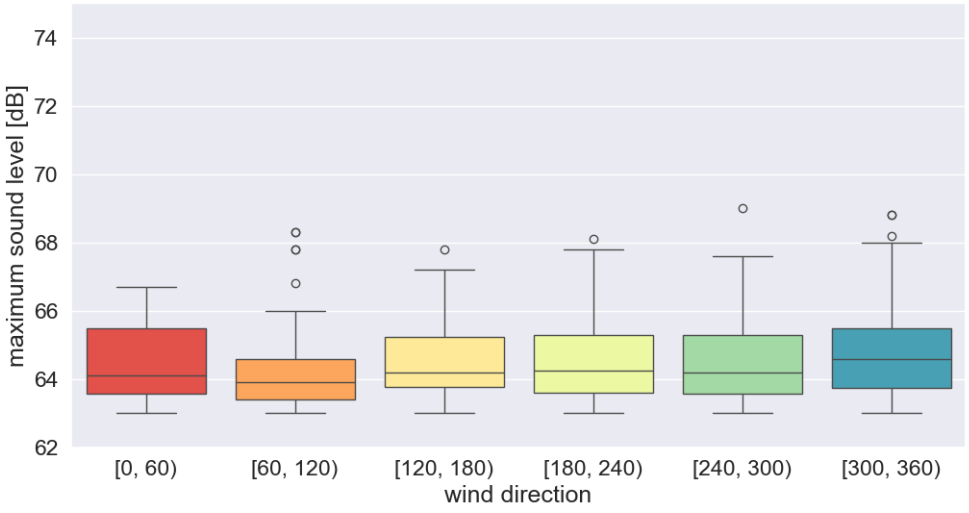


Figure 6.20.: NMT 03 wind direction boxplot

Figure 6.21.: Boxplot for NMT 02 and NMT 03 grouped by 60° wind direction intervals

Table 6.5.: ANOVA wind direction results for NMT 02 and NMT 03

| NMT 02 | $sum^2$ | df | $mean^2$ | F-value | p-value | $\eta^2$ | $\omega^2$ |
|---|---|---|---|---|---|---|---|
| C(wind direction) | 20.88 | 5.00 | 4.18 | 1.18 | 0.32 | 0.01 | 0.00 |
| Residual | 3338.27 | 942.00 | 3.54 | | | | |
| NMT 03 | $sum^2$ | df | $mean^2$ | F-value | p-value | $\eta^2$ | $\omega^2$ |
| C(wind direction) | 7.21 | 5.00 | 1.44 | 0.50 | 0.78 | 0.02 | -0.02 |
| Residual | 331.32 | 114.00 | 2.91 | | | | |

Table 6.6.: Wind direction statistics for NMT 02 and NMT 03

| | Variable | N | Mean | SD | SE | 95% Conf. | Interval |
|---|---|---|---|---|---|---|---|
| NMT 02 | value | 948.00 | 66.65 | 1.88 | 0.06 | 66.53 | 66.77 |
| NMT 03 | value | 120.00 | 64.59 | 1.69 | 0.15 | 64.29 | 64.89 |

If the wind comes from the direction of the NMT in comparison to the location of the airplane, i.e. the source is located upwind to the receiver, we expect a reduction in the measured noise emissions due to refraction [38]. Similarly, we expect an increase in the measured noise emissions when the wind comes from the direction of the aircraft, i.e. the source is downwind of the receiver [38]. To test this dependency, we divide the measured noise levels into groups of 60° intervals. The population $p_1$ contains all measurement in the interval [0°, 60°), population $p_2$ contains all measurement in the interval [60°, 120°), ..., and $p_6$ includes all measured values in [300°, 360°). We define the first null hypothesis $H_0$ that all population means are equal:

**Hypothesis 1:** $H_0$: $\mu_1 = \mu_2 = \mu_3 = \mu_4 = \mu_5 = \mu_6$

where $\mu_n$ for n $\in [1, 6]$ is the mean of the population $p_n$.

Table (6.6) shows the ANOVA table for both NMT 02 and NMT 03. For both NMTs, the p-value is not significant. Both $\eta^2$ and $\omega^2$ show that the effect sizes are negligible. The $\omega^2$ value is negative for NMT 03 in this case because the F-value is less than one. This result, together with the boxplots where we can see virtually no differences in the mean values between the wind direction groups, indicates that we cannot prove any dependence of the value $L_{AS,max}$ on the wind direction for these two measuring stations. One reason for this could be that the routes during take-off differ much more than is the case during landings. The distance from the NMT is a decisive factor. However, the variance of this parameter in the measurement data is very large, which can also be seen in figure (6.18). Another reason for NMT 02 could also be that the NMT is located in the middle of a curve in the departure route and the aircraft are therefore in many different directions. The wind direction as a simple parameter is then no longer sufficient. A consideration of the wind direction component in the direction of sound propagation for each aircraft would be necessary here.

Figure 6.22.: NMT 02 wind direction residuals QQ-plot (left), and histogram (right)

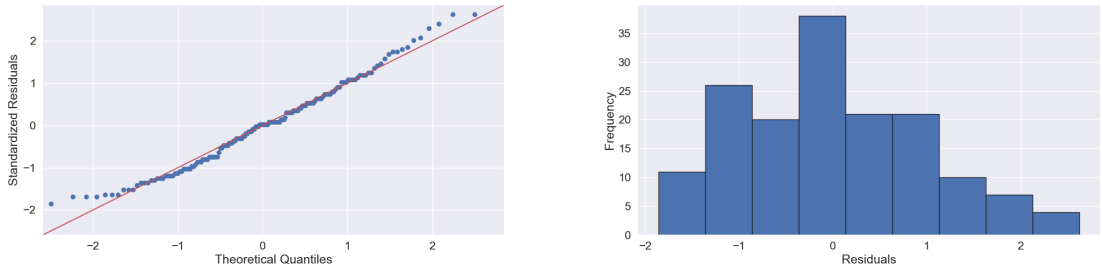


Figure 6.23.: NMT 02 wind direction residuals QQ-plot (left), and histogram (right)

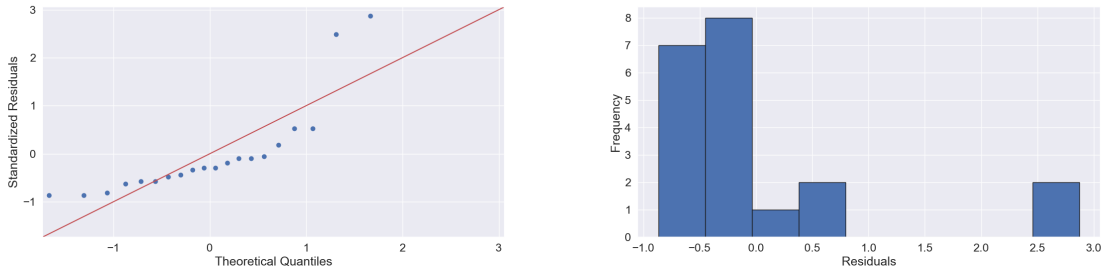


When considering weather parameters, it is therefore important to take local conditions such as topography and departure or approach routes into account.

We perform the Shapiro-Wilk test for normality on the normalized residuals. These equal the normalized differences between each element and the column mean where the columns represent the grouped wind direction intervals. The Shapiro-Wilk test results in significant p-values for both NMTs. Therefore, we reject the null hypothesis that the data is sampled from data following a normal distribution. However, the residuals for NMT 02 seem normally distributed with a heavy tail when we visually look at them with a quantile-quantile plot or a histogram. The residuals for NMT 03 however don't seem to be normally distributed looking at the quantile-quantile plot and the histogram. We conclude that the results from parametric methods such as the ANOVA are not reliable.

To test the homogeneity of variance assumption we perform the Levene test (see chapter 5) for unequal variances. We test the null hypothesis that the population variances are equal. Both for NMT 02 and NMT 03 the p-values are well above 0.05 and therefore not significant. We keep the null hypothesis that the variances between the wind direction intervals are equal.

Table 6.7.: Levene test for NMT 02 and 03 residuals

| | Parameter | NMT 02 | NMT 03 |
|---|---|---|---|
| 0 | Test statistics (W) | 0.42 | 0.56 |
| 1 | Degrees of freedom (Df) | 5.00 | 5.00 |
| 2 | p-value | 0.83 | 0.73 |

**Temperature gradients** In this paragraph, we want to analyze and compare the influence of the atmosphere on sound propagation at the NMT 14 Lurup. This NMT is located in the south-west of the airport. Therefore, planes that either start on runway 23 or land on runway 05 will fly over this station. Again, we only consider the Airbus A320 aircraft type and we'll use data from starts and landings of this aircraft separately.
We want to focus on the effect of temperature gradients in the atmosphere but also look at the influence of the wind again. The equation for the sound speed (3.2) in the atmosphere shows that a higher temperature will lead to a higher sound speed. If we consider an inhomogeneous atmosphere we see that the temperature generally decreases with height until we reach the tropopause at a height of around 15km. However, in the ABL, sometimes temperature inversions occur as can be seen in the temperature profile plot from the weather mast in Hamburg (6.25). The temperature gradients lead to vertical sound speed gradients, where a positive gradient $\frac{dc_{eff}}{dz} > 0$ leads to downward refraction of the sound waves and a negative gradient $\frac{dc_{eff}}{dz} < 0$ leads to upward refraction of the sound waves.

Taking temperature gradients into account when calculating the influence on noise is difficult because the airport's NMTs only measure the temperature directly above the ground. The weather mast at the University of Hamburg measures the temperature at various heights between 2m and 280m. However, it is located at a distance of approx. 14.5 km from the airport. Therefore, we must first determine whether and to what extent we can use the measured values from the weather mast to investigate noise immissions in the vicinity of NMT 14 Lurup, which is located at a distance of approx. 16.15 km from the weather mast.
The vertical temperature gradient for a given height is the difference of the temperature measurement above the given height $T(h_i)$ minus the temperature measurement below the given height $T(h_r)$ divided by the distance between $h_i$ and $h_r$ in meters:

$$\frac{dT}{dz} = \frac{T(h_i) - T(h_r)}{h_i - h_r} \tag{6.2}$$

With equation (6.2) we compute the temperature gradient for all heights [10m, 50m, 70m, 110m, 175m, 250m]. For each of these altitudes, we divide the measured values into three populations: negative temperature gradient $_1$, no temperature gradient $p_2$, and positive temperature gradient $p_3$.

We define the null hypotheses $H_0$ that all population means are equal:

**Hypothesis 2:** $H_0$: $\mu_1 = \mu_2 = \mu_3$

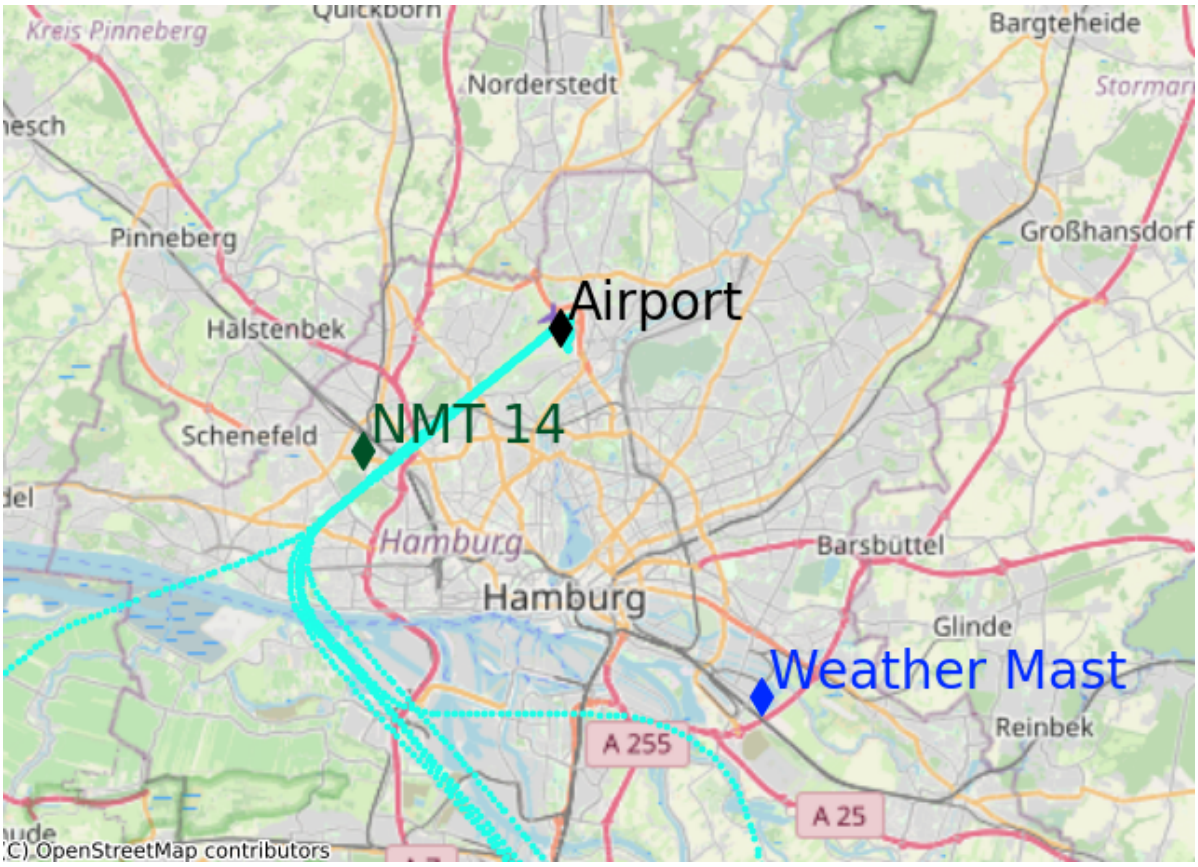


Figure 6.24.: Departure and arrival routes for NMT 14 Lurup

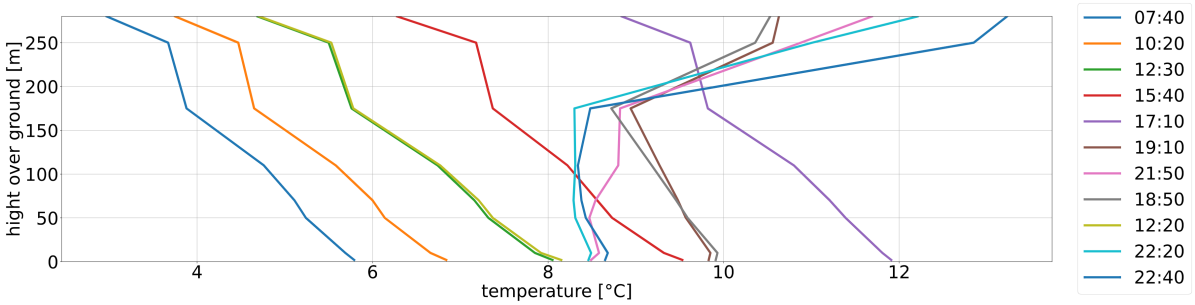


Figure 6.25.: Temperature profiles measured at the Weathermast Hamburg on April 20th, 2023 measured at 2m, 10m, 50m, 70m, 110m, 175m, 250m and 280m. During the day we observe a negative temperature gradient (orange and green lines), whereas in the evening and at night we observe positive temperature gradients (pink and light blue lines).

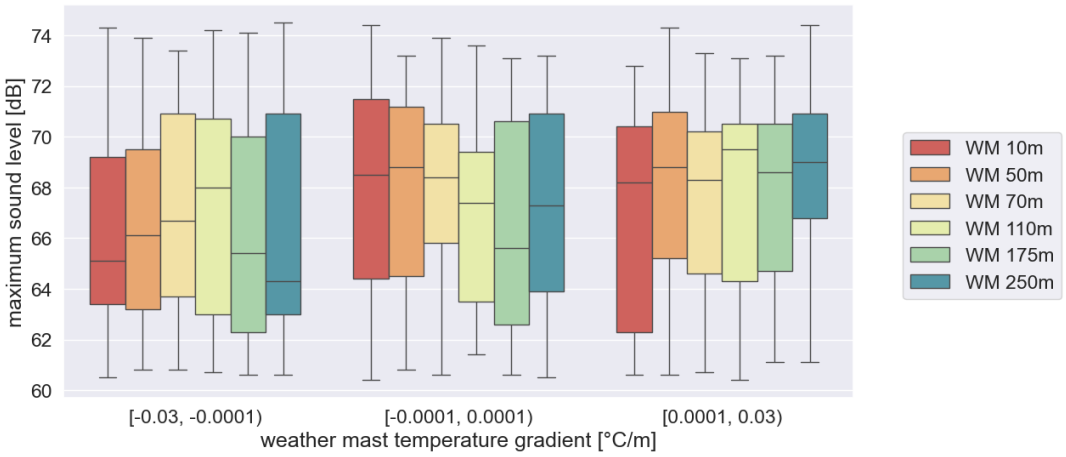


Figure 6.26.: Boxplot for NMT 14 Lurup grouped by temperature gradient

where $\mu_n$ for n $\in [1,3]$ is the mean of the population $p_n$.

Figure (6.26) shows the boxplot for each of the three temperature gradient groups for each altitude for which we can calculate a temperature gradient. In general, we can observe the trend that the maximum sound level increases when we go from a negative temperature gradient to a positive temperature gradient. A color represents a certain height of the weather mast and its temperature gradient. For all heights, we see that the $L_{AS,max}$ values increase from left to right. The lowest values for all heights are at negative temperature gradients. The highest values, on the other hand, are for positive temperature gradients at all heights. According to the theory (3), we expect that with a negative temperature gradient, the sound is refracted away from the ground and sound shadow zones are created. The boxplot seems to confirm this based on the measured values.

The sum of squares ($sum^2$ column) for entries where the p-value is $> 0.05$ is noticeably larger, is because the value shows the sum of squared differences between the observed dependent variables and the overall mean. A high p-value indicates that there are no significant differences between the means of the groups. Therefore, the value tends to be small when the means of the groups don't differ significantly.

For each height (except the lowest height of 2m and the highest height of 280m, because the calculation of a gradient is not possible here) we calculate the p-value and the effect size in the table (6.8). We observe that the p-value is only significant for the two gradients at 175m and 250. Also, $\eta^2$ and $\omega^2$ show medium effect sizes of 0.06 in these two cases. Since the ANOVA does not yet tell us how exactly positive and negative gradients differ, we carry out a post-hoc test in the next step. Since the p-values for the heights $10m, 50m, 70m,$ and$110m$ are not significant, only $175m$ and $250m$ are considered. One reason for this could be that the atmospheric conditions near the ground at the weather mast and the NMT differ more than is the case above 150m.

At an altitude of 175m, the noise level increases by an average of 2.36 dB between a negative and positive temperature gradient. With a p-value of 0.01, the statement is meaningful. The

Table 6.8.: ANOVA Table Resulted from the categorization into temperature gradients where $n = 394$ for each group $[-2.00, 0.01)\frac{^{\circ}C}{100m}$ and $[0.01, 3.00)\frac{^{\circ}C}{100m}$

| | sum$^2$ | df | mean$^2$ | F-value | p-value | $\eta^2$ | $\omega^2$ |
|---|---|---|---|---|---|---|---|
| C(temp. grad. 10m) | 37.02 | 2.00 | 18.51 | 1.17 | 0.31 | 0.02 | 0.00 |
| Residual | 2094.42 | 132.00 | 15.87 | | | | |
| C(temp. grad. 50m) | 7.48 | 2.00 | 3.74 | 0.30 | 0.74 | 0.00 | -0.01 |
| Residual | 1633.12 | 132.00 | 12.37 | | | | |
| C(temp. grad. 70m) | 30.45 | 2.00 | 15.23 | 1.09 | 0.34 | 0.02 | 0.00 |
| Residual | 1838.25 | 132.00 | 13.93 | | | | |
| C(temp. grad. 110m) | 1.59 | 2.00 | 0.79 | 0.06 | 0.94 | 0.00 | -0.01 |
| Residual | 1835.57 | 132.00 | 13.91 | | | | |
| C(temp. grad. 175m) | 152.37 | 2.00 | 76.19 | 4.78 | 0.01 | 0.07 | 0.05 |
| Residual | 2102.79 | 132.00 | 15.93 | | | | |
| C(temp. grad. 250m) | 153.57 | 2.00 | 76.78 | 5.19 | 0.01 | 0.07 | 0.06 |
| Residual | 1954.58 | 132.00 | 14.81 | | | | |

Table 6.9.: Tukey HSD for temperature gradients at NMT 14

| | groups $\left[\frac{^{\circ}C}{100m}\right]$ | mean difference | std error | t-value | p-value | 95 % CI lower CI | 95 % CI upper CI |
|---|---|---|---|---|---|---|---|
| 10m | - | - | - | - | > 0.05 | - | - |
| 50m | - | - | - | - | > 0.05 | - | - |
| 70m | - | - | - | - | > 0.05 | - | - |
| 110m | - | - | - | - | > 0.05 | - | - |
| 175m | (-0.01, 0.01) : (0.01, 3.00) | 2.13 | 0.60 | 2.51 | 0.04 | 5.50 | -1.25 |
| | (-3.00, -0.01) : (0.01, 3.00) | 2.36 | 0.57 | 2.92 | 0.01 | 5.73 | -1.01 |
| 250m | (-3.00, -0.01) : (0.01, 3.00) | 2.61 | 0.57 | 3.26 | 0.00 | 5.99 | -0.76 |

Table 6.10.: Levene test for temperature gradients residuals

| | Parameter | 10m | 50m | 70m | 110m | 175m | 250m |
|---|---|---|---|---|---|---|---|
| 0 | Test statistics (W) | 0.05 | 0.07 | 0.47 | 0.01 | 1.08 | 0.99 |
| 1 | Degrees of freedom (Df) | 2.00 | 2.00 | 2.00 | 2.00 | 2.00 | 2.00 |
| 2 | p-value | 0.95 | 0.94 | 0.62 | 0.99 | 0.34 | 0.37 |

values for 250m are similar. Here it gets louder by 2.61 dB on average with a p-value of 0.00. The group no gradient - positive gradient is also in the 2 dB range, but with a higher p-value of 0.04. Overall, we observe that a positive temperature gradient is audibly louder. This result is in line with theory, as we expect the sound to be refracted towards the colder ground in this case.

Finally, we examine whether the assumptions of the ANOVA are fulfilled and whether our results are reliable. In figure (6.33) we see the standardized residuals of the temperature gradients for each investigated altitude. The quantile-quantile plots for 10m and 175m look a bit curved, like an S. This could indicate that the tails of the distribution are a bit heavier than a standard normal distribution but it could also just be a normal distribution skewed by randomness. However, this should have less impact on mean-referenced analyses.

Finally, the homoscedasticity of the standardized residuals is tested using the Levene test. We see that for all groups the p-value is greater than 0.05 and therefore not significant. We do not reject the null hypothesis and stick to the assumption that the variances of the groups are equal.

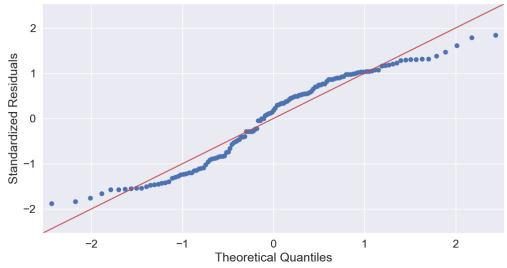


Figure 6.27.: 10m

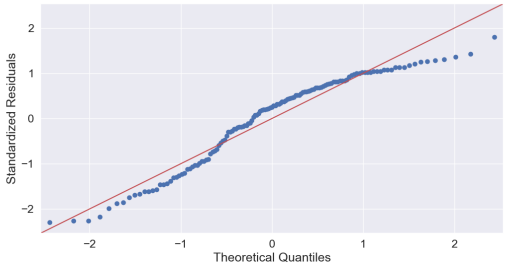


Figure 6.28.: 50m

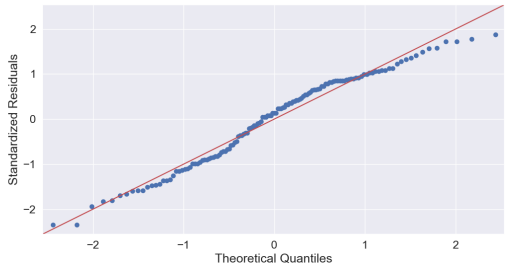


Figure 6.29.: 70m

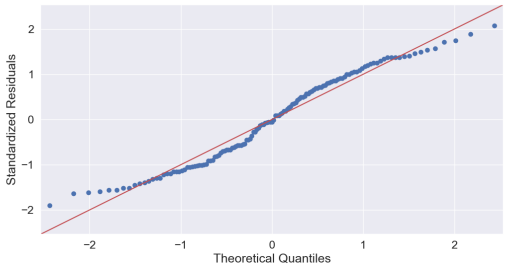


Figure 6.30.: 110m

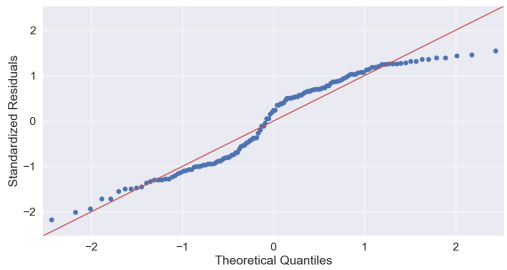


Figure 6.31.: 175m

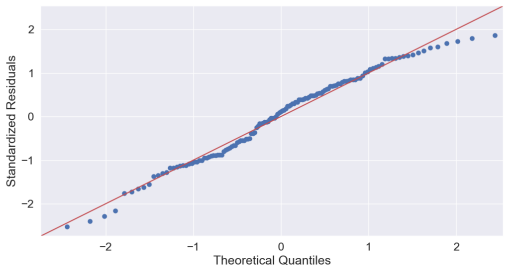


Figure 6.32.: 250m

Figure 6.33.: NMT 14 QQ-plots for all measured temperature gradients standardized residuals

**Upwind/Downwind** Vertical gradients in the effective sound speed given by equation (3.5) govern the refraction of sound waves. In this chapter, we'll focus on the horizontal wind component $Vcos(\alpha)$ in this equation. We'll quantify its effect on the mean maximum sound level in decibels for starts and landings on runway 33/15. The angle $\alpha$ describes the angle between the wind and the direction of sound propagation in (3.5). We keep the definition of $\alpha$ from the HARMONOISE project [29]. The wind direction is the direction from which the wind is blowing. The position of 0° is north, 90° is east, and so on. Contrary, the sound direction is the direction to which the sound propagates, again with 0° north. We'll illustrate the semantics with an example: The observer is looking at the airplane to the west at 270°. In this case, the sound propagates to 90° east. The wind is blowing from the direction of the airplane at 270° into the face of the observer. For $\alpha$ we get $270° - 90° = 180°$. In equation (3.5) we get a positive sign for the horizontal wind component. With a look at table 6.11 we are in the downwind scenario and would expect more noise from the airplane at the position of the observer due to refraction.

**Methodology** To compute the angle $\alpha$ between the wind direction and the direction of sound propagation $\gamma$ we need the position of the airplane relative to the microphone at the NMT. The wind speed and direction are directly measured at NMT 11 Norderstedt, Reitstall Ohlenhoff some meters above the ground. The position of the aircraft is determined by the radar from the airport. The time $TLAS_{max}$ where the maximum sound level $LAS_{max}$ is measured is noted. For each noise measurement at NMT 11, we look up the position in latitude and longitude at the time $TLAS_{max}$. For the calculation of the angle between the airplane and the NMT about 0° N it is assumed that the ground is a flat plane. The error regarding the calculation of the angle introduced by this assumption is negligible because of the small distances between the aircraft and the NMT. The arctangent function is used to calculate the angle between the aircraft and the NMT. In Python the function *math.atan2(y, x)* calculates the angle in radians between a point (x,y) and the center (0,0) starting from the x-axis rotating counterclockwise. The NMT is assumed to be at position (0,0) with x being the longitude and y being the latitude. The difference $dx$ in longitude and latitude $dy$ between the aircraft and the NMT is used as point (x,y) for atan2(dy, dx).

$$\begin{aligned} dx &= \text{aircraft.longitude} - \text{NMT.longitude} \\ dy &= \text{aircraft.latitude} - \text{NMT.latitude} \end{aligned} \tag{6.3}$$

To get a distance in meters the coordinate reference system (CRS) is transformed to the WGS 84 Web Mercator projection (EPSG identifier 3857) before making the calculations. The angle between the x-axis and the point is converted to the angle starting at 0° N rotating clockwise.

```
(90 - math.degrees(math.atan2(dy, dx))) % 360.
```
(6.4)

The result is angle $\gamma$ in degrees between the aircraft and the NMT with 0° in the north as a point of reference. Therefore, this angle represents the angle from which the sound is coming from the point of view of the microphone at the NMT. To get the direction to which the sound

is traveling we add $\gamma^{'} = (180^{\circ} + \gamma) \mod 360^{\circ}$. With the direction of sound propagation angle $\alpha$ between the wind direction is calculated.

| wind class | u(z = 10m) | |
|---|---|---|
| V1 | < -10 m/s | upwind |
| V2 | -10 ... - 6 m/s | |
| V3 | -6 ... - 3 m/s | |
| V4 | -3 ... - 1 m/s | |
| V5 | -1 ... + 1 m/s | crosswind or no wind |
| V6 | +1 ... +3 m/s | downwind |
| V7 | +3 ... +6 m/s | |
| V8 | +6 ... +10 m/s | |
| V9 | >10 m/s | |

Table 6.11.: European HARMONOISE project [29] upwind/downwind classes V1 to V9 and according to wind components u at 10m above ground in the direction of sound propagation.

Noise measurement and radar data from the time frame 01.08.2022 - 31.08.2023 were matched with a database-like inner join using the combination of the flight ID and $TLAS_{max}$ as a common key pair. For class V2 we get 10 flights, for class V3 110 flights, for class V4 375 flights, for class V5 570 flights, for class V6 672 flights, for class V7 358 flights, for class V8 21 flights and for class V9 98 flights that could be matched with an accuracy of 1s to position data. $LAS_{max}$ and distance-to-NMT values below the 1 %-quantile and above the 99 %-quantile are removed as outliers. This is done to remove exceptional or incorrect data from the set, i.e. cases where the microphone measured noise above 100 dB. Such a value could only be measured if the A320 flew directly over the microphone which is highly irregular for airliner operations. Measurements from classes V2 and V8 (very strong upwind/ very strong downwind) are also removed because there are not enough values to make meaningful conclusions.

**Results** It is essential for aircraft operations that they start and land against the wind to increase lift. In figure 6.37 we can see that the wind during a landing typically comes from a southeast direction directly against the direction of the airplane. From the point of view of NMT 11 Norderstedt, Reitstall Ohlenhoff the sound mainly comes from the southwest (6.38) since the station is located to the northeast of the glide path.

Landings and starts of aircraft need to be looked at separately (see chapter 5.3.) because the measured sound levels differ vastly. The difference in sound levels makes it difficult to distinguish meteorological influences. For this reason, the data set is separated into landings on runway 15 and starts on runway 33. Runway 15 and Runway 33 are the same physical

runway, only the direction of operation differs. Aircraft on runway 15 land in a direction of 150° and aircraft on runway 33 start in a direction of 330°. For the landings, we have 98 values for both the up- and downwind class that are sampled from the population. All values are from A320-200 variants, namely the A3202 (without winglets) and the A320A (with winglets) type. Aircraft on an instrument approach generally follow a 3-degree glide slope toward the runway. In figure (6.35) we can see that almost all of the positions during time $TLAS_{max}$ are on this glide slope close to the NMT.


Figure 6.34.: starts

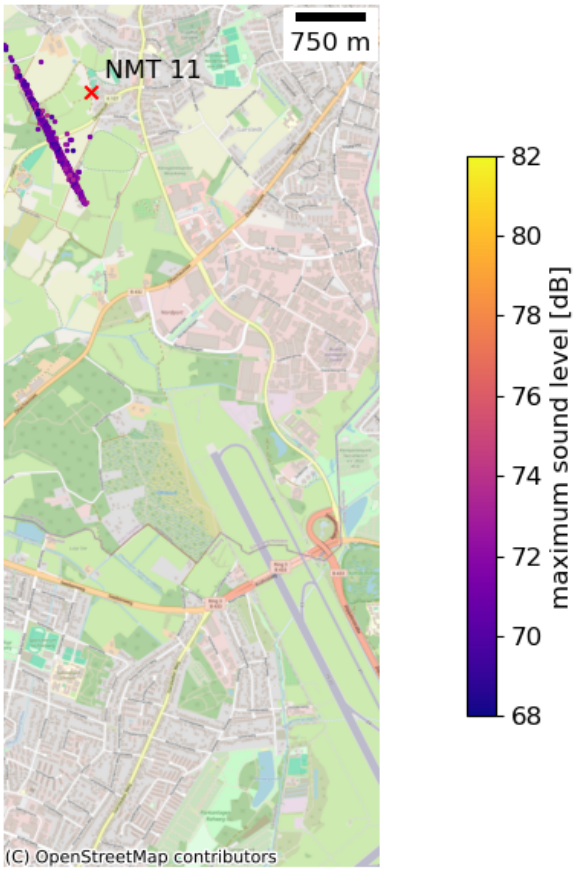


Figure 6.35.: landings

Figure 6.36.

We observe that starts in figure (6.34) and landings in figure (6.35) are very distinguishable from two characteristics. First, the position of the aircraft during starts is much more distributed in space. This can be explained by the strict procedures that planes have to adhere to during the approach. Both vertical and horizontal positions are predetermined by the glide slope given by the instrument landing system. During departure, there is no such requirement. Depending on the weight and take-off performance the aircraft can make a relatively quick turn towards either side. The height during departures also vastly varies due

to aircraft weight even when we only look at Airbus A320 aircraft variants. Not all flights are fully booked or the aircraft might not be fully loaded with freight. Second, the measured maximum sound level also vastly differs due to the aforementioned reasons. A difference of around 5 dB between starts and landings can be measured on average at this NMT, see figure (6.11)
We aim to filter out the influence of meteorology on the measured noise level at the NMT. Since measured noise levels and parameters such as aircraft weight, distance to the NMT, and altitude vary greatly during take-off, this goal is difficult to achieve when we look at data from take-offs. Meteorology has a comparatively small influence on noise compared to the other parameters. The analysis of variance for data from departures shows that the wind classes have no statistically significant influence on the mean values of the maximum measured sound level of the groups.

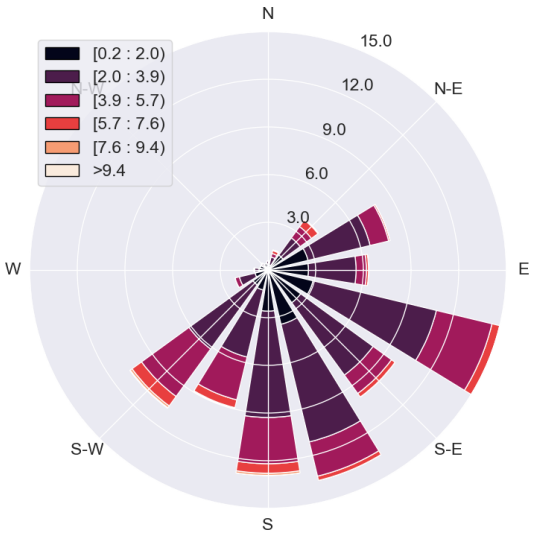


Figure 6.37.

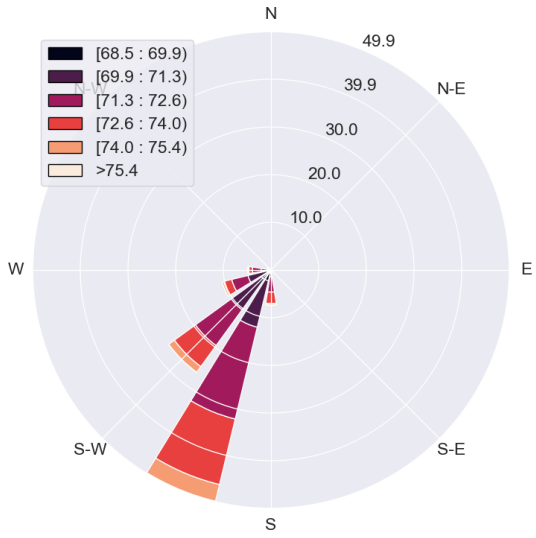


Figure 6.38.

Figure 6.39.: (6.37) wind direction [°] and wind speed [m/s] measured at NMT 06 for landings on runway 15
(6.38) direction from which the sound comes [°] from the point of view of NMT 11 and measured maximum sound level [dB] at the NMT

We plot the wind rose from wind data measured at NMT 06 Lufthansa Werft. The NMT is exactly located at 53°37′25.5"N, 9°59′08.4"E next to the Lufthansa Technik base at the airport. Wind direction and wind speed are measured by NMT 06 and used for this NMT, see NMT list (4.1). For each wind direction in degrees, the value of the corresponding wind speeds is drawn in figure (6.37). The length of the bar represents the total number of measurements for that direction. The colors distinguish the different wind speed intervals. In figure (6.37) we do the same but for $LAS_{max}$ measurements. Mathematically the direction of sound propagation

is the direction to which the sound travels. However, this plot shows the sound propagation from the point of view of the NMT. Therefore, plot (6.38) shows the direction from which the sound is coming towards the NMT. We expect the sound to increase if the sound and wind come from the same direction and we expect the sound to decrease if the wind comes from the opposite direction. If the airplane lands on Runway 33 and we measure an N-E cross wind we expect the noise to be minimal at the NMT for instance. A series of statistical tests will be performed to test of hypothesis on measured data.

We define the null hypothesis $H_0$ that we test. All population means of the noise measurements of the up/downwind classes are equal for noise measurements from A320 landings on runway 15 measured at NMT 11 Reitstall Ohlenhoff. The populations $p_{Vn}$ are defined as the maximum sound level measurements grouped into up/downwind classes.

**Hypothesis 3:** $H_0$: $\mu_{V3} = \mu_{V4} = \mu_{V5} = \mu_{V6} = \mu_{V7} = \mu_{V9}$

where $\mu_{Vn}$ for n $\in 3, 4, 5, 6, 7, 9$ is the mean of the population $p_{Vn}$.

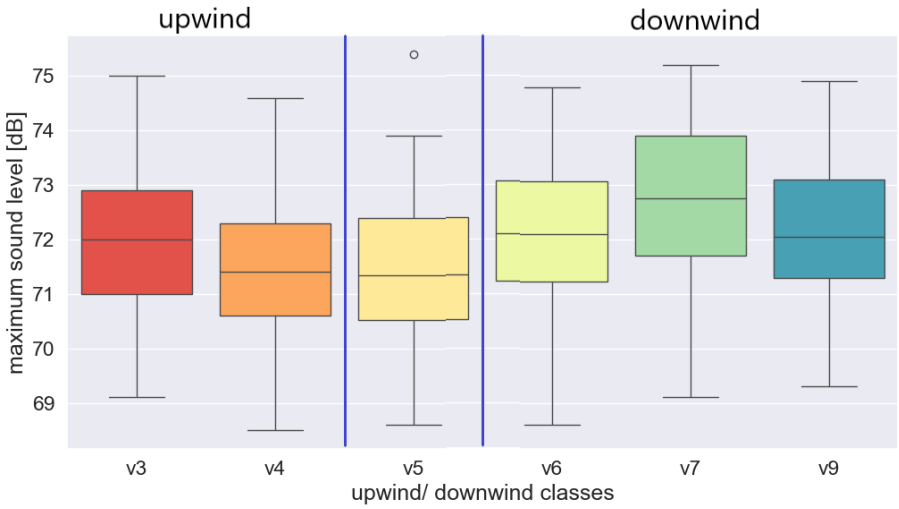


Figure 6.40.: Boxplot for NMT 11 Norderstedt, Reitstall Ohlenhoff maximum sound levels [dB] grouped by up/downwind classes V3-V7, V9

The boxplot (6.40) shows the distribution, locality, and outliers for the various upwind and downwind classes. For the range V4 - to V7, i.e. light upwind to medium downwind, we see an increase in the noise level. According to theory, we would also expect the immissions at the receiver to be louder when sound and wind come from the same direction. The boxplot seems to confirm this for the measured values. Only the groups v3 (medium strong upwind) and v9 (very strong downwind) break the trend a little. One possible reason for this could be that there are relatively few measured values for these very high wind speeds. This means that it is not as easy to obtain representative data from the measurements by sampling since the number of samples is low.

Table 6.12.: ANOVA Table Resulted from the categorization into up/downwind classes at NMT 11

| | $sum^2$ | df | $mean^2$ | F-value | p-value | $\eta^2$ | $\omega^2$ |
|---|---|---|---|---|---|---|---|
| C(up/downwind class) | 111.37 | 5.00 | 22.27 | 12.64 | 0.00 | 0.10 | 0.09 |
| Residual | 1025.71 | 582.00 | 1.76 | | | | |

In the next step, we run the ANOVA again to test whether there are significant differences in the mean value of the wind classes. With a p-value of 0.00, there is a statistically significant difference, therefore we reject the null hypothesis that the group means are the same. The effect size, indicated by $\eta^2$ and $\omega^2$, is medium to high at 0.09 - 0.10. We now use a posthoc test to determine which groups and by how many decibels they differ.

Table 6.13.: Tukey HSD for up/downwind classes at NMT 11

| | pairwise group comparisons | mean difference | std error | t-value | p-value | 95 % confidence interval lower CI | upper CI |
|---|---|---|---|---|---|---|---|
| 1 | V3 : V5 | -0.56 | 0.13 | 3.00 | 0.04 | -1.10 | -0.04 |
| 3 | V3 : V7 | 0.71 | 0.14 | 3.56 | 0.00 | 0.18 | 1.23 |
| 6 | V4 : V6 | 0.65 | 0.13 | 3.51 | 0.00 | 0.13 | 1.17 |
| 7 | V4 : V7 | 1.22 | 0.14 | 6.23 | 0.00 | 0.70 | 1.74 |
| 8 | V4 : V9 | 1.22 | 0.13 | 4.03 | 0.00 | 0.8 | 1.74 |
| 9 | V5 : V6 | 0.69 | 0.13 | 3.65 | 0.00 | 0.17 | 1.22 |
| 10 | V5 : V7 | 1.26 | 0.14 | 6.30 | 0.00 | 0.74 | 1.79 |
| 11 | V5 : V9 | 0.77 | 0.13 | 4.16 | 0.00 | 0.23 | 1.32 |

In the table (6.13) the pairwise comparisons of the up/downwind classes for Tukey's HSD test (equation 5.13) are shown. Only pairs with a significant p-value (< 0.05) are shown. Overall, the mean differences are in the range of 0.6 - 1.3 dB. Differences in the sound pressure level of approx. 1 dB are audible, so the differences are relatively small. However, if we look at pairs of strong downwind and strong upwind the difference can be particularly pronounced. For the pair V4-V7 the 95% confidence interval is $[0.70, 1.74]$. In summary, it can be said that at least at NMT 11 wind speeds from -3 m/s to 3 m/s have hardly any influence on the perceived noise. However, the results indicate that strong wind conditions have a noticeable influence on the noise. It should be added that very little data is available for the extreme wind classes V1 and V9. This is partly because these wind speeds do not occur so often, but also due to the bias that flight operations are only possible to a limited extent or not at all at such high wind speeds, and therefore no noise measurements are available. However, these cases in particular would be interesting for an investigation concerning noise, as the strongest effects due to refraction would be expected here.

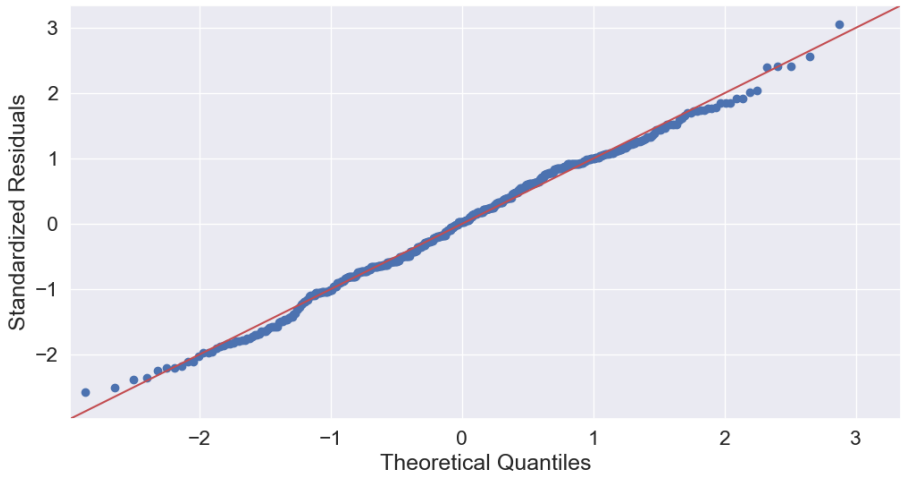


Figure 6.41.: QQ-plot comparing standardized $LAS_{max}$ residuals from NMT 11 landing measurements to a theoretical normal distribution

The standardized residuals of the noise measurements grouped by wind class are first compared in a quantile-quantile plot with a theoretical normal distribution to test the ANOVA assumptions. We can see that the data are normally distributed. The homogeneity of the variances is tested using the Levene test on the standardized noise measurement regressions. With a very clear p-value of 0.99, we don't reject the null hypothesis that there is equality of variance. The assumptions of the ANVOA are thus given and the results should therefore be reliable.

Table 6.14.: Levene test for temperature gradient residuals

| | Parameter | Value |
|---|---|---|
| 0 | Test statistics (W) | 0.07 |
| 1 | Degrees of freedom (Df) | 4.00 |
| 2 | p-value | 0.99 |

# 7. Feature Selection for the Prediction of Noise

After we first built a model from the measurement data in the last chapter and performed statistics according to the model, we now go one step further and make predictions about $L_{AS,max}$. We are particularly interested in the importance of meteorological parameters in the prediction of noise compared to non-meteorological parameters such as distance. We want to answer the following research questions:

- How can we predict noise measurements of overflights or noise events?
- Which data do we need for that?
- Can we filter out the influence factors of the weather on the measurements with AI methods?

AI methods such as neural networks are often used for the prediction of time series or regression and classification. The major disadvantage of these or similar methods is that the results are no longer reproducible in retrospect. We cannot say exactly which parameters are related and how, and how the network decided to link the parameters in a certain way. Our research questions are aimed precisely at these issues. We want to understand exactly what effect meteorology has. In addition to the prediction of noise, it is also of interest which weather constellations lead to a prediction no longer being possible, e.g. whether particularly humid air or rapidly changing wind directions could lead to less accurate predictions.

For these reasons, the random forest model from Breiman et al. [39] is used for this chapter. A random forest model is an ensemble of decision trees. The target variable $L_{AS,max}$ is calculated in a regression method. In regression, each decision tree is given a different sampled subset of the data set. The trees are formed by supervised learning so that we receive a value from each tree. The prediction is found by averaging the output of the decision trees. A similar approach was used by Iannace et al. [40] in relation to the noise prediction of wind turbines.

The data set used for the random forest model is the data set from NMT 11 Norderstedt, Reitstall Ohlenhoff. In contrast to earlier chapters, the data set here is explicitly not divided into take-offs and landings. It is important to note, however, that the parameter "Start" [True/False] is not included in the set of parameters as a categorical variable. As we have seen in the previous chapters, this parameter is very meaningful. We test if the machine learning model can identify and use it to make predictions.

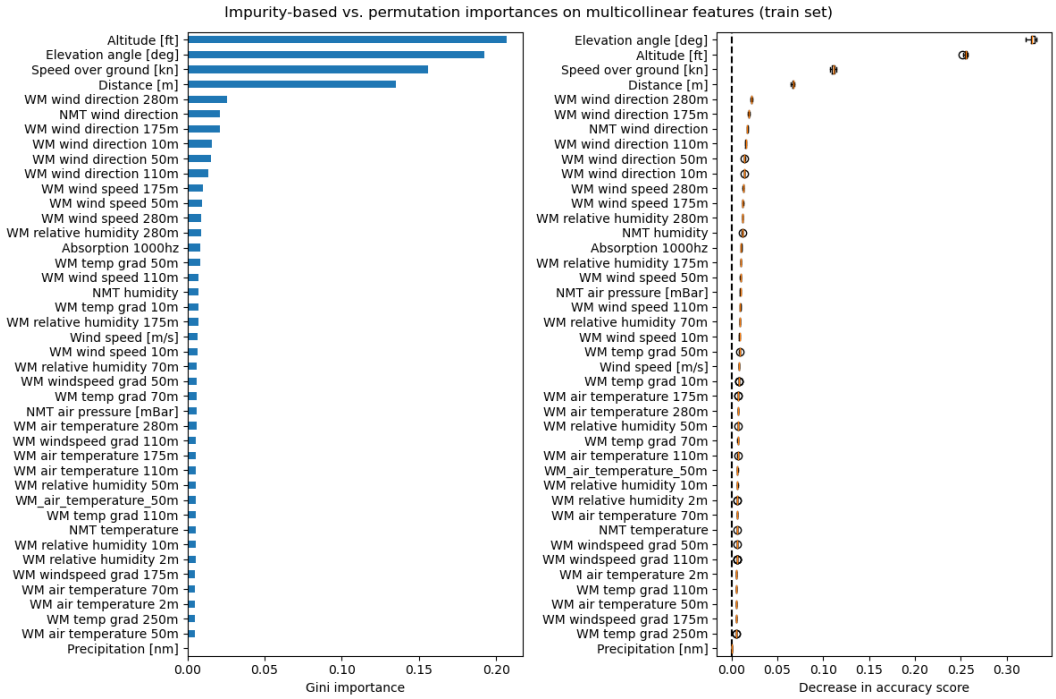


Figure 7.1.: Impurity-based vs. permutation importances A320 NMT11 measurements

## 7.1. Impurity-based and permutation importance

The **permutation importance** is a possible metric to evaluate the influence of a parameter on the performance of the model. When we calculate the permutation importance for a single parameter we randomly permutate its values and observe the change of the score of the model or how much it degrades. By randomly shuffling a parameter. By doing this we can better observe the relationship of the two. It is important to note that permutation importance does not reflect the predictive value of a parameter but rather how important it is for a certain model. The value of the permutation importance can be between -1 and 1. Negative values indicate that the model would become more accurate if we remove a parameter.

The permutation importance $PI$ for each parameter $j$ in scikit-learn [1] is defined as

$$PI_j = s - \frac{1}{K}\sum_{k=1}^{K} s_{k,j} \tag{7.1}$$

where for each repetition $K$, we randomly shuffle the values of parameter $j$ to generate an altered version of the data set, on which we compute the score $s_{k,j}$ and subtract it from the reference score $s$.

The measurements of meteorological parameters, such as the measurement of temperature at different altitudes, are highly collinear features. When we consider collinear parameters

[1] https://scikit-learn.org/stable/modules/permutation_importance.html#permutation-importance

such as the temperature at the heights $175m$ and $250m$ and shuffle one of them to calculate the permutation importance, the models tend to assign little predictive value to either one of the parameters as it can always get the same information from the other collinear parameter. In figure (7.1) we see that the permutation-based feature importance evaluation drops the accuracy by more than 0.02. This contradicts the accuracy on the train set of 0.972 as none of the parameters would be important for the model even though the model has a high accuracy.

**Impurity-based importance** can be used as an alternative to permutation-based importance for tree-based models. For impurity-based parameter importance, it is important to note that [2]

1. they are biased towards high-cardinality parameters, i. e. categorical parameters that have a lot of different labels;
2. they are computed on the training set and, therefore are not suited to make predictions that generalize to the test set.

The decision trees in the random forest model are trained with different subsets of the data. Making a prediction from a group of decision trees works best if the subgroups are not strongly correlated. Therefore, the random forest can choose the best splitting point among a random subset of parameters and parameter values. In scikit-learn [3] this is implemented as follows.
For a training vector $x_i \in \mathbb{R}^n$, $i = 1, ..., n$ a label vector $y \in \mathbb{R}^l$ a decision tree recursively partitions the parameter space. The data at a node $m$ is represented by $Q_m$ with $n_m$ samples. For each split $\theta = (j, t_m)$ for parameter $j$ and threshold $t_m$, the data is partitioned into $Q_m^{left}(\theta)$ and $Q_m^{right}(\theta)$ where the left partition contains all value-labels pairs lower or equal to the threshold and the right partition the other values.

Then the impurity function or loss function $H$ is used to determine the split of each candidate

$$G(Q_m, \theta) = \frac{n_m^{left}}{n_m} H(Q_m^{left}(\theta)) + \frac{n_m^{right}}{n_m} H(Q_m^{right}(\theta)). \tag{7.2}$$

The parameter that minimizes the impurity is chosen

$$\theta^* = argmin_\theta G(Q_m, \theta). \tag{7.3}$$

The location for splits in the regression case is determined by the Mean Squared Error (MSE). MSE selects the learned mean value $\overline{y}_m$ as the predicted value

$$\overline{y}_m = \frac{1}{n_m} \sum_{y \in Q_m} y. \tag{7.4}$$

The impurity function for the MSE is defined as

$$H(Q_m) = \frac{1}{n_m} \sum_{y \in Q_m} (y - \overline{y}_m)^2. \tag{7.5}$$

[2] https://scikit-learn.org/stable/auto_examples/inspection/plot_permutation_importance.html#sphx-glr-auto-examples-inspection-plot-permutation-importance-py
[3] https://scikit-learn.org/stable/modules/tree.html#mathematical-formulation

## 7.2. Reducing the parameter set

Another way to deal with the collinear parameters is to apply **hierarchical clustering** to the **Spearman rank-order correlations**, pick a threshold, and pick a parameter from each cluster [4]. Figure (7.2) shows Spearman's rank correlation coefficient in a heatmap of the correlated features. We manually pick a threshold from the left figure. From each group below the threshold, one parameter is kept, thus reducing the set of parameters. The accuracy on the training set was **0.972** while the accuracy on the test set was **0.827**. As a threshold, we choose **0.5**. With the removed parameters the accuracy on the test set only drops to **0.8**.

The correlated features are shown in figure (7.2). The meteorological measurements of the Hamburg weather mast are strongly correlated. The horizontal profiles are shown as clusters in the heat map, as we would expect. The temperature and humidity form two very distinct clusters. The absorption is also located in this part of the heat map as it's computed from these two parameters. It can also be seen that the measured values of the weather mast are strongly correlated with those of the measuring point at the airport. This finding is important, as in the future it may be possible to supplement the measurements from the airport with precise and comprehensive measurements from the weather mast. The wind direction parameter is partly correlated with the distance, altitude, elevation angle, and start parameters and the information on whether the noise measurement is from a start or a landing. Because airplanes usually take off and land into the wind, wind direction is a crucial factor when we look at measurements from a particular runway, in this case, runway 33. The height profiles of the weather parameters are grouped. For a machine learning model, it is therefore probably sufficient to look at one altitude per measurement variable.

[4] https://scikit-learn.org/stable/auto_examples/inspection/plot_permutation_importance_multicollinear.html#sphx-glr-auto-examples-inspection-plot-permutation-importance-multicollinear-py

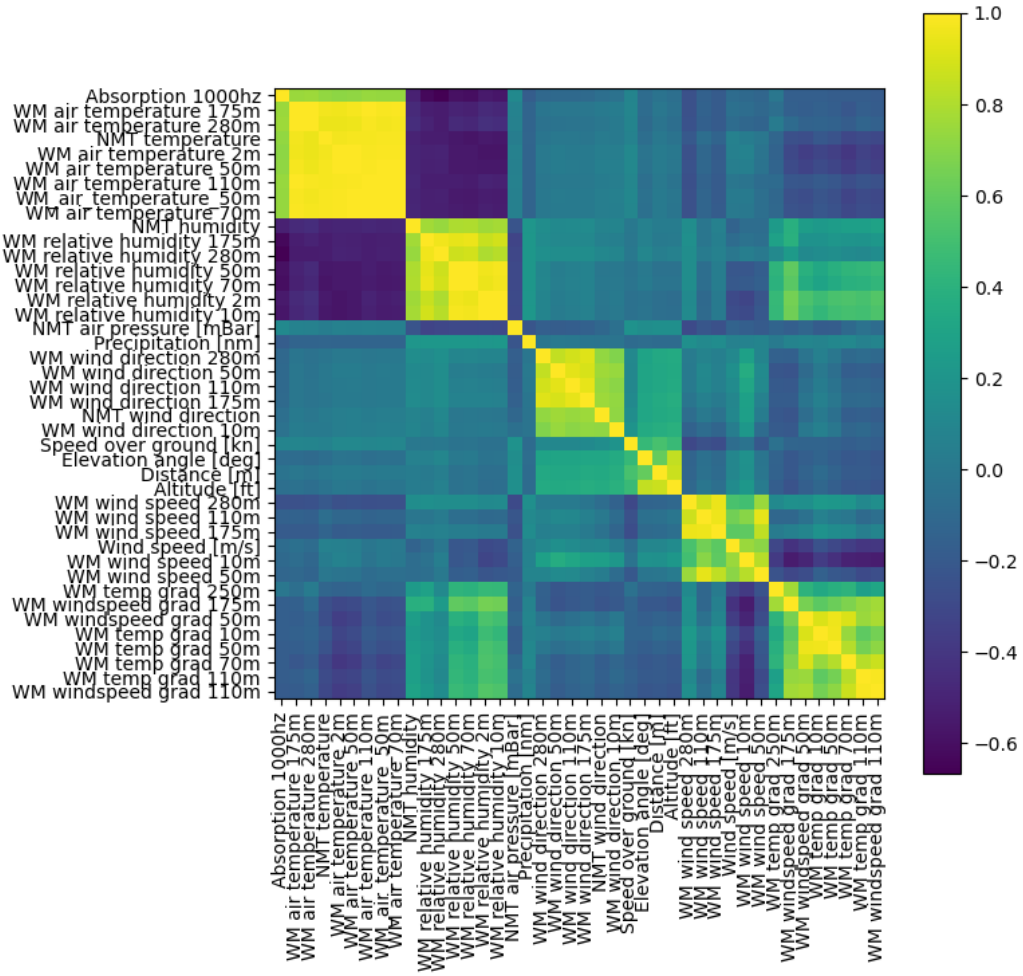


Figure 7.2.: Spearman's rank correlation matrix (heatmap) of the correlated parameters for A320 measurements at NMT 11 Norderstedt, Reitstall Ohlenhoff. Dark blue values indicate a negative monotonic relation (Spearman's coefficient < 0.0) between the parameters while bright yellow values (Spearman's coefficient > 0.0) indicate a positive monotonic relationship between the two parameters. No relationship between a pair of parameters is indicated as a blue color with a value of 0.0.

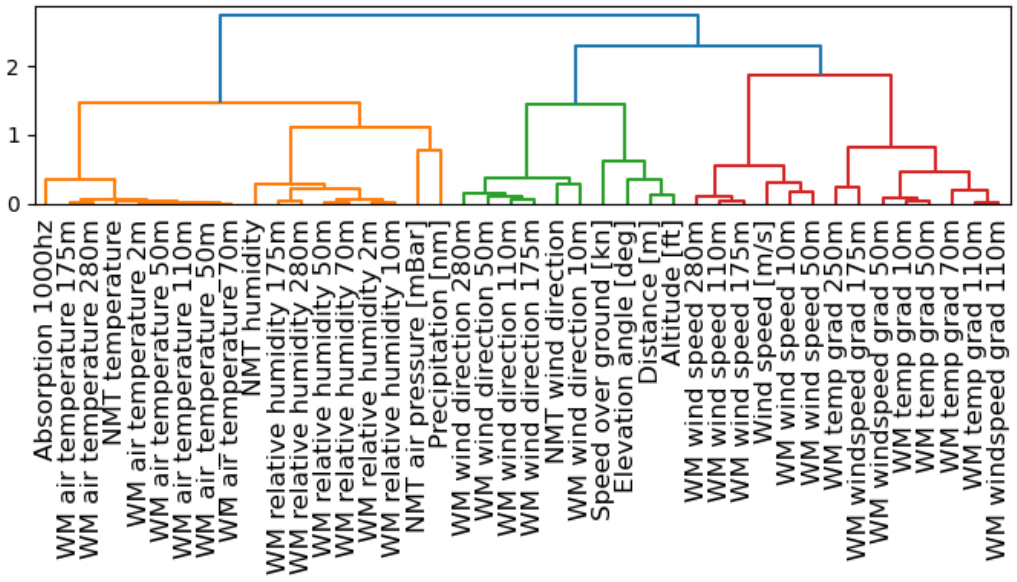


Figure 7.3.: Hierarchical Clustering (dendrogram) of the parameters of the A320 measurements at NMT11

Figure (7.3) shows the hierarchical clustering of the parameters. It is important to note that the y-axis has no label. The height of the cluster or data points can be understood as a metric of closeness. For example, the elevation angle, the distance, and the altitude are equally distant from the speed over ground because they join each other before they join the speed over ground. We chose to set the threshold at 0.5 below which parameters are grouped. Since the threshold is 0.5 the speed of the aircraft remains a non-grouped parameter due to its distance from the aforementioned three parameters that could be described as the distance between aircraft and NMT. The distance, elevation angle, and altitude of the aircraft to the NMT are grouped as a new "distance" parameter. All wind direction parameters and all temperature measurements are grouped into their respective groups. The other parameters are not important to the model as can be seen in figure (7.4) which shows the permutation importance on the test set. The sklearn method *scipy.cluster.hierarchy.dendrogram* [5] and the *scipy.stats.spearmanr* method [6] have been used to create figure (7.2) and figure (7.3).

[5]https://scikit-learn.org/stable/auto_examples/cluster/plot_agglomerative_dendrogram.html
[6]https://docs.scipy.org/doc/scipy/reference/generated/scipy.stats.spearmanr.html

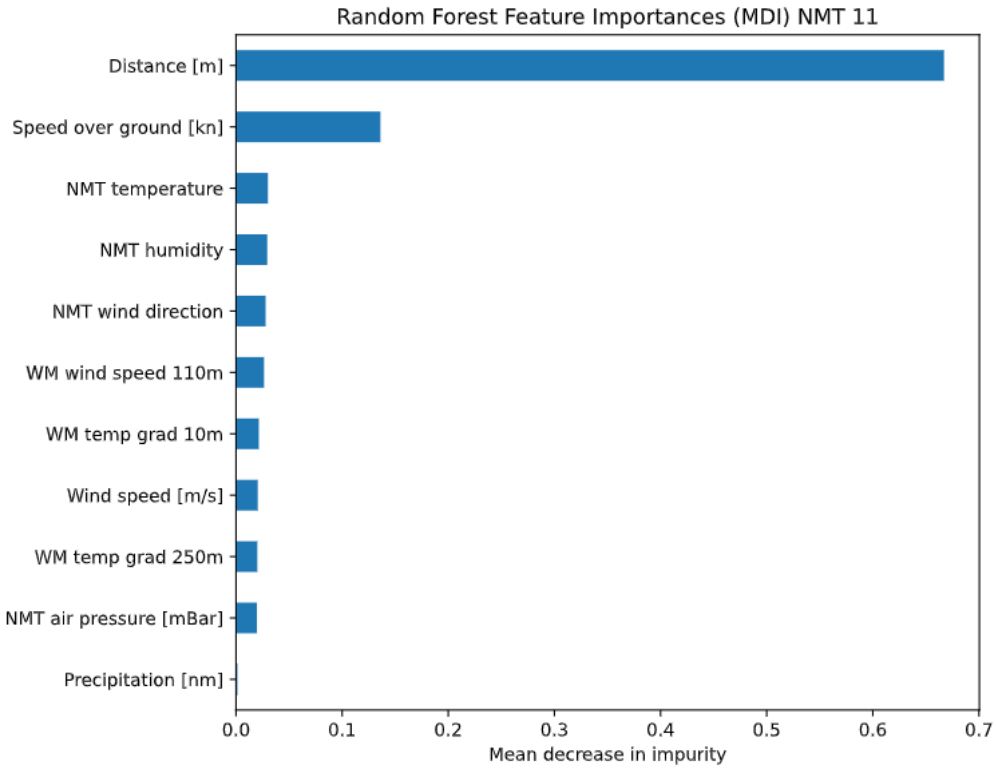


Figure 7.4.: Feature importance using the Mean Decrease in Accuracy on multicollinear A320 training data set at NMT11 with the reduced parameter set

## 7.3. Predicting $L_{AS,max}$

The new model can now be used to predict values of $L_{AS,max}$. After fitting the model to the training data set we predict the values of $L_{AS,max}$ on the test. Table (7.1) shows the results. The mean absolute error is around 0.89 dB meaning the error of the model is almost not noticeable by the human ear.

We plot the test values for $L_{AS,max}$ as a histogram and plot the predictions of the model in the same figure (7.5). The data is comprised of noise measurements from starts and landings. Therefore, we see two peaks in the data set. The lower peak with the less loud noise measurements are the landings while the other peak contains all the measurements from the starts. This division was also visible in the PCA of the same data set (5.1). Overall, the random forest was able to identify the two distinct groups of measurements even though the parameter "Start" [True/False] was not included in the training data set and to predict noise values up to an accuracy that would not be noticeable in practice.

The meteorological parameters make up for 14.85 % of the accuracy in the training data when we look at the Mean Decrease in Impurity (MDI). The parameters in figure (7.5) are the parameters that resulted from hierarchical clustering.

| | |
|---|---|
| Mean Absolute Error | 0.89 |
| Mean Squared Error | 1.43 |
| Root Mean Squared Error | 1.20 |
| Accuracy | 98.81% |

| Mean decrease in accuracy (MDI) | % |
|---|---|
| Distance [m] | 66.70% |
| Elevation angle [deg] | 13.61% |
| Altitude [ft] | 2.05% |
| Speed over ground [kn] | 2.79% |
| WM Wind speed [m/s] | 3.01% |
| NMT wind direction | 2.94% |
| NMT temperature | 1.97% |
| NMT humidity | 0.13% |
| NMT air pressure [mBar] | 2.64% |
| Precipitation [nm] | 2.15% |
| WM air temperature 2m | 2.01% |

Table 7.1.: (left) Prediction results with the reduced parameter set random forest model. (right) Mean decrease in accuracy (MDI) per parameter in the random forest model. The prefix NMT denotes the measurements at the noise measuring station while WM denotes measurements at the weather mast.

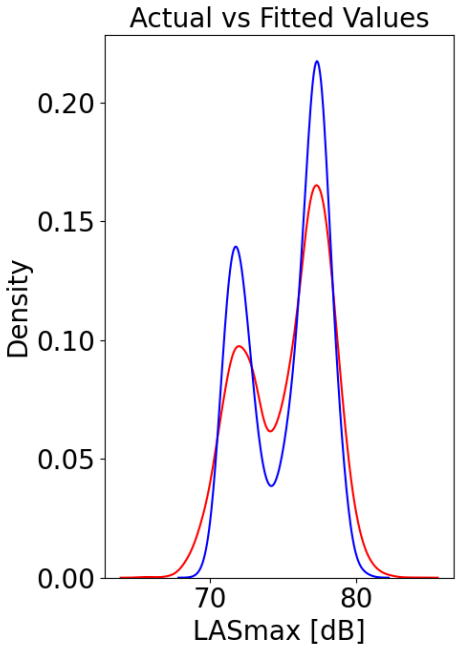


Figure 7.5.: Prediction results for $L_{AS,max}$ of the random forest model

# 8. Conclusion

To be able to take suitable measures to reduce noise, the noise propagation outdoors must first be quantified and the influencing factors identified. In this work, we have chosen a data-oriented approach to analyze noise pollution using the example of Hamburg Airport. This lays the first foundations for predicting noise events in the future. In this way, the effectiveness of future measures can be better evaluated.

We were able to work out the influencing factors from the measurement data and quantify the dependence of the noise value $L_{AS,max}$ on the parameters in decibels in chapter (6) which are the temperature gradient and the wind class. Flight data and noise measurements from the Airbus A320-200 from one year were combined with weather data. To be able to draw conclusions about the weather, we looked at various stations in detail. Concerning aircraft noise in the vicinity of an airport, noise refraction has proven to be an important meteorological influencing factor. By classifying the wind direction and speed into established headwind and crosswind classes, we were able to determine a difference of up to 1.2 dB at a distance of approx. 700 m between the aircraft and the measuring station using the ANOVA method. While such effects are often neglected in models in practice, we found that they make an audible difference for people living near the airport. Measuring vertical temperature gradients requires more complex measuring methods such as weather masts or radiosondes, which are generally not available at airports. By including data from the Hamburg weather mast, we were also able to investigate these influencing factors. Temperature profiles during the day and night differ greatly and influence the direction in which the sound is refracted. Here we were able to determine a difference of up to 2.6 dB between day and night temperature profiles at a certain station. However, we have also found that it is not always possible to work out meteorological influences, depending on the measuring station and the flight routes. Flight routes do not always provide optimal measurement conditions and the permanent noise measurement on the ground is also susceptible to interference factors that require a lot of manual work to process such as bird or car noise. Overall, there is an average difference of around 10 dB in noise exposure between the quietest and loudest measuring stations in the vicinity of Hamburg Airport. These differences can mainly be explained by the fact that the aircraft are much closer to the measuring station shortly after take-off or shortly before landing than is the case at more distant measuring stations.

Up to now, outdoor sound propagation has mainly been analyzed using numerical simulations. In chapter (5.3) and chapter (7) machine learning approaches were used to filter out influencing factors. The PCA method was used to identify groups and correlations in the data set. Take-offs and landings can be identified and should be considered separately for further analysis. A random forest model is fitted to the noise data at a specific measurement point.

With an accuracy of 98.81 %, the model was able to predict $L_{AS,max}$ values. In addition, we were able to draw conclusions from the model that the speed and distance to the measuring station make by far the greatest contribution to the accuracy of the model. The wind direction, followed by the temperature, turned out to be the most important meteorological parameter. For a specific NMT with its topographical conditions and a specific aircraft type, a simple machine-learning model is sufficient to make predictions with an accuracy of 1 dB. Knowing at which NMT the measurement takes place, the predictions could probably be extended to the entire area if a model is trained for each NMT, although this would require further work. The machine learning model could be trained with approx. 14,500 A320-200 measurements at NMT 11 Norderstedt, Reitstall Ohlenfhoff. Not as much data was available for other aircraft types, so it was not possible to train a model for other types. Overall, meteorological parameters were responsible for 14.85 % of the accuracy in the training data when we look at the Mean Decrease in Impurity (MDI).

In contrast to previous work, we have supplemented the measurement data for wind speed and direction, temperature, and humidity with vertical profiles. Using these measurement data, we were able to show that meteorology is not a negligible component of noise models. Even in best practice models, the inclusion of these parameters makes an audible difference. Future work can investigate how measurement data from weather masts can further contribute to making accurate noise predictions. In the long term, a noise forecast can be made similarly to a weather forecast. Residents living near airports will benefit from better noise protection, especially if air traffic continues to increase. Planners of noise-reducing measures also benefit from such forecasts, as this simplifies planning.

# A. Appendix

In the Appendix, PCA is applied to the noise and weather data of each NMT. A reduced set of parameters is shown for most NMTs so that the names of the parameters are still easy to read in the plot. For NMT 5 and 14 the complete parameter set is shown. NMT 5 does not measure any weather data. For NMT 14, in addition to the weather parameters wind, temperature and relative humidity measured at the station, all measurements of the weather mast are also shown, i.e. the measurements of these parameters at the heights 2m, 10m, 70m, 110m, 175m, 250m, 280m. For NMT 05, these are supplemented by the NMT without comparative values. In some plots, e.g. NMT 05, 07, and 11, you can see the division into two groups. Here there are measurements of both take-offs and landings. The red dots are individual noise events from take-offs, the purple dots represent measured noise events from landings. The plot shows how closely the weather measurements of the weather mast correlate with the measurements of the NMTs. This is interesting if you want to supplement the airport measurements with height profiles of wind and temperature. The NMTs are located at different altitudes and the local topographies may differ, so the data, represented by the principal components, will look different for each NMT, although they may come from the same overflights if the NMTs are placed one behind the other in relation to flight paths. Performing a complete PCA analysis with eigenvalues and tabulated loadings for each NMT, as shown in chapter (5.3), would be too extensive for the work. However, since the data is available and can provide interesting insights and can be used to compare the NMTs with each other, the plots appear here in the appendix.

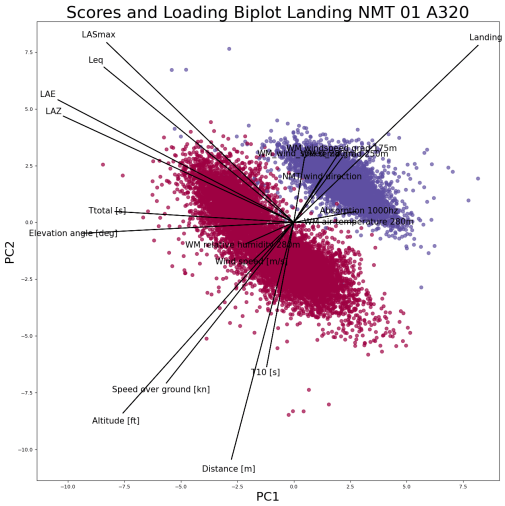


Figure A.1.: PCA NMT 01, only A320 data

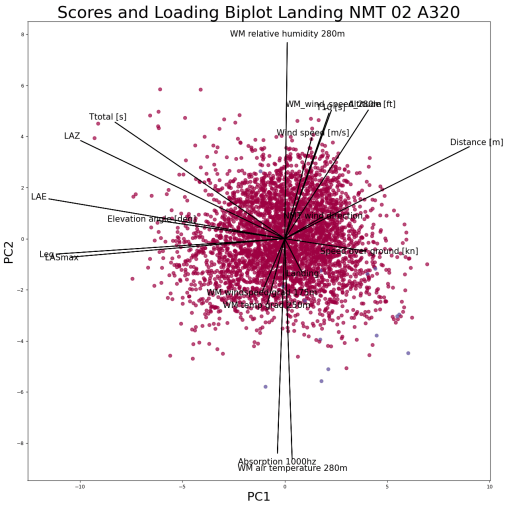


Figure A.2.: PCA NMT 02, only A320 data

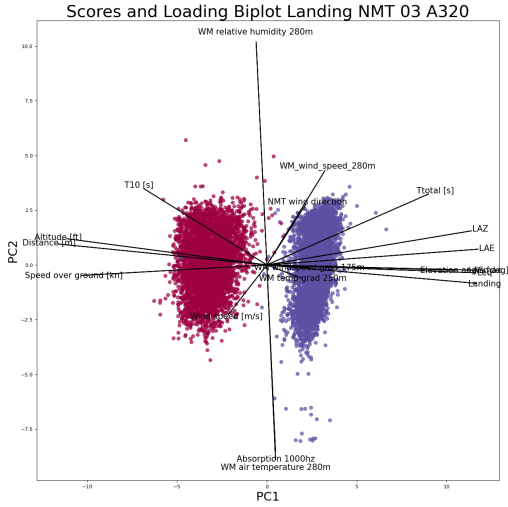


Figure A.3.: PCA NMT 03, only A320 data

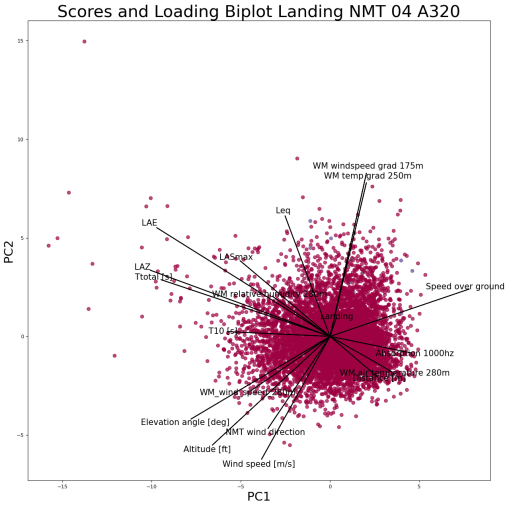


Figure A.4.: PCA NMT 04, only A320 data

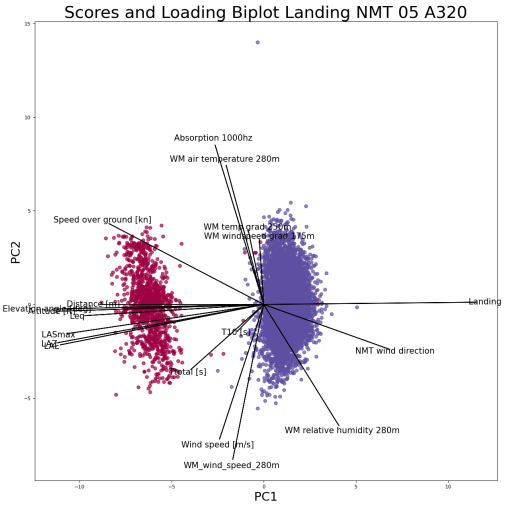


Figure A.5.: PCA NMT 05, only A320 data

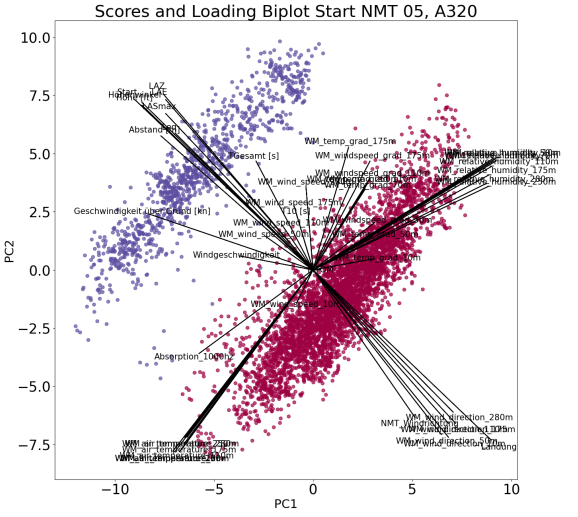


Figure A.6.: PCA NMT 05 complete, only A320 data

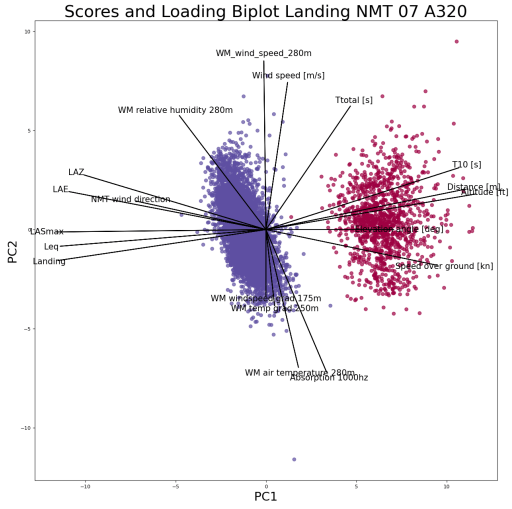


Figure A.7.: PCA NMT 07, only A320 data

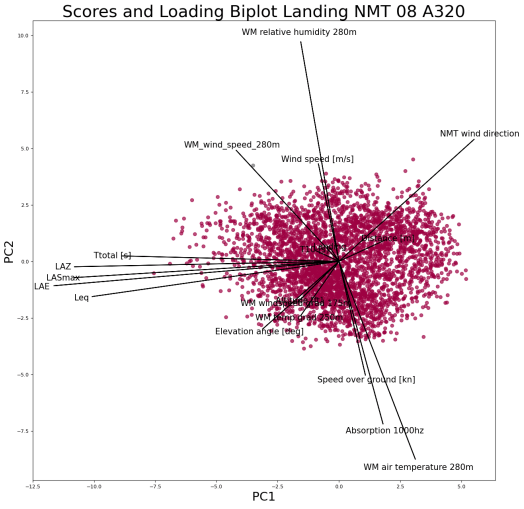


Figure A.8.: PCA NMT 08, only A320 data

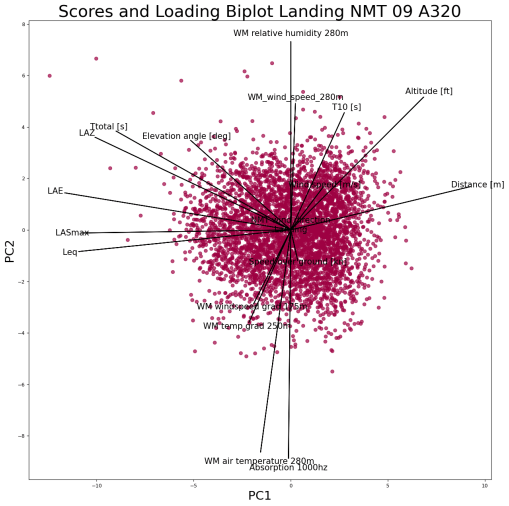


Figure A.9.: PCA NMT 09, only A320 data

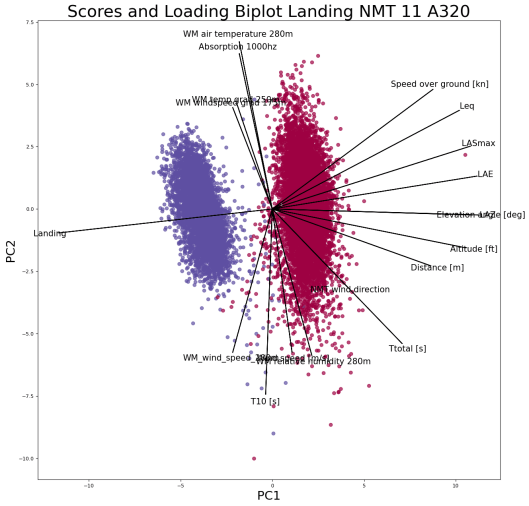


Figure A.10.: PCA NMT 11, only A320 data

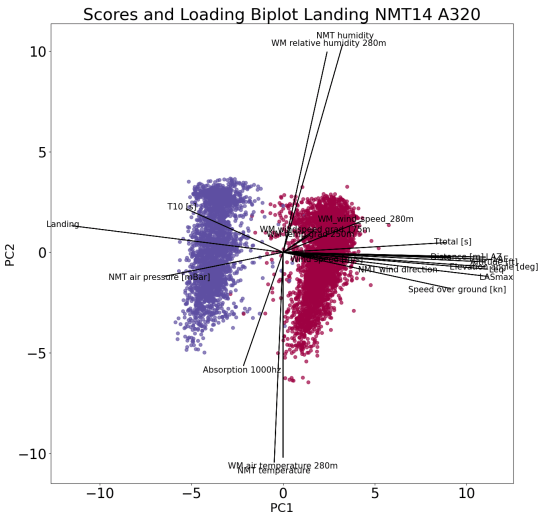


Figure A.11.: PCA NMT 14, only A320 data

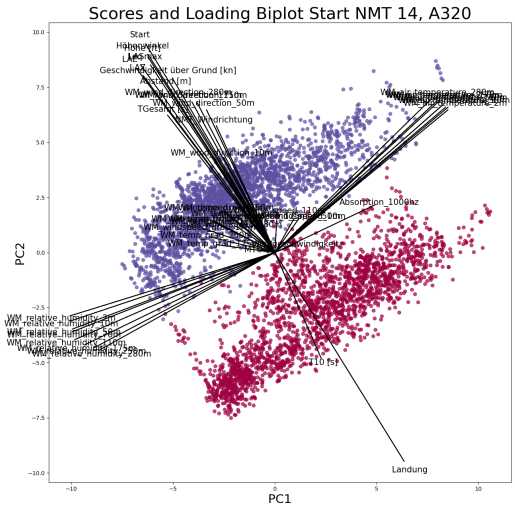


Figure A.12.: PCA NMT 14 complete, only A320 data

# List of Figures

# List of Tables

# Acronyms

**ABL** atmospheric boundary layer. 5, 49

**ADS-B** Automatic Dependent Surveillance-Broadcast system. 12, 17

**ANOVA** Analysis of Variance. 4

**CRS** Coordinate Reference System. 13

**f** frequency [Hz]. 6

**ICAO** International Civil Aviation Organization. 3

$L_{AE}$ A-weighted sound exposure level (immission at certain observer), [dBA]. 22

$L_{AS,max}$ maximum A-weighted sound pressure level of the aircraft with the "SLOW" rating (immission at a certain observer) [dBA]. 8, 19, 22, 27–30, 33–36, 39, 40, 42, 45, 47, 51, 62, 68, 70, 71

$L_E$ single event sound level [dB]. 8

$L_{eq}$ equivalent continuous sound level, [dBA]. 8, 22

$L_{\overline{p}}$ mean of the sound pressure level $L$ over a series of noise events $L_i$, [dBA]. 9, 40, 42

**NMT** Noise Monitoring Terminal. 2

$\hat{p}$ sound pressure amplitude [Pa]. 6

**PCA** principal component analysis. 22

**SPL** sound pressure level [dB]. 8, 9, 40

**SVD** singular value decomposition. 23

**T** temperature [$^{\circ}C$]. 8, 14

$T_{Las,max}$ time where the maximum sound pressure level $L_{AS,max}$ is measured. 12, 39, 40, 45

# Bibliography


[1] U. Isermann and L. Bertsch. "Aircraft noise immission modeling". In: *CEAS Aeronautical Journal* 10.1 (2019), pp. 287–311. ISSN: 1869-5582. DOI: 10.1007/s13272-019-00374-5.

[2] R. Blumrich and D. Heimann. "A linearized Eulerian sound propagation model for studies of complex meteorological effects". In: *The Journal of the Acoustical Society of America* 112.2 (2002), pp. 446–455.

[3] D. Heimann and G. Gross. "Coupled simulation of meteorological parameters and sound level in a narrow valley". In: *Applied Acoustics* 56.2 (1999), pp. 73–100.

[4] D. Heimann, A. Schady, and J. Feng. "Atmospheric Acoustics published in Atmospheric Physics". In: (2012). DOI: 10.1007/978-3-642-30183-4.

[5] M. Greenacre, P. J. F. Groenen, T. Hastie, A. I. D'Enza, A. Markos, and E. Tuzhilina. "Principal component analysis". In: *Nature Reviews Methods Primers* 2.1 (2022). DOI: 10.1038/s43586-022-00184-w.

[6] H. Abdi and L. J. Williams. "Principal component analysis". In: *WIREs Computational Statistics* 2.4 (2010), pp. 433–459. DOI: https://doi.org/10.1002/wics.101. eprint: https://wires.onlinelibrary.wiley.com/doi/pdf/10.1002/wics.101. URL: https://wires.onlinelibrary.wiley.com/doi/abs/10.1002/wics.101.

[7] M. Kaltenbach, C. Maschke, and R. Klinke. "Health consequences of aircraft noise". In: *Deutsches Arzteblatt international* 105.31-32 (2008), pp. 548–556. DOI: 10.3238/arztebl.2008.0548.

[8] E. A. M. Franssen, C. M. A. G. van Wiechen, N. J. D. Nagelkerke, and E. Lebret. "Aircraft noise around a large international airport and its impact on general health and medication use". In: *Occupational and Environmental Medicine* 61.5 (2004), pp. 405–413. ISSN: 1470-7926. DOI: 10.1136/oem.2002.005488. URL: https://oem.bmj.com/content/oemed/61/5/405.full.pdf.

[9] The Assembly of the United Nations. "Consolidated statement of continuing ICAO policies and practices related to environmental protection - General provisions, noise and local air quality, Resolution A41-20". In: (ASSEMBLY – 41st SESSION, 2022).

[10] F. Yunus, D. Casalino, F. Avallone, and D. Ragni. "Toward inclusion of atmospheric effects in the aircraft community noise predictions". In: *The Journal of the Acoustical Society of America* 150.2 (2021), pp. 759–768. ISSN: 0001-4966. DOI: 10.1121/10.0005733.

[11] A. Johansson and K. Bolin. "Analysis of landing noise from Airbus A321neo using long term noise measurements and flight recorder data". In: *The Journal of the Acoustical Society of America* 153.6 (2023), pp. 3482–3492. ISSN: 0001-4966. DOI: 10.1121/10.0019713.

[12] J. W. Tukey. "Comparing individual means in the analysis of variance". In: *Biometrics* (1949), pp. 99–114.

[13] D. B. Richardson, G. B. Hamra, R. F. MacLehose, S. R. Cole, and H. Chu. "Hierarchical regression for analyses of multiple outcomes". In: *American journal of epidemiology* 182.5 (2015), pp. 459–467. DOI: 10.1093/aje/kwv047.

[14] C. Zellmann, B. Schäffer, J. M. Wunderli, U. Isermann, and C. O. Paschereit. "Aircraft Noise Emission Model Accounting for Aircraft Flight Parameters". In: *Journal of Aircraft* 55.2 (2018), pp. 682–695. ISSN: 0021-8669. DOI: 10.2514/1.C034275.

[15] L. Bertsch. *Noise Prediction within Conceptual Aircraft Design*. Tech. rep. Technische Universität Braunschweig, Aug. 2013. URL: https://elib.dlr.de/84386/.

[16] L. Bertsch, B. Schäffer, and S. Guérin. "Uncertainty Analysis for Parametric Aircraft System Noise Prediction". In: *Journal of Aircraft* 56.2 (2019), pp. 529–544. ISSN: 0021-8669. DOI: 10.2514/1.C034809.

[17] U. Römer, L. Bertsch, S. B. Mulani, and B. Schäffer. "Uncertainty Quantification for Aircraft Noise Emission Simulation: Methods and Limitations". In: *AIAA Journal* 60.5 (2022), pp. 3020–3034. ISSN: 0001-1452. DOI: 10.2514/1.J061143.

[18] L. Bertsch, W. Dobrzynski, and S. Guérin. "Tool development for low-noise aircraft design". In: *Journal of Aircraft* 47.2 (2010), pp. 694–699.

[19] J. Hoffman, J. Jansson, and C. Johnson. "New Theory of Flight". In: *Journal of Mathematical Fluid Mechanics* 18.2 (2016), pp. 219–241. ISSN: 1422-6928. DOI: 10.1007/s00021-015-0220-y.

[20] R. B. Stull. *An introduction to boundary layer meteorology*. Vol. 13. Springer Science & Business Media, 2012.

[21] E. M. Salomons. *Computational atmospheric acoustics*. Springer Science & Business Media, 2001.

[22] D. Heimann, M. Bakermans, J. Defrance, and D. Kühner. "Vertical sound speed profiles determined from meteorological measurements near the ground". In: *Acta Acustica united with Acustica* 93.2 (2007), pp. 228–240.

[23] G. Taraldsen, T. Berge, F. Haukland, B. H. Lindqvist, and H. Jonasson. "Uncertainty of decibel levels". In: *The Journal of the Acoustical Society of America* 138.3 (2015), EL264–EL269. ISSN: 0001-4966. DOI: 10.1121/1.4929619.

[24] H. E. Bass, L. C. Sutherland, and A. J. Zuckerwar. "Atmospheric absorption of sound: Update". In: *The Journal of the Acoustical Society of America* 88.4 (1990), pp. 2019–2021. ISSN: 0001-4966. DOI: 10.1121/1.400176.

[25] *ISO 9613-1: Acoustics, Attenuation of Sound During Propagation Outdoors. Calculation of the absorbtion of sound by the atmosphere. Part 1*. International standard. International Organization for Standardization, 1993. URL: https://books.google.de/books?id=8yG0zQEACAAJ.

[26] THE EUROPEAN COMMISSION. "COMMISSION IMPLEMENTING REGULATION (EU) 2020/587: amending Implementing Regulation (EU) No 1206/2011 laying down requirements on aircraft identification for surveillance for the single European sky and Implementing Regulation (EU) No 1207/2011 laying down requirements for the performance and the interoperability of surveillance for the single European sky". In: *Official Journal of the European Union* (29 April 2020). URL: https://eur-lex.europa.eu/legal-content/EN/TXT/?uri=CELEX%3A32020R0587.

[27] U. Isermann and B. M. Vogelsang. "Messung und Beurteilung von Fluggeräuschen–Vorstellung der neuen DIN 45643". In: (2011).

[28] T. Joppa and F. Berber. *"Übersicht der Wetterstationen am Flughafen Hamburg" – Persönliche Mitteilung vom 11. 09. 2023*.

[29] J. Defrance, E. Salomons, I. Noordhoek, D. Heimann, B. Plovsing, G. Watts, H. Jonasson, X. Zhang, E. Premat, I. Schmich, et al. "Outdoor sound propagation reference model developed in the European Harmonoise project". In: *Acta Acustica united with Acustica* 93.2 (2007), pp. 213–227.

[30] Fraport AG. *DIN 45643:2011-02 Umsetzung bei Fraport*. URL: https://www.fraport.com/content/dam/fraport-company/images/umwelt/schallschutz/flugl%C3%A4rm/dokumente/Umstellung%20des%20Messverfahrens.pdf/_jcr_content/renditions/original./Umstellung%20des%20Messverfahrens.pdf.

[31] Ingo Lange. *Wind- und Temperaturdaten vom Wettermast Hamburg des Meteorologischen Instituts der Universität Hamburg für den Zeitraum August 2022 bis August 2023. – Persönliche Mitteilung vom 11. 10. 2023*.

[32] T. Kurita. "Principal component analysis (PCA)". In: *Computer Vision: A Reference Guide* (2019), pp. 1–4.

[33] Svante Wold. "Principal Component Analysis". In: *Chemometrics and Intelligent Laboratory Systems, 2 (1987) 37-52* ().

[34] J. L. Gastwirth, Y. R. Gel, and W. Miao. "The impact of levene's test of equality of variances on statistical theory and Practice". In: *Statistical Science* 24.3 (2009). DOI: 10.1214/09-sts301.

[35] N. H. Augustin, E.-A. Sauleau, and S. N. Wood. "On quantile quantile plots for generalized linear models". In: *Computational Statistics & Data Analysis* 56.8 (2012), pp. 2404–2409.

[36] L. St»hle and S. Wold. "Analysis of variance (ANOVA)". In: *Chemometrics and Intelligent Laboratory Systems* 6.4 (1989), pp. 259–272. DOI: 10.1016/0169-7439(89)80095-4.

[37] H. Abdi. "Honestly significant difference (HSD) test". In: *Encyclopedia of Research Design* (2010). DOI: 10.4135/9781412961288.n181.

[38] Keith Attenborough and Timothy Van Renterghem. *Predicting Outdoor Sound [2 ed.]* CRC Press, 2021. ISBN: 978-1498740074.

[39] L. Breiman. "Random forests". In: *Machine learning* 45 (2001), pp. 5–32.

[40] G. Iannace, G. Ciaburro, and A. Trematerra. "Wind turbine noise prediction using random forest regression". In: *Machines* 7.4 (2019), p. 69.